AN ABSTRACT OF THE THESIS OF

NARENDER KUMAR NAGPAL for the DOCTOR OF PHILOSOPHY
(Name) (Degree)

in SOILS presented on Feb 19, 1971
(Major) (Date)

Title: MEASUREMENT AND INTERPRETATION OF PHYSICAL PROPERTIES OF SOILS

Redacted for Privacy

Abstract approved: _____
Larry Boersma

One of many important physical properties that must be known to understand transport phenomena in soils is pore size distribution. Presently the pore size distributions of soils are most commonly obtained from soil water characteristic curves. The soil water characteristic curves are usually obtained by the pressure plate technique. It is a very laborious and time consuming procedure, with questionable reproducibility.

Use of the mercury intrusion porosimeter in determining pore size distributions of soils was evaluated. Eight soils differing in clay content were used. Upon applying appropriate computational techniques the two methods were found to give identical results. Adoption of mercury intrusion as a standard laboratory procedure is suggested.

Thermal conductivities of three size classes of glass beads, 53-74 μ, 74-105 μ, and 149-210 μ, were predicted using the model

developed by de Vries. Predicted and experimental values of thermal conductivity showed good agreement. Since vapor transfer under temperature gradients is one of the components of heat transfer, it was hypothesized that pore size distribution by its controlling action on vapor flow would affect the thermal conductivity of the media. The results showed no influence of pore size distribution on thermal conductivity.

It was observed however that pore size distribution does affect the rate of water loss from porous beds subjected to diurnal temperature fluctuations. Smaller pores resist rapid loss of water vapor and as a result total heat exchanged in beds made up of small particles was much smaller than observed for beds made up of large particles. The evaporative flux constitutes a major part of the total heat flux. Incoming radiation was observed to be used more efficiently in moist samples than in dry samples.

Measurement and Interpretation of Physical Properties of Soils

by

Narender Kumar Nagpal

A THESIS

submitted to

Oregon State University

in partial fulfillment of
the requirements for the
degree of

Doctor of Philosophy

June 1971

APPROVED:

Redacted for Privacy

Professor of Soils

in charge of major

Redacted for Privacy

Head of Department of Soils

Redacted for Privacy

Dean of Graduate School

Date thesis is presented Feb. 19, 1971

Typed by Clover Redfern for Narender Kumar Nagpal

ACKNOWLEDGMENTS

I wish to express my gratitude to Doctor Larry Boersma for his valuable guidance, encouragement and constructive criticism during the course of this study as well as in the preparation of this manuscript.

My appreciation is also expressed to Doctor M. D. Dawson, Doctor W. P. Lowry and Doctor R. H. Brooks for acting as members of my Graduate Committee and for their valuable advice in selecting courses relevant to this study.

I further wish to thank Mr. Gary Jarman for his valuable technical assistance.

Financial support from the Office of Water Resources Research, United States Department of the Interior (grant No. B-001-ORE), and the Oregon Agricultural Experiment Station (project 419), is gratefully acknowledged.

TABLE OF CONTENTS

	Page
INTRODUCTION	1
PORE SIZE DISTRIBUTION AND SOIL WATER CHARACTERISTIC CURVES	4
Introduction	4
Materials and Methods	7
Porosimeter	7
Equipment and Procedure	8
Calculation of Pore Aperture Size Distribution	11
Soil Water Characteristic Curves as Derived from Porosimeter Data	13
Results and Discussion	14
Sources of Disagreement Between Methods	16
Conclusions	21
Epilogue	24
THERMAL CONDUCTIVITY	52
Introduction	52
Thermal Conductivity of Dry Soils	52
Thermal Conductivity of Wet Soils	53
Calculation of Thermal Conductivity	54
Materials and Methods	56
Experimental Measurement of Thermal Conductivity	56
Theoretical Calculation of Thermal Conductivity	58
Results and Discussion	62
Conclusions	70
SIMULTANEOUS TRANSFER OF HEAT AND WATER	71
Introduction	71
Materials and Methods	74
Experimental Configuration	74
Heating of the Sample	76
Temperature Measurements	79
Water Content Measurements	82
Equipment	85
Results and Discussion	87
Experiments I and V: Air Dry; 53-74 Microns and 149-210 Microns	87

Page

Experiments II and VI: Saturated; 53-74 Microns and 149-210 Microns 93
Analysis of the Experimental Results 100
Experiments III and VII: Initially Saturated; 53-74 Microns and 149-210 Microns 107
Experiments IV and VIII: Initial Water Content 34% for 53-74 Microns and 30% for 149-210 Microns Glass Beads 119
Heat Flux 131
Dry Samples 133
Saturated Samples 134
Initially Saturated Samples 136
Initially Unsaturated Samples 138
Conclusions 140

SUMMARY AND CONCLUSION 151

BIBLIOGRAPHY 154

APPENDIX 159

LIST OF TABLES

Table		Page
1.	Pore size distribution of Quincy soil as determined by the mercury intrusion porosimeter.	12
2.	Pressure correction for hanging mercury column in penetrometer.	13
3.	Water retention characteristics of Quincy soil as calculated from porosimeter data.	15
4.	Mechanical analysis of soils used as obtained with the hydrometer method.	15
5.	List of experiments conducted for the study of simultaneous transfer of heat and water in glass bead beds.	76
6.	A sample of tables prepared for each group of thermistors to convert chart reading to temperature.	82
7.	Maximum temperature (°C) and time lag (minutes) observed for air dry samples subjected to a diurnal temperature cycle.	93
8.	Maximum temperature (°C) and time lag (minutes) observed for saturated samples subjected to a diurnal temperature cycle.	94
9.	Values of parameters used in the calculations of the temperature (°C) at a depth of 2 cm in the 53-74 microns size glass bead beds.	99
10.	Calculated maximum temperature (°C) and time lag (minutes) for air dry samples, based on a 14 hour period.	105
11.	Calculated maximum temperature (°C) and time lag (minutes) for saturated samples, based on a 14 hour period.	106
12.	Maximum temperature in °C observed for the initially saturated columns subjected to a diurnal radiation cycle.	112

Table		Page
13.	Time lag in minutes observed for the initially saturated columns subjected to a diurnal radiation cycle.	113
14.	Percent change in water content at the end of each day for initially saturated samples subjected to a diurnal temperature cycle.	118
15.	Maximum temperature in °C observed for initially unsaturated columns subjected to a diurnal temperature cycle.	124
16.	Time lag in minutes observed for initially unsaturated columns subjected to a diurnal temperature cycle.	125
17.	Percent change in water content at the end of each day in initially unsaturated columns subjected to a diurnal temperature cycle.	126
18.	Quantity of heat exchanged at the surface of dry glass beads beds.	134
19.	Quantity of heat exchanged at the surface of saturated glass beads beds.	135
20.	Quantity of heat exchanged at the surface of initially saturated glass beads beds.	136
21.	Quantity of heat exchanged at the surface of initially unsaturated glass beads beds.	139

LIST OF FIGURES

Figure		Page
1.	Front view of the mercury intrusion porosimeter.	9
2.	Mercury intrusion porosimeter penetrometer assembly.	10
3.	Soil water characteristic curve for Sand II.	26
4.	Soil water characteristic curve for Quincy soil.	27
5.	Soil water characteristic curve for Ephrata soil.	28
6.	Soil water characteristic curve for Cloquato soil.	29
7.	Soil water characteristic curve for Woodburn soil.	30
8.	Soil water characteristic curve for Chehalis soil.	31
9.	Soil water characteristic curve for Dayton soil.	32
10.	Soil water characteristic curve for Kenutchen soil.	33
11.	Pore size distribution curves determined by mercury intrusion and by the pressure plate apparatus, Sand II.	34
12.	Pore size distribution curves determined by mercury intrusion and by the pressure plate apparatus, Qunicy.	35
13.	Pore size distribution curves determined by mercury intrusion and by the pressure plate apparatus, Ephrata.	36
14.	Pore size distribution curves determined by mercury intrusion and by the pressure plate apparatus, Cloquato.	37
15.	Pore size distribution curves determined by mercury intrusion and by the pressure plate apparatus, Woodburn.	38
16.	Pore size distribution curves determined by mercury intrusion and by the pressure plate apparatus, Chehalis.	39
17.	Pore size distribution curves determined by mercury intrusion and by the pressure plate apparatus, Dayton.	40

Figure		Page
18.	Pore size distribution curves determined by mercury intrusion and by the pressure plate apparatus, Kenutchen.	41
19.	Pore size distribution curves determined by the mercury intrusion porosimeter, after correction, and by the pressure plate and the pressure membrane apparatus.	42
20.	Pore size distribution curves determined by the mercury intrusion porosimeter, after correction, and by the pressure plate and the pressure membrane apparatus.	43
21.	Pore size distribution curves determined by the mercury intrusion porosimeter, after correction, and by the pressure plate and the pressure membrane apparatus.	44
22.	Pore size distribution curves determined by the mercury intrusion porosimeter, after correction, and by the pressure plate and the pressure membrane apparatus.	45
23.	Pore size distribution curves determined by the mercury intrusion porosimeter, after correction, and by the pressure plate and the pressure membrane apparatus.	46
24.	Pore size distribution curves determined by the mercury intrusion porosimeter, after correction, and by the pressure plate and the pressure membrane apparatus.	47
25.	Pore size distribution curves determined by the mercury intrusion porosimeter, after correction, and by the pressure plate and the pressure membrane apparatus.	48
26.	Pore size distribution curves determined by the mercury intrusion porosimeter, after correction, and by the pressure plate and the pressure membrane apparatus.	49
27.	The percent pore space correction required to make the mercury intrusion and the pressure plate determined pore size distribution curves coincide, as a function of clay content of the soil.	50
28.	Correlation between clay content and water content at 15.0 bars for clay soils from various geographic regions.	51

Figure		Page
29.	Rise in temperature of the thermal conductivity probe inserted in a sample as a function of time.	59
30.	The thermal conductivity of three samples of glass beads as a function of water content.	63
31.	The thermal conductivity of three samples of glass beads as a function of water suction.	65
32.	Soil water characteristic curves for three samples of glass beads as obtained with the mercury intrusion porosimeter.	66
33.	Experimental arrangement used for the study of simultaneous transfer of heat and water in glass bead beds.	75
34.	Heat input from the heat source as a function of time.	78
35.	Positions at which temperature measurements in glass bead samples were made.	80
36.	The calibration curve for the temperature recorder, showing the relation between chart reading and resistance.	81
37.	Positions at which water content measurements were made.	88
38.	Diurnal temperature variations in air dry column of the 53-74 microns size glass beads at 2 cm, 4 cm, and 7 cm depths.	89
39.	Diurnal temperature variations in air dry column of the 53-74 microns size glass beads at 11 cm, 18 cm, and 38 cm depths.	90
40.	Diurnal temperature variations in air dry column of the 149-210 microns size glass beads at 2 cm, 4 cm, and 7 cm depths.	91
41.	Diurnal temperature variations in air dry column of the 149-210 microns size glass beads at 11 cm, 18 cm, and 38 cm depths.	92

Figure		Page
42.	Diurnal temperature variations in saturated column of the 53-74 microns size glass beads at 2 cm, and 7 cm depths.	95
43.	Diurnal temperature variations in saturated column of the 53-74 microns size glass beads at 18 cm, and 38 cm depths.	96
44.	Diurnal temperature variations in saturated column of the 149-210 microns size glass beads at 2 cm, and 7 cm depths.	97
45.	Diurnal temperature variations in saturated column of the 149-210 microns size glass beads at 18 cm, and 38 cm depths.	98
46.	Comparison of the observed and the calculated temperature as a function of time at a depth of 2 cm in saturated samples of glass beads.	103
47.	Comparison of the observed and the calculated temperature as a function of time at a depth of 2 cm in air dry samples of glass beads.	104
48.	Diurnal temperature variations in initially saturated column of the 53-74 microns size glass beads at 2 cm, and 7 cm depths.	108
49.	Diurnal temperature variations in initially saturated column of the 53-74 microns size glass beads at 18 cm, and 38 cm depths.	109
50.	Diurnal temperature variations in initially saturated column of the 149-210 microns size glass beads at 2 cm, and 7 cm depths.	110.
51.	Diurnal temperature variations in initially saturated column of the 149-210 microns size glass beads at 18 cm, and 38 cm depths.	111
52.	Percent change in water content as a function of time in initially saturated column of the 53-74 microns size glass beads at 2 cm, 3 cm, and 33 cm depths.	114

Figure		Page
53.	Percent change in water content as a function of time in initially saturated column of the 53-74 microns size glass beads at 5 cm, and 17 cm depths.	115
54.	Percent change in water content as a function of time in initially saturated column of the 149-210 microns size glass beads at 2 cm, 3 cm, and 33 cm depths.	116
55.	Percent change in water content as a function of time in initially saturated column of the 149-210 microns size glass beads at 5 cm, 9 cm, and 17 cm depths.	117
56.	Diurnal temperature variations in initially unsaturated column of the 53-74 microns size glass beads at 2 cm, 4 cm, and 7 cm depths.	120
57.	Diurnal temperature variations in initially unsaturated column of the 53-74 microns size glass beads at 11 cm, 18 cm, and 38 cm depths.	121
58.	Diurnal temperature variations in initially unsaturated column of the 149-210 microns size glass beads at 2 cm, 4 cm, and 7 cm depths.	122
59.	Diurnal temperature variations in initially unsaturated column of the 149-210 microns size glass beads at 11 cm, 18 cm, and 38 cm depths.	123
60.	Percent change in water content as a function of time in initially unsaturated columns of the 53-74 microns size glass beads at 2 cm, 3 cm, and 33 cm depths.	127
61.	Percent change in water content as a function of time in initially unsaturated column of the 53-74 microns size glass beads at 5 cm, 9 cm, and 17 cm depths.	128
62.	Percent change in water content as a function of time in initially unsaturated column of the 149-210 microns size glass beads at 2 cm, 3 cm, and 33 cm depths.	129
63.	Percent change in water content as a function of time in initially unsaturated columns of the 149-210 microns size glass beads at 5 cm, and 17 cm depths.	130

Figure		Page
64.	Heat flux variations in air dry column of the 53-74 microns size glass beads.	143
65.	Heat flux variations in air dry column of the 149-210 microns size glass beads.	144
66.	Heat flux variations in saturated column of the 53-74 microns size glass beads.	145
67.	Heat flux variations in saturated column of the 149-210 microns size glass beads.	146
68.	Heat flux variations in initially saturated column of the 53-74 microns size glass beads.	147
69.	Heat flux variations in initially saturated column of the 149-210 microns size glass beads.	148
70.	Heat flux variations in initially unsaturated column of the 53-74 microns size glass beads.	149
71.	Heat flux variations in initially unsaturated column of the 149-210 microns size glass beads.	150

MEASUREMENT AND INTERPRETATION OF PHYSICAL PROPERTIES OF SOILS

INTRODUCTION

The properties of soils that govern the flow of heat and water are of great interest to several disciplines. Soil scientists and agronomists are concerned with problems of heat and water movement in the soil which are potent regulators of soil-plant-water relationships. Rates of biological and chemical reactions and hence rates of plant growth are influenced by the temperature of the soil.

Soil water characteristic curves are an expression of the relationship between water content and matric suction. They are presently obtained with a method developed by Richards (1947, 1949a, 1949b). The technique has certain limitations (Hillel and Mottes, 1966) that impair its reproducibility. It is, furthermore, extremely time consuming. Drake and Ritter (1945) developed a technique to measure pore aperture size distributions of porous media. This technique is based on the forcing of mercury into the porous material. Pore size apertures corresponding to applied pressure can be calculated with the pressure of displacement equation. The volume of mercury forced into the pores provides a measure of pore volume. Since a soil water characteristic curve is a function of pore size distribution, it can be obtained from porosimeter data. This technique

seems to offer certain advantages over the pressure plate method. Experiments were designed to evaluate the potential use of the mercury intrusion method in the soils laboratory as a tool to obtain pore size distribution and soil water characteristic curves.

In the description of heat transfer in soils, knowledge of thermal conductivity is important. The literature indicates the effect of structure, texture, bulk density, porosity, and water content on the thermal conductivity of soil. Models have been developed that allow calculation of the thermal conductivity of porous materials from the volume fractions of its constituents and the shape of the particles (de Vries, 1966). These calculations allow for the transfer of heat in the form of vapor movement under the influence of thermal gradients in the porous medium. Experiments were conducted to evaluate the validity of these theoretical models. These experiments had the additional objective of evaluating the relation between pore size distribution and thermal conductivity.

Heat and water are two major components of the environment in which roots grow. The availability of water and the temperature of the soil determine in large measure how well a plant is going to develop. The soil water content and the soil temperature are part of a constantly changing scene. The importance of being able to predict future changes in these parameters is clear. These parameters were expected to be influenced by other soil variables such as pore size

distribution and initial soil water content. Experiments were designed to study the effect of these soil variables on the distribution of moisture and temperature in soils under diurnal temperature variations. Since changes in heat content give a good indication of temperature and water content changes in soils subjected to thermal gradients, this parameter was also calculated and studied (Gardner and Hanks, 1966).

PORE SIZE DISTRIBUTION AND SOIL WATER CHARACTERISTIC CURVES

Introduction

The relation between soil water content and matric or soil water suction is usually referred to as the soil water characteristic curve. The relationship is not unique and depends on the previous history of water uptake and water withdrawal (Rose, 1966). It reflects the behavior of fluids in a porous material as governed by the relationship between capillary pressure, or suction, and the liquid content held in the pores at that suction. In a soil water system, this relationship gives the familiar soil water characteristic curves (Childs, 1940).

Soil water characteristic curves are obtained by a method first introduced by Richards (1941). A saturated sample, supported by a porous plate, is subjected to a certain pressure. The corresponding water content is determined when the soil sample reaches equilibrium conditions.

Since the method was first developed, several modifications have been introduced. Ceramic plates (Richards, 1948), alundum filter discs (Tanner, Bourget and Holmes, 1954), fritted glass beads (Nielson and Phillips, 1958) and other porous materials have been used to retain the soil sample as the soil water is released under applied pressure. It has usually been assumed that the soil water

characteristic curves thus obtained are independent of the plate or membrane, provided the bubbling pressure of the porous plate or membrane is not exceeded. Jackson et al. (1965) and Hillel and Mottes (1966), however, recognized the influence of the porous plate or membrane on the soil water characteristic curve. They have also discussed the effects of wetting methods and aging on soil water retention curves. All these factors are considered reasons for the rather poor reproducibility of soil water characteristic curves.

Pore size distributions of soils are easily obtained from soil water characteristic curves (Schofield, 1939; Leamer and Lutz, 1940; Childs, 1940). The relation used to convert water release curves into pore size distribution is:

$$P = \frac{2\sigma\cos\theta}{r}, \qquad (1)$$

where P is the capillary pressure, or suction, with which water is held in the pores, r is the radius of the pore, σ is the surface tension of water, and θ is the angle of contact between water and solid. The theory of this conversion has been discussed by Klock (1968). Since the pores are very irregular in shape, the interfaces are, in general, not truly spherical. Equation (1) gives an effective or equivalent pore size.

Washburn (1921) first suggested the use of mercury intrusion

under pressure to determine the pore size distribution of porous solids. He proposed the relationship given in Equation (1) and defined r as the radius of the pore being intruded by mercury of surface tension σ, under pressure P, and at contact angle θ with the material.

Ritter and Drake (1945) published experimental data and developed a method for determining the macropore size distribution in porous solids. They applied external pressure to force mercury, a nonwetting liquid, into porous materials and measured the volume of mercury intruded as a function of pressure.

The question of which value to use for the contact angle for mercury in contact with various solids has not been established with certainty. As an average value for many materials, Ritter and Drake (1945) used 140 degrees. In an experiment designed to test the validity of the method, Juhola and Wiig (1949) forced mercury, at known pressures, into fine, calibrated glass capillaries and found a value of 140 degrees for the contact angle in two separate experiments. Winslow and Shapiro (1959) found 130 degrees to be a useful average value for the contact angle.

Purcell (1949) developed further the technique of Ritter and Drake to apply to materials having pore sizes of the magnitude found in natural rock formations. He also compared mercury capillary pressure curves (capillary pressure versus percent of total pore space

occupied by liquid) with curves obtained with water and air for various types of rock formations. A relatively close agreement between the two methods was observed over the range of porosities tested.

The advantages of the mercury injection method are that it is much faster than the standard pressure plate technique and that the range of capillary pressures is considerably greater than for the porous plate or membrane method.

The experiments to be described were conducted to compare soil water characteristic curves obtained by means of mercury intrusion with those obtained by the conventional pressure plate techniques.

Materials and Methods

Porosimeter

The mercury intrusion porosimeter is a device used to force mercury into the pores of a substance while measuring the volume of mercury taken up by pores. The principle underlying this technique is simple and was first used by Washburn in 1921. He recognized that the pressure required to force a nonwetting fluid, such as mercury, into a pore is a function of pore size as indicated by Equation (1), where σ now becomes the surface tension of mercury. Surface tension σ, and contact angle θ are constant parameters in Equation (1). Using a value of 130 degrees for the contact angle between

mercury and solid (soil) and 473 dynes/cm for the surface tension of mercury, the equation reduces to:

$$D = \frac{175}{P} , \qquad (2)$$

where D is the pore diameter in microns and P is the absolute pressure (psia).

Equipment and Procedure

The Aminco-Winslow porosimeter, model 5000 psi, shown in Figure 1, was used to determine the pore size distribution of various soil samples. This particular model has a pressure range of 0-5000 psi. The maximum possible sample pore volume determined by the penetrometer stem is 0.2 cm^3 (Figure 2). Pores, ranging from about 500 microns to 0.035 microns in diameter, and pore volumes as small as 0.001 cm^3 can be measured. Klock (1968) has described this porosimeter in detail.

Air dry soils are passed through a 2 mm sieve. The sample cup is filled with soil and then slid gently, shielded with the cupholder, into the penetrometer assembly. The penetrometer is inserted into the filling device which is evacuated to a pressure of less than 50 microns. Once this pressure is reached, the lower tip of the penetrometer is immersed in the mercury by tilting the lower end of the

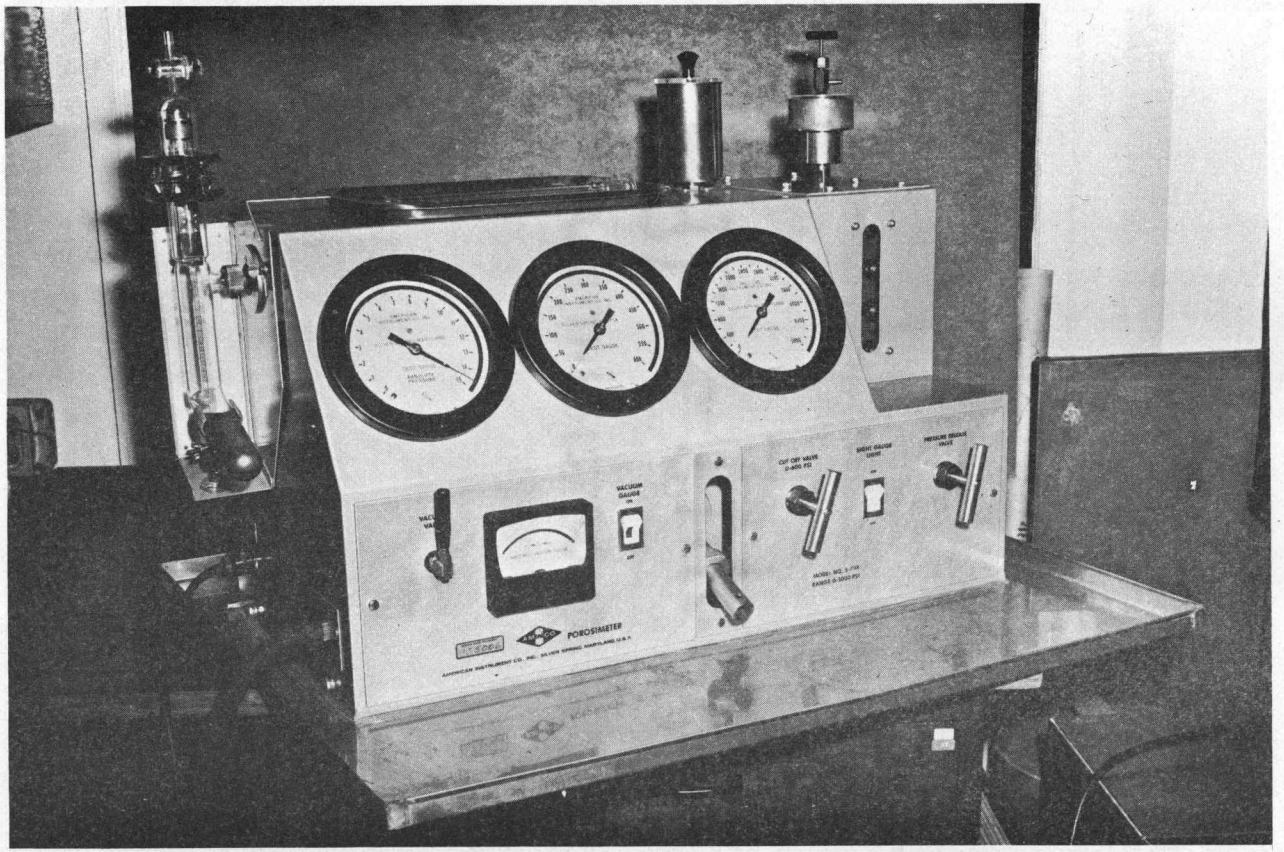

Figure 1. Front view of the mercury intrusion porosimeter.

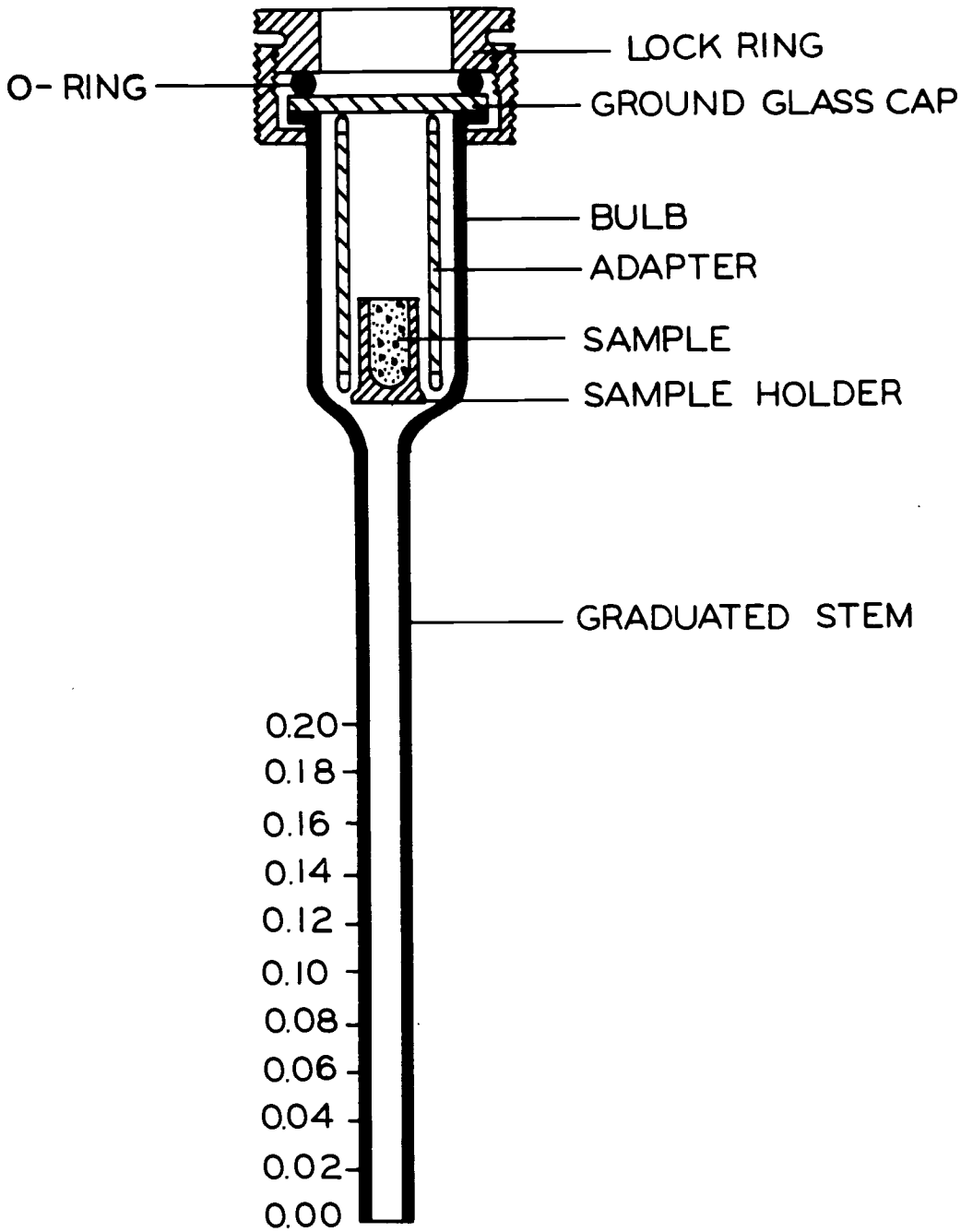

Figure 2. Mercury intrusion porosimeter penetrometer assembly.

filling chamber forward. Pressure is released into the evacuated chamber slowly by controlling the motion of a stopcock which is situated at the top of the chamber and opens into the atmosphere. Pressure is allowed to increase until it reads 6.0 psi on the 0-15 psi gauge. This initial pressure is required to fill the penetrometer with mercury. One must insure at this time that no air bubble is trapped in the penetrometer stem. The entire assembly is repositioned into the vertical position which disengages the penetrometer stem from the mercury pool and the mercury level in the graduated stem is recorded. The pressure in the chamber is then increased step by step. At each pressure, stem readings are recorded. When the pressure in the chamber reaches 14.5 psi (ambient pressure) the penetrometer assembly is transferred to the pressure vessel. Pressure is increased further, in steps, up to 5000 psi. The pressure increment for each step is determined by the rate of volume change in the penetrometer.

Calculation of Pore Aperture Size Distribution

Equation (2) allows the calculation of pore diameter as a function of absolute pressure. In order to use this equation the absolute pressure must be known. Porosimeter data are tabulated as shown in Table 1. The absolute pressure (D) applied is the difference between the applied pressure (B + C) and the Hg-head (A). Calculation for

Table 1. Pore size distribution of Quincy soil as determined by the mercury intrusion porosimeter.

Hg-Head Pressure (A)	0-15 Gage Reading (B)	Pressure Gage Reading (C)	Total Absolute Pressure (D)	Penetrometer Stem Reading (E)	Cumulative Volume (F)	Pore Diameter (G)	Percent Pore Volume (H)
psi	psi	psi	psi	cc	cc	μ	%
5.029	5.35		0.321	0.00	0.180	545.2	45.2
5.002	9.00		3.998	0.002	0.178	43.8	44.7
4.989	12.00		7.001	0.003	0.177	25.0	44.5
4.963	14.50		9.537	0.005	0.175	18.2	44.0
4.936	14.50	0.0	9.564	0.007	0.173	18.3	43.5
4.857	14.50	1.0	10.643	0.013	0.167	16.4	42.0
4.658	14.50	2.0	11.842	0.028	0.152	14.8	38.2
4.300	14.50	3.5	13.700	0.055	0.125	12.8	31.4
3.995	14.50	5.0	15.505	0.078	0.102	11.3	25.6
3.571	14.50	7.5	18.429	0.110	0.070	9.54	17.6
3.492	14.50	10.0	21.008	0.116	0.064	8.37	16.1
3.200	14.50	20.0	31.300	0.138	0.042	5.68	10.5
2.988	14.50	50.0	61.502	0.154	0.026	2.85	6.5
2.869	14.50	150.0	161.631	0.163	0.017	1.08	4.3
2.790	14.50	400.0	411.710	0.169	0.011	0.425	2.8
2.710	14.50	1200.0	1211.790	0.175	0.005	0.144	1.3
2.670	14.50	2500.0	2511.830	0.178	0.002	0.070	0.5
2.644	14.50	3900.0	3911.856	0.180	0.000	0.044	0.0
2.644	14.50	5000.0	5011.856	0.180	0.000	0.035	0.0

converting mercury head to pressure units at any stem reading are given in Appendix I and are tabulated as shown in Table 2. Column E, the penetrometer reading in cm^3, indicates volumes of pores filled with mercury. Column (F) is derived from column (E) and each value in this column is obtained by subtracting the stem reading at any pressure P from the stem reading at 5000 psi. It indicates the cumulative volume of the pores smaller in diameter than the corresponding pore diameter in column (G). Column (H) shows the pore volume expressed in percent.

Table 2. Pressure correction for hanging mercury column in penetrometer.

Penetrometer Reading	Pressure Correction
cm^3	psi
0.00	5.029
0.02	4.764
0.04	4.499
0.06	4.234
0.08	3.969
0.10	3.704
0.12	3.439
0.14	3.174
0.16	2.909
0.18	2.644
0.20	2.379

Soil Water Characteristic Curves as Derived from Porosimeter Data

Table 3 shows how the soil water characteristic curve is

obtained from porosimeter data. Columns (D) and (F) are the same as presented in Table 1. Column (I) represents the effective pore diameter which is obtained by multiplying the pore diameter calculated with Equation (2) (Column (G), Table 1) by a factor of 1.31. This correction was suggested by Klock, Boersma, DeBacker (1969). When trying to predict permeabilities of porous media based on pore size distributions obtained with the mercury intrusion porosimeter, they found that the results obtained from the porosimeter needed this correction. Column (H) indicates the percent pore space smaller than the indicated pore diameter calculated as follows:

$$\text{Percent pore space} = \frac{\text{cumulative pore volume (F)}}{\text{volume of the cup}} \times 100. \quad (3)$$

Results and Discussion

Soil water characteristics curves obtained with the pressure plate and the pressure membrane apparatus for eight soils are shown in Figures 3 through 10. Pore size distribution data for the same soils were obtained with the mercury intrusion method. Results calculated according to the procedure shown in Table 1 are shown in Figures 11 through 18. The data obtained from the pressure plate and the pressure membrane apparatus were also plotted in these Figures. Percent sand, silt and clay of the soils determined by the hydrometer method is shown in Table 4.

Table 3. Water retention characteristics of Quincy soil as calculated from porosimeter data.

Absolute Total Pressure (D)	Absolute Total Pressure or Suction (M)	Cumulative Pore Volume (F)	Percent Water by Volume (H)	Pore Diameter (I)
psi	bars	cc	%	μ
0.321	0.022	0.180	45.2	714.2
3.998	0.276	0.178	44.7	57.4
7.001	0.483	0.177	44.5	32.7
9.537	0.658	0.175	44.0	24.0
9.564	0.660	0.173	43.5	24.0
10.643	0.734	0.167	42.0	21.5
11.842	0.817	0.152	38.2	19.4
13.700	0.945	0.125	31.4	16.8
15.505	1.069	0.102	25.6	14.8
18.429	1.271	0.070	17.6	12.5
21.008	1.449	0.064	16.1	11.0
31.300	2.159	0.042	10.6	7.44
61.502	4.242	0.026	6.5	3.73
161.631	11.15	0.017	4.3	1.41
411.710	28.39	0.011	2.8	0.557
1211.790	83.57	0.005	1.3	0.189
2511.830	173.2	0.002	0.5	0.092
3911.856	269.8	0.000	0.0	0.058
5011.856	345.6	0.000	0.0	0.046

Table 4. Mechanical analysis of the soils used as obtained with the hydrometer method.

Soil	Percent			Textural Class
	Sand	Silt	Clay	
Sand II	100	0	0	Sand
Quincy	90	6	4	Sand
Ephrata	84	11	5	Loamy sand
Cloquato	43	37	20	Loam
Woodburn	19	50	31	Silty clay loam
Dayton	18	46	36	Silty clay loam
Chehalis	16	47	37	Silty clay loam
Kenutchen	20	23	57	Clay

Examination of Figures 11 through 18 indicates that the pore size distribution curves obtained by the two methods agree well for soils with a low clay content. As the clay content increases the curves obtained by the two methods show similar trends but do not coincide. They can be made to coincide by transposing the curves obtained by the mercury intrusion method to the right. This transposition, the results of which are shown in Figures 19 through 26, implies the addition of a constant pore volume to the results obtained by mercury intrusion. The pore volume to be added increases as the clay content of the soil increases. Figure 27 shows the amount of pore space added as a function of the clay content of the soil. The diagram suggests that the mercury intrusion method according to the procedure used underestimates the pore volume by a constant amount which is a linear function of the clay content. The required correction is given by the equation:

$$\text{Percent pore volume correction} = 2.189 + 0.403 \times \%\ \text{clay}. \quad (4)$$

Sources of Disagreement Between Methods

1. The major disagreement between the pore size distribution curves obtained by the two methods is the result of the computational procedures used. The curve based on the mercury intrusion data was constructed by arbitrarily setting the

pore volume at the maximum pressure reached equal to zero. At this point a certain pore volume was not penetrated by the mercury. The procedure presented does not allow an estimate of this volume. The total pore volume is known since a known weight of soil is contained in a known volume. But the amount of mercury entering the large pores when the penetrometer is initially filled with mercury is not known. This leaves the two end points of the pore size distribution obtained by the mercury intrusion porosimeter undetermined. The pore volume ignored by setting the volume at the maximum pressure reached equal to zero is, according to Figure 27, closely correlated to the clay content. The point of maximum pressure may be chosen to correspond to a suction of 15 bars. The actual position, therefore, can be obtained by using the relation between clay content and pore volume at a suction of 15 bars. A correlation similar to the one shown in Figure 27 was reported by Lund (1959) and Stakman (1969). The latter report points out that the correlation which exists between water content at a suction of 15 bars and clay content on the one hand and between this water content and the total surface area of clay particles on the other hand indicates that at these low water contents the retention of water depends on the active surface area of the particles. The

coverage of this surface with exchangeable cations which can be hydrated further influences the amount of water retained.

The correlation between clay content and cations adsorbed and water content at 15 bars may therefore be expected to vary from region to region. Figure 28 shows this correlation for various regions. The relationship shown in Figure 27 has been replotted in Figure 28. The correlation for Willamette Valley soils (curve 6) corresponds closely to that for the river deposited clay found in the Netherlands (curve 5). This may logically be expected. The climatic conditions in the two regions are similar, the agricultural use in the two regions is similar and circumstances under which the soils were formed were probably similar.

Texture is one of the criteria used as family differentiation in the Comprehensive System of Soil Classification. A strong relationship is considered to exist between clay content and percent water content at 15 bars suction. In soils that do not disperse well, clay content used is the higher of either measured clay, or 2.5 times the 15-bar moisture percentage, if one-half or more of the control section has a 15-bar moisture to clay ratio of 0.6 or more (U.S. Soil Conservation Service, 1967).

2. A further cause for discrepancy between the two methods may be that the curves obtained with the pressure plate and the pressure membrane apparatus are desaturation curves, whereas the curves obtained with the porosimeter are imbibition curves. Since the voids in soils are very irregular in shape, the desaturation suction is determined by the largest effective radius of the connecting channels of pores, whereas the criterion governing sorption by the voids is the maximum diameter of the void itself. It implies that at any suction the amount of water retained in a soil will be greater when approached in the desaturation process rather than in the saturation process. Since a clayey soil tends to have a wider range of pore sizes than a sandy soil, the hysteresis effect is more pronounced in fine textured soils.
3. The nature of the fluid is another factor that contributes to the discrepancy. Water, unlike mercury, is a polar compound and is adsorbed on the surface of the solid particles. In soils that contain clays such as montmorillonite, adsorption and desorption of water results in swelling and shrinking of soils and hence a continuous change in the pore size distribution. The results obtained from the Kenutchen soil that contains montmorillonitic type clays demonstrate this. The two curves in Figure 26 do not coincide, even after

transposition.

4. The validity of Equation (1) should also be considered. The equation has three variables--pressure, contact angle, and surface tension--and a constant factor of two. The pressure applied is measured easily and accurately. The surface tension of mercury has been thoroughly measured and is given in handbooks (Weast, 1964). This value should not be expected to change with pressure within the range of pressures applied. The question of an appropriate contact angle is more complicated. There is an apparent lack of measurements of the contact angle of mercury in soils. The constant two is developed from the geometry of a capillary tube with one radius of curvature. Use of this equation assumes that the connecting pores have the same geometry as capillary tubes. In soils, however, this is not true. It is quite possible that the pore shape factor must be considered in an evaluation of the constant.
5. Discrepancies can also arise from a difference in the bulk density of the samples in the porosimeter and the standard method. The penetrometer containing the sample is subjected to a vacuum and the subsequent contact with mercury under pressure may result in a change in bulk density of the sample. The discrepancy noted between the two curves for

the Quincy and Ephrata soils for the large pores (> 10μ, Figures 20 and 21) was associated with bulk density differences. The total pore space of these two soils was about 5 percent greater in the penetrometer sample. The pore volume represented by this 5 percent was mostly made up of pores with a diameter around 20 microns. These spaces represent the largest pores of the group which occupies most of the pore space. These are the pores which would indeed be expected to fill first with solid material if a denser packing were obtained, as was the case with the packed cores used in the pressure plate procedure.

Conclusions

The importance of soil water characteristic curves in the understanding of soil-plant-water relationships necessitates their precise determination. The validity of these curves determined by the standard methods involving the use of the porous plate and porous membrane has been questioned (Hillel and Mottes, 1966). In the present investigation, the results obtained by the porosimeter technique are compared with those of the standard techniques. Figures 11 through 18 indicate that the pore size distribution curves for various soil samples determined by the porosimeter method are very reproducible. These curves, after correction, when superimposed on the curves

obtained by the standard technqiue tend to coincide except near the saturation point, as shown in Figures 18 through 25. For each set of curves, in these Figures, this agreement extends from a suction of 0.02-15.0 bars, a range of soil water suction which determines available water in soils for plant growth.

The disagreement between the pore size distribution curve determined by the mercury intrusion method on the one hand and the pressure plate method on the other hand is considered to be entirely due to the computational procedure used, except for those curves where differences in bulk density occur. In this procedure the pore volume at the maximum pressure reached was arbitrarily set equal to zero. The required correction allows for this pore volume ignored in the analysis of the porosimeter data. It is closely correlated with the clay content of the soil as was demonstrated for the soils used in these experiments. The correlation was further substantiated with literature data.

Several additional causes for the discrepancy between porosimeter data and pressure plate results were suggested. Errors introduced from these causes are considered to be small.

The results presented in Figures 11 through 27, therefore, show that the mercury intrusion porosimeter can be used in determining the soil water characteristic curves. Further, this technique being a great deal faster has an advantage over the standard methods.

The use of porosimeter, however, is questionable for soils that contain montmorillonitic type clays (Figure 26).

A procedure to construct a soil water characteristic curve with the mercury intrusion porosimeter is given below:

1. Pass air dry soil through a 2 mm sieve. Fill a sample cup of known volume with the soil. To ensure a constant bulk density in each replication, tap the sample cups an equal number of times.
2. Place the cup containing the sample in the penetrometer bulb. Seal the top of the penetrometer assembly. Insert the penetrometer assembly into the filling chamber. Be sure the mercury level in the chamber is sufficient. Evacuate the chamber to a pressure of 50 microns.
3. Follow the procedure given in the "Equipment and Procedure" section and obtain penetrometer stem readings as a function of applied pressure. Using Equation (2) calculate the pore aperture size distribution of the soil from the above data as shown in Table 1.
4. Take 50 grams of air dry soil and determine its clay content with the hydrometer method.
5. Read the corresponding correction factor for the pore volume from Figure 27. To get the corrected pore volume, add this factor to column (H) of Table 3. In order to obtain the

effective diameter, multiply the results from the mercury intrusion procedure, column (G), Table 1, by a factor of 1.31.

6. Convert the effective pore diameter to soil water suction using Equation (1) where σ is surface tension of water and θ is the angle of contact between soil solid and water. Plot soil water suction versus pore volume (Figures 19 through 26).

Epilogue

Upon conclusion of the analysis of the porosimeter results it was realized that a more complete procedure for obtaining the curves shown in Figures 19 through 26 can be established. The porosimeter can be calibrated so that the total amount of mercury intruded in the sample is known. This would solve the major problem associated with the porosimeter procedure as discussed under "Sources of Disagreement Between Methods."

The calibration procedure would be carried out as follows: (1) replace the glass cup used to retain the sample (Figure 2) with a replica in which the sample space is also filled with a solid, (2) fill the penetrometer with mercury according to the usual procedure, (3) weigh the complete assembly, (4) repeat the same weighing after completion of the intrusion procedure, (5) make adjustments in the

last weighing to allow for differences in the mercury level of the penetrometer stem. The difference in the adjusted weighings divided by the specific weight of mercury is the total sample volume intruded by mercury. This volume subtracted from the total pore volume of the sample known from its bulk density establishes the endpoint of the pore size distribution curve.

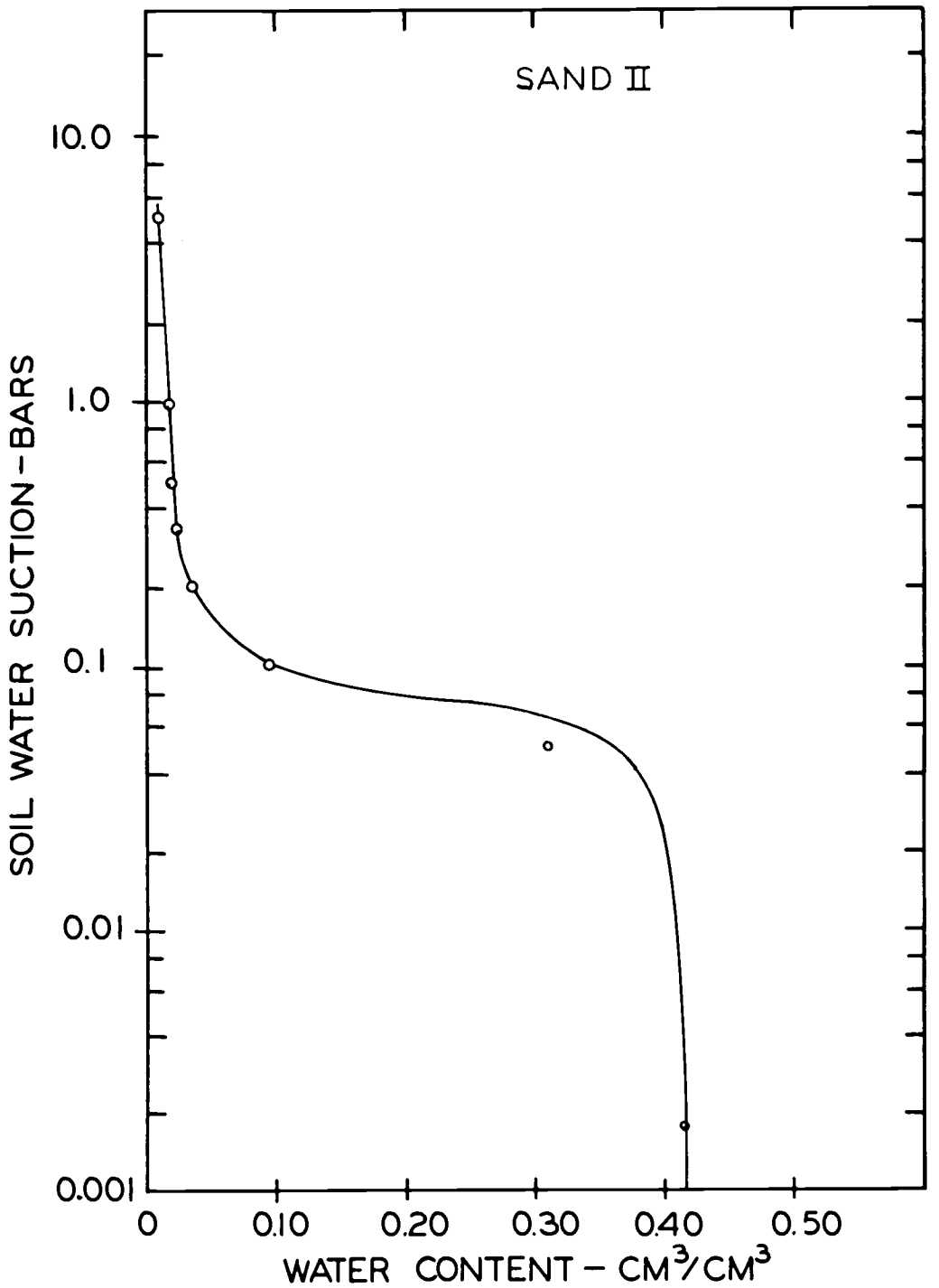

Figure 3. Soil water characteristic curve for Sand II. The data points shown were obtained with the pressure plate and the pressure membrane techniques. Packed cores were used for the measurements at suction less than 6 bars and loose samples were used for the measurements at higher suctions.

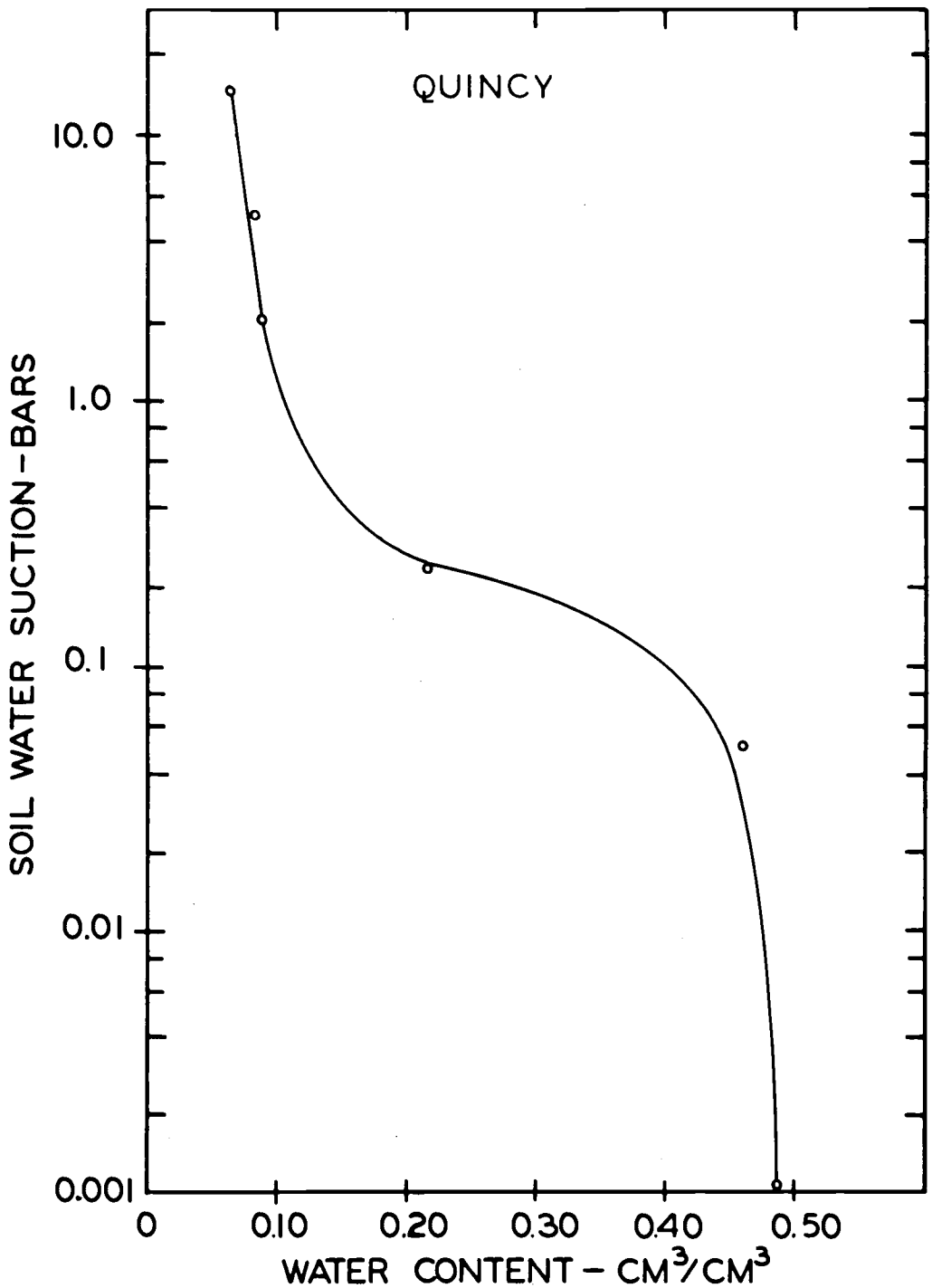

Figure 4. Soil water characteristic curve for Quincy soil. The data points shown were obtained with the pressure plate and the pressure membrane techniques. Packed cores were used for the measurements at suctions less than 6 bars and loose samples were used for the measurements at higher suctions.

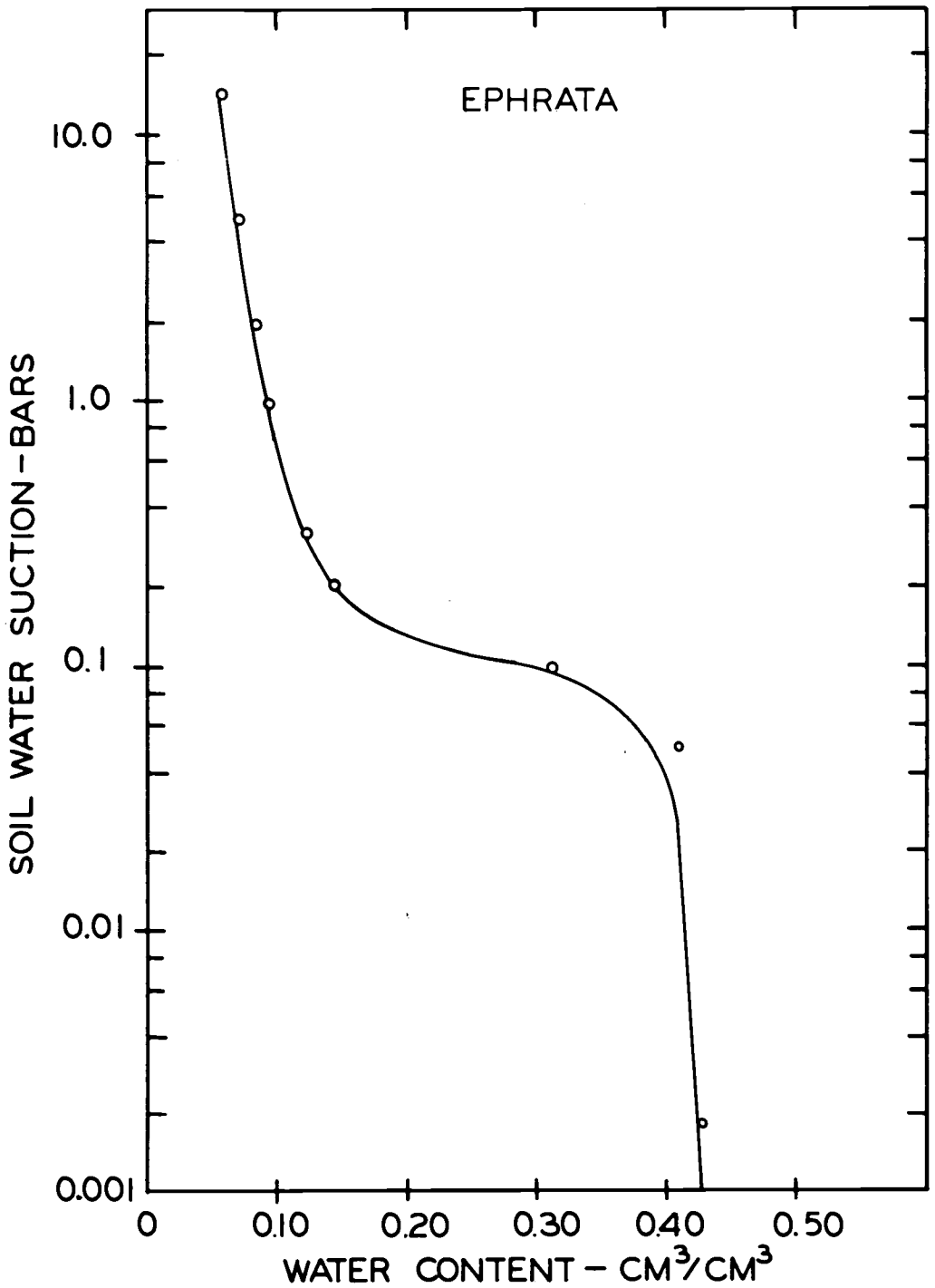

Figure 5. Soil water characteristic curve for Ephrata soil. The data points shown were obtained with the pressure plate and the pressure membrane techniques. Packed cores were used for the measurements at suctions less than 6 bars and loose samples were used for the measurements at higher suctions.

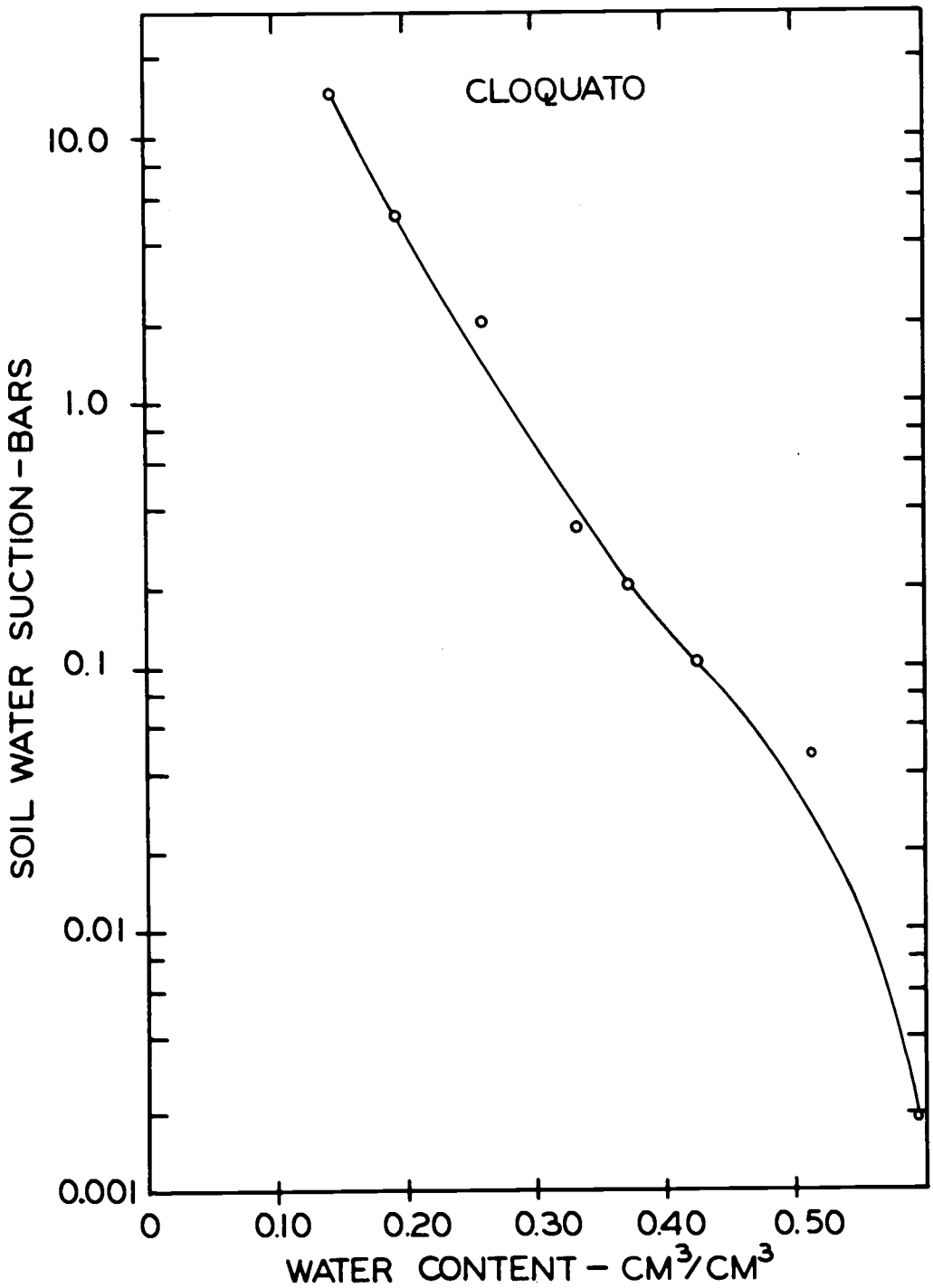

Figure 6. Soil water characteristic curve for Cloquato soil. The data points shown were obtained with the pressure plate and the pressure membrane techniques. Packed cores were used for the measurements at suctions less than 6 bars and loose samples were used for the measurements at higher suctions.

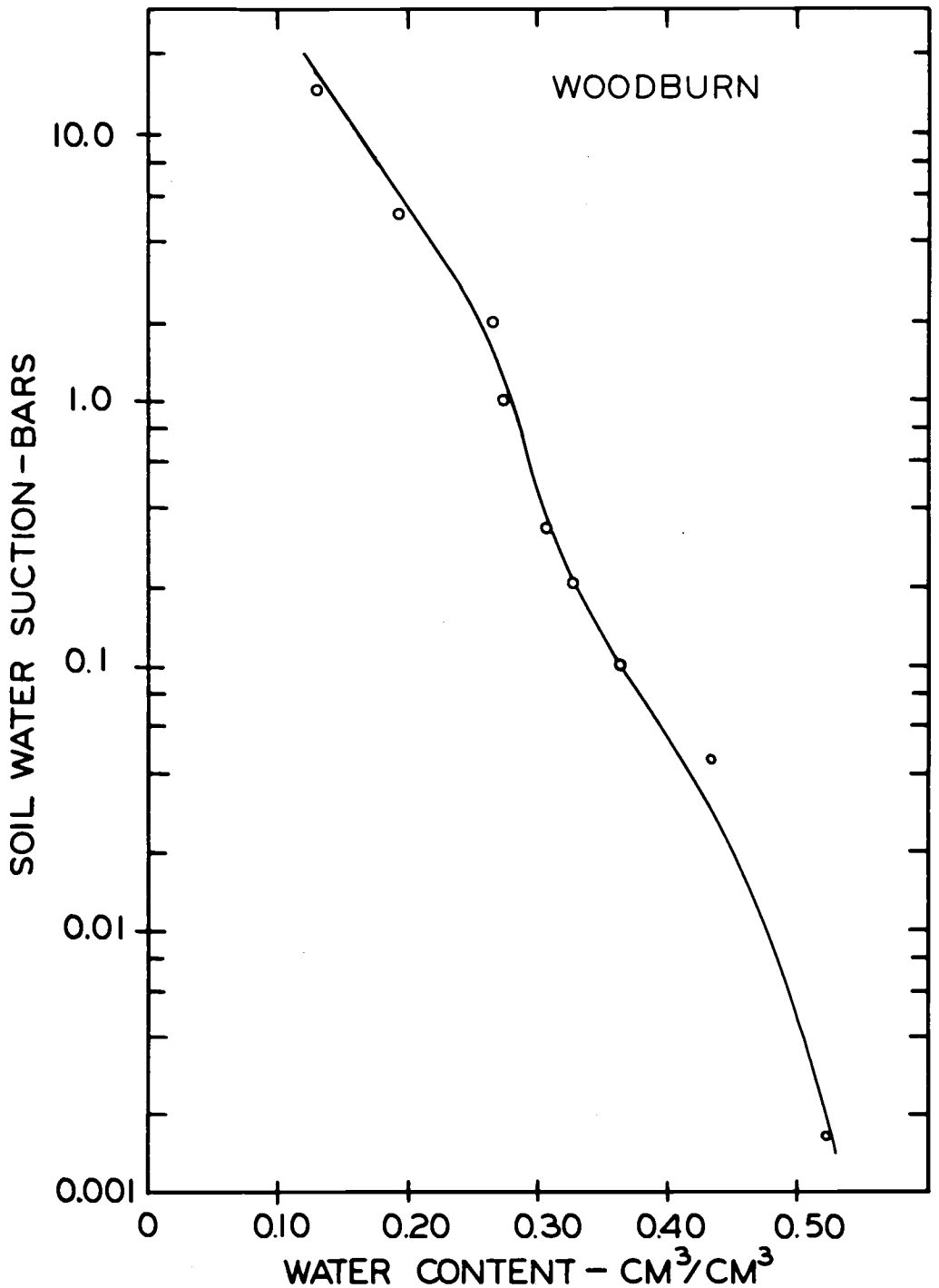

Figure 7. Soil water characteristic curve for Woodburn soil. The data points shown were obtained with the pressure plate and the pressure membrane techniques. Packed cores were used for the measurements at suctions less than 6 bars and loose samples were used for the measurements at higher suctions.

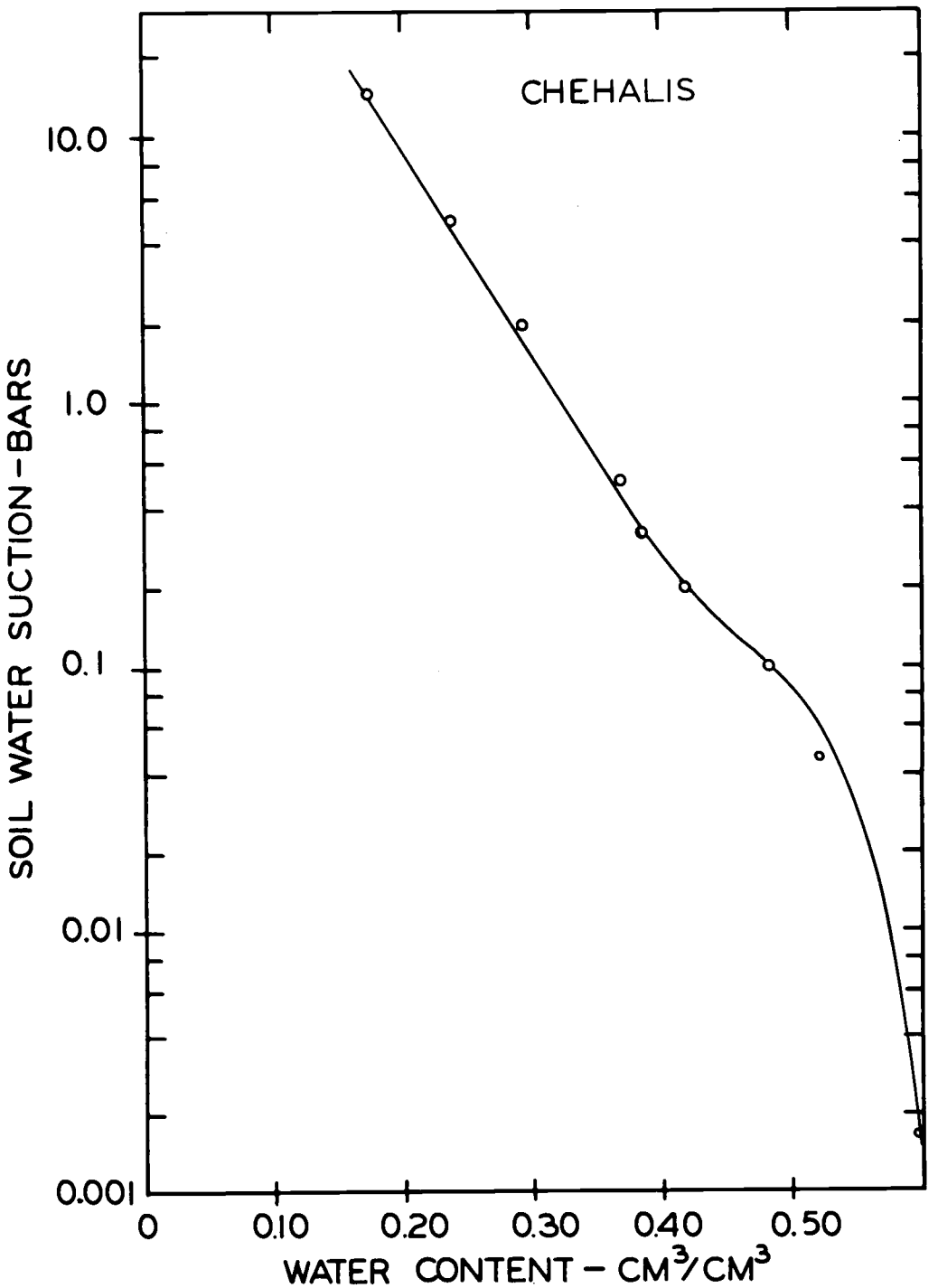

Figure 8. Soil water characteristic curve for Chehalis soil. The data points shown were obtained with the pressure plate and the pressure membrane techniques. Packed cores were used for the measurements at suctions less than 6 bars and loose samples were used for the measurements at higher suctions.

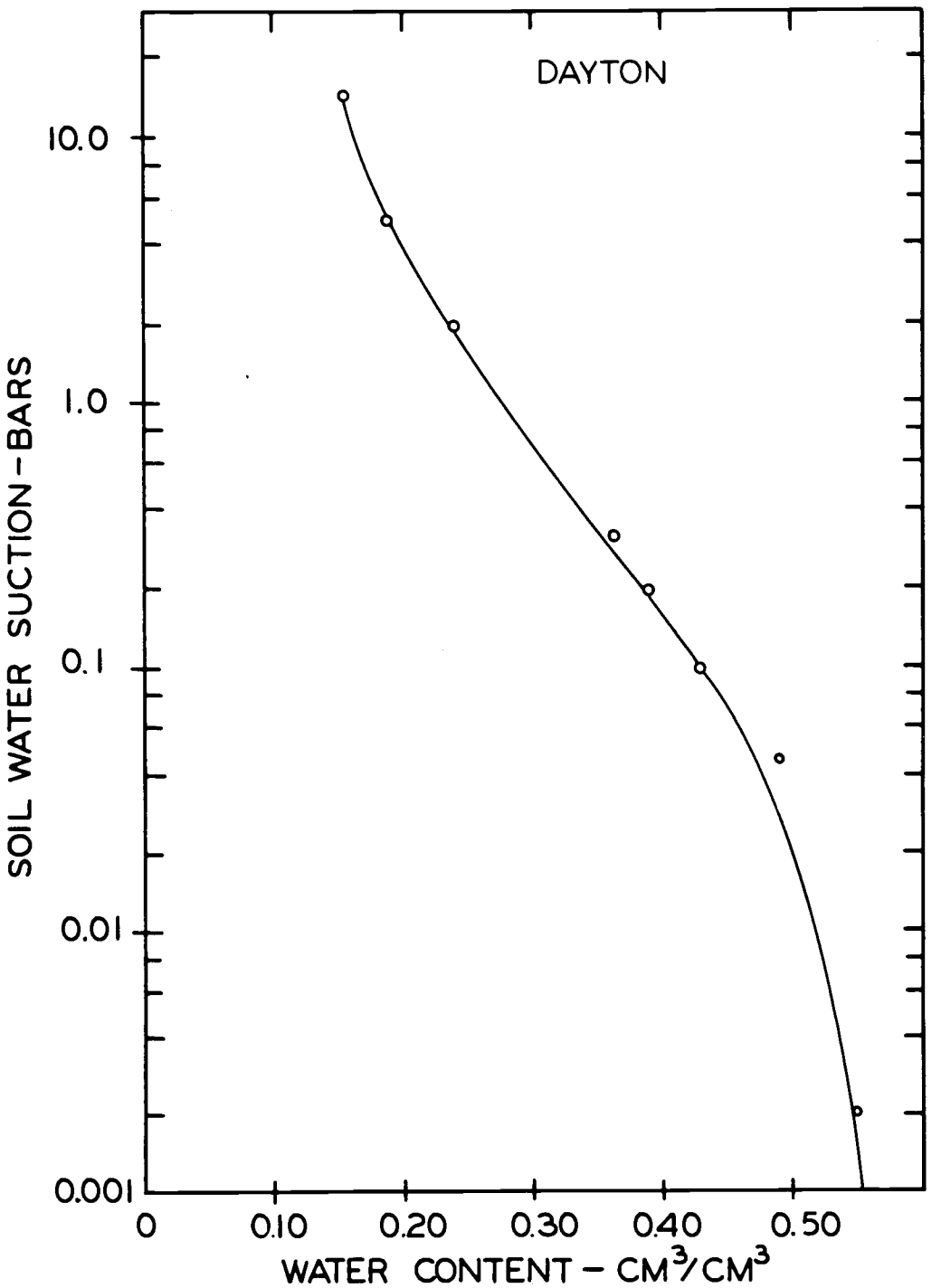

Figure 9. Soil water characteristic curve for Dayton soil. The data points shown were obtained with the pressure plate and the pressure membrane techniques. Packed cores were used for the measurements at suctions less than 6 bars and loose samples were used for the measurements at higher suctions.

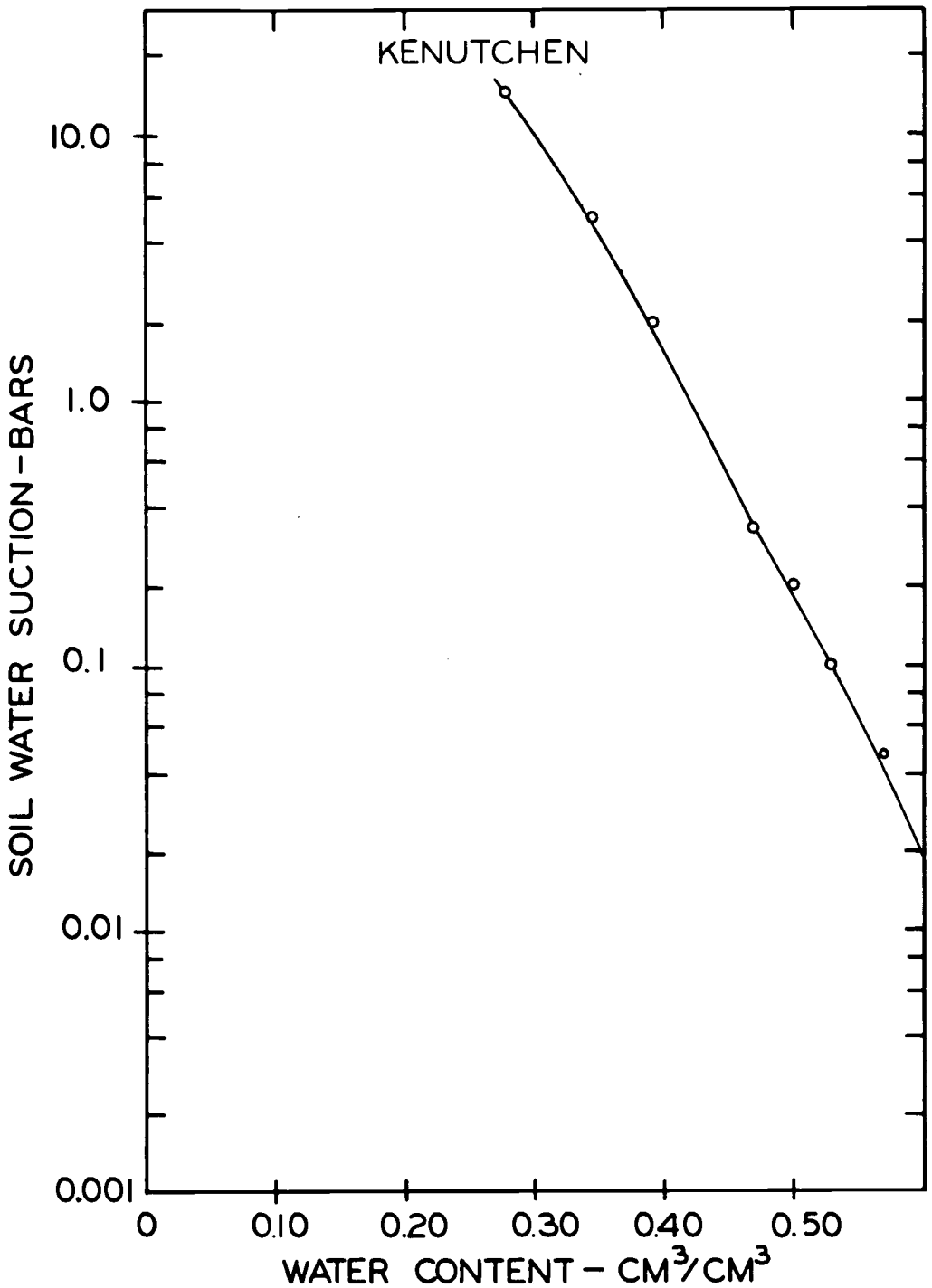

Figure 10. Soil water characteristic curve for Kenutchen soil. The data points shown were obtained with the pressure plate and the pressure membrane techniques. Packed cores were used for the measurements at suctions less than 6 bars and loose samples were used for the measurements at higher suctions.

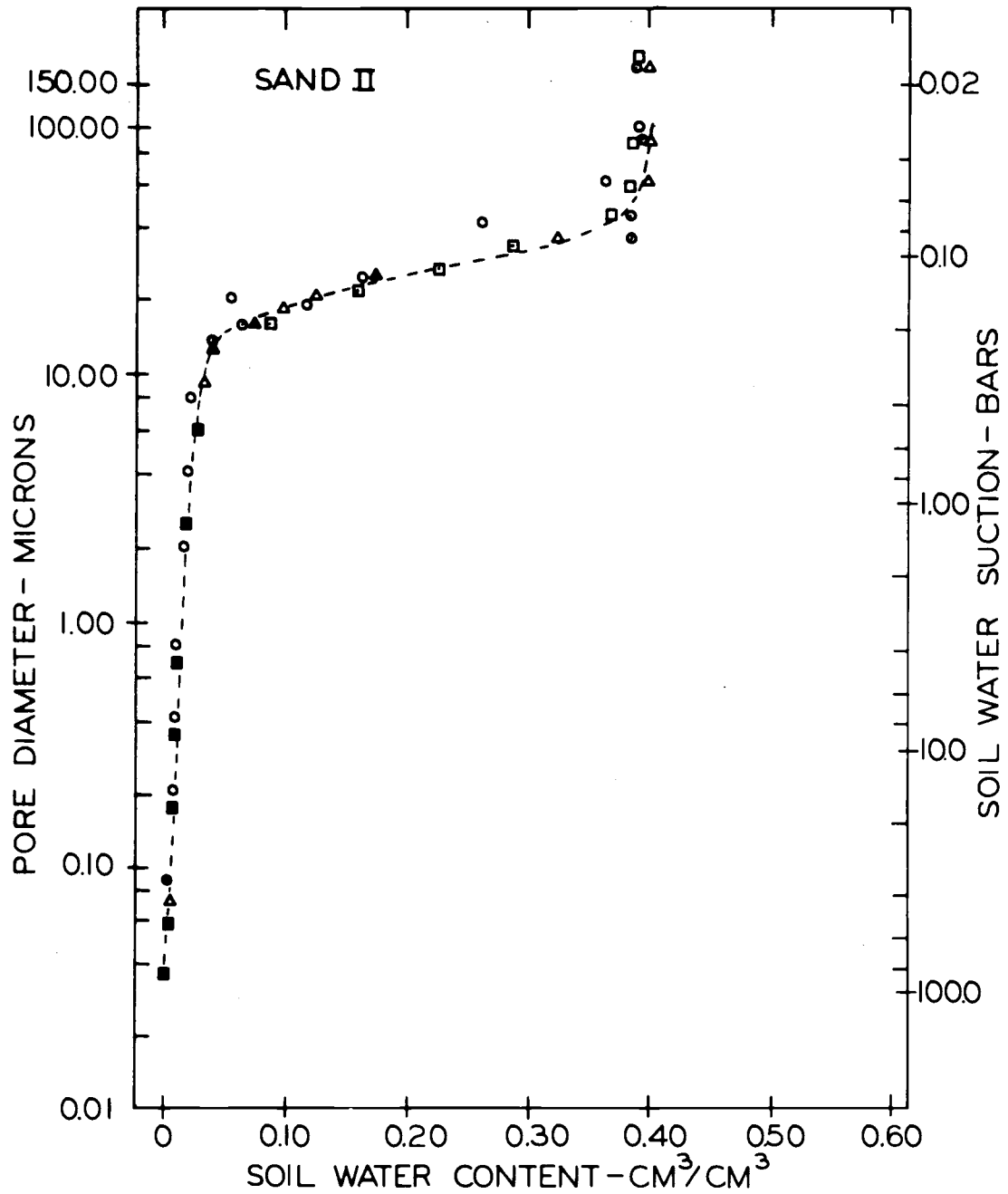

Figure 11. Pore size distribution curves determined by mercury intrusion (● , ■ , and △) and by the pressure plate apparatus (O). The data obtained by mercury intrusion represent three samples showing the reproducibility of this technique.

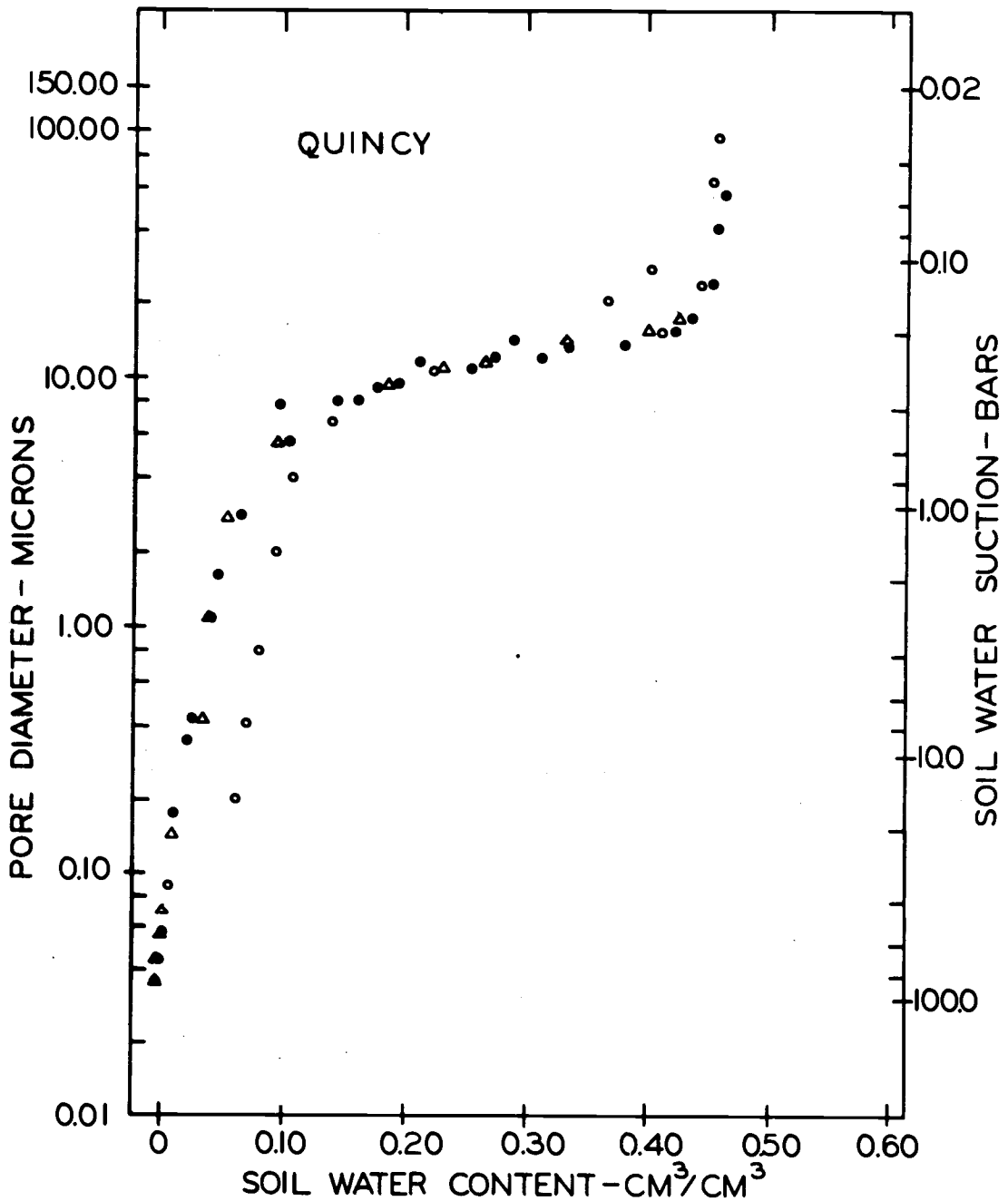

Figure 12. Pore size distribution curves determined by mercury intrusion (●, △) and by the pressure plate apparatus (○). The data obtained by mercury intrusion represent two samples showing the reproducibility of this technique.

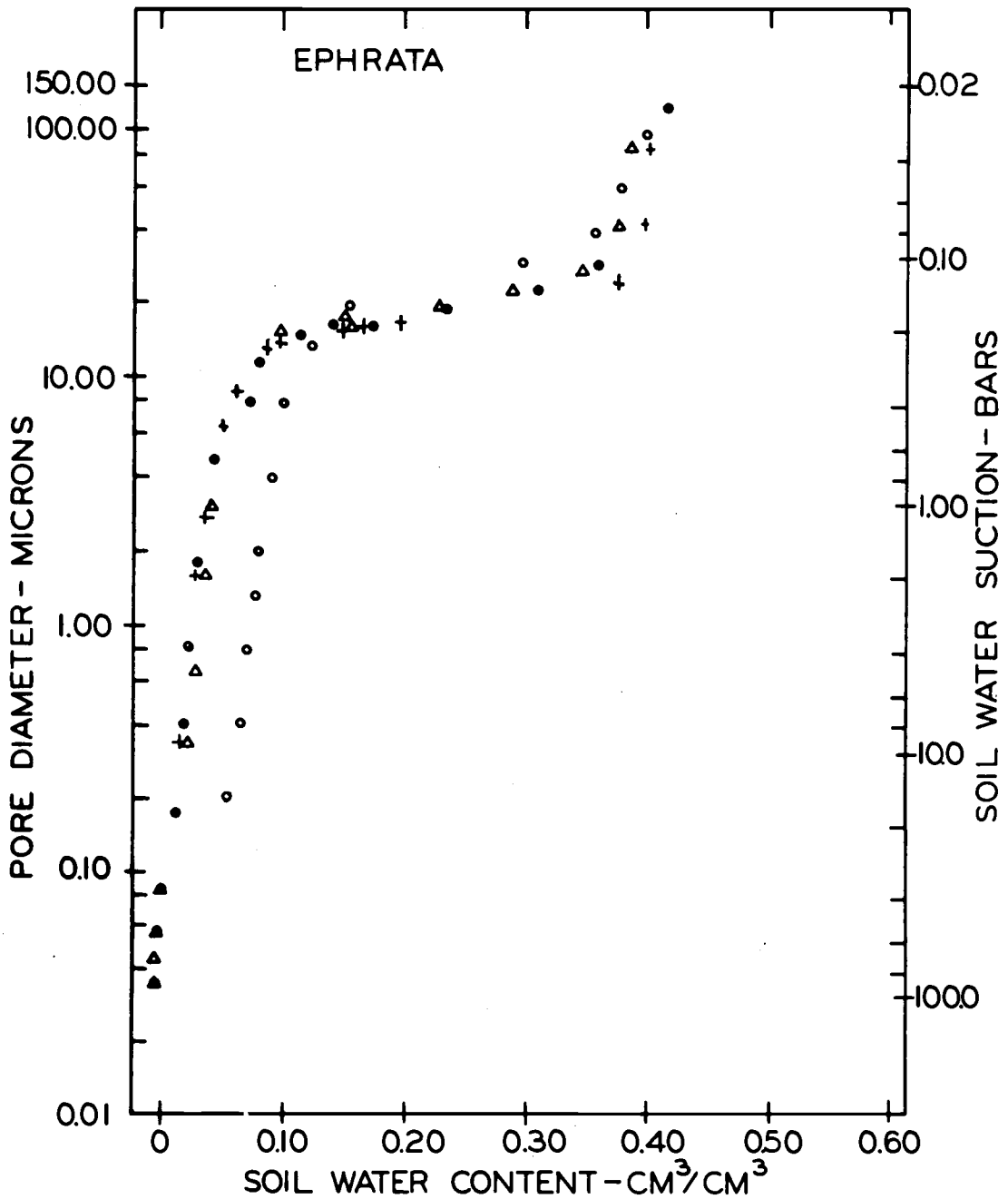

Figure 13. Pore size distribution curves determined by mercury intrusion (●, △, and +) and by the pressure plate apparatus (○). The data obtained by mercury intrusion represent three samples showing the reproducibility of this technique.

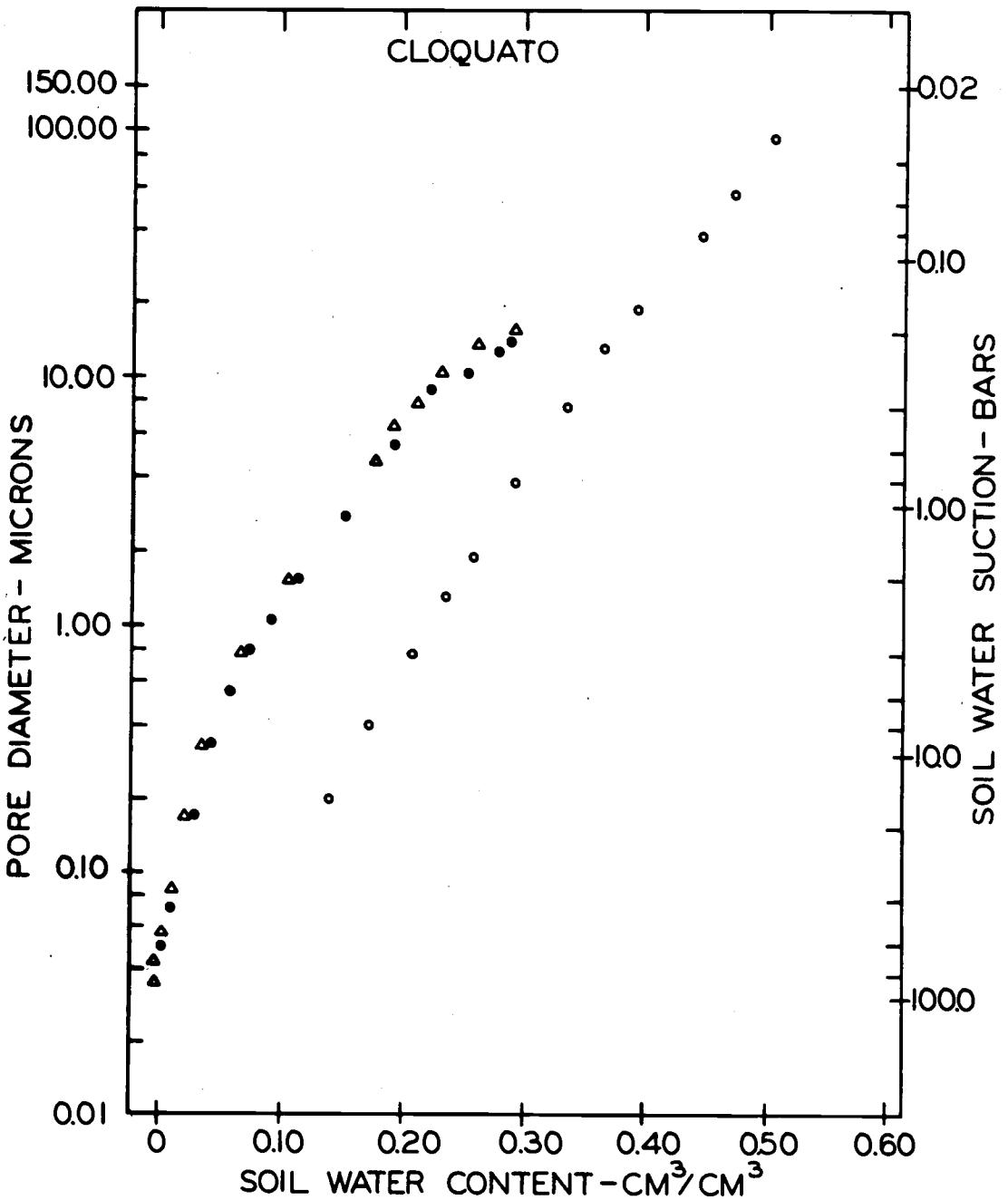

Figure 14. Pore size distribution curves determined by mercury intrusion (●, △) and by the pressure plate apparatus (○). The data obtained by mercury intrusion represent two samples showing the reproducibility of this technique.

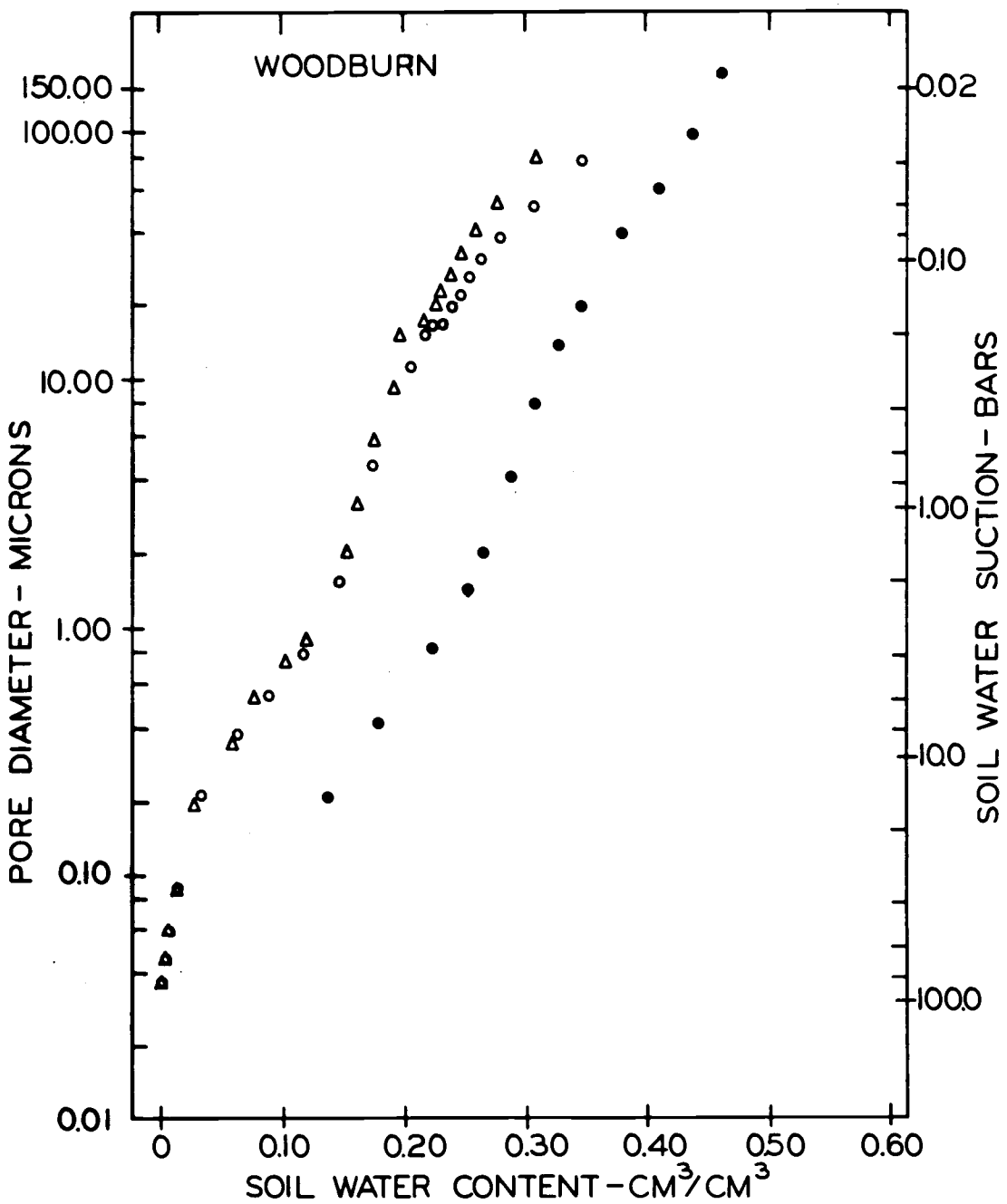

Figure 15. Pore size distribution curves determined by mercury intrusion (○, △) and by the pressure plate apparatus (●). The data obtained by mercury intrusion represent two samples showing the reproducibility of this technique.

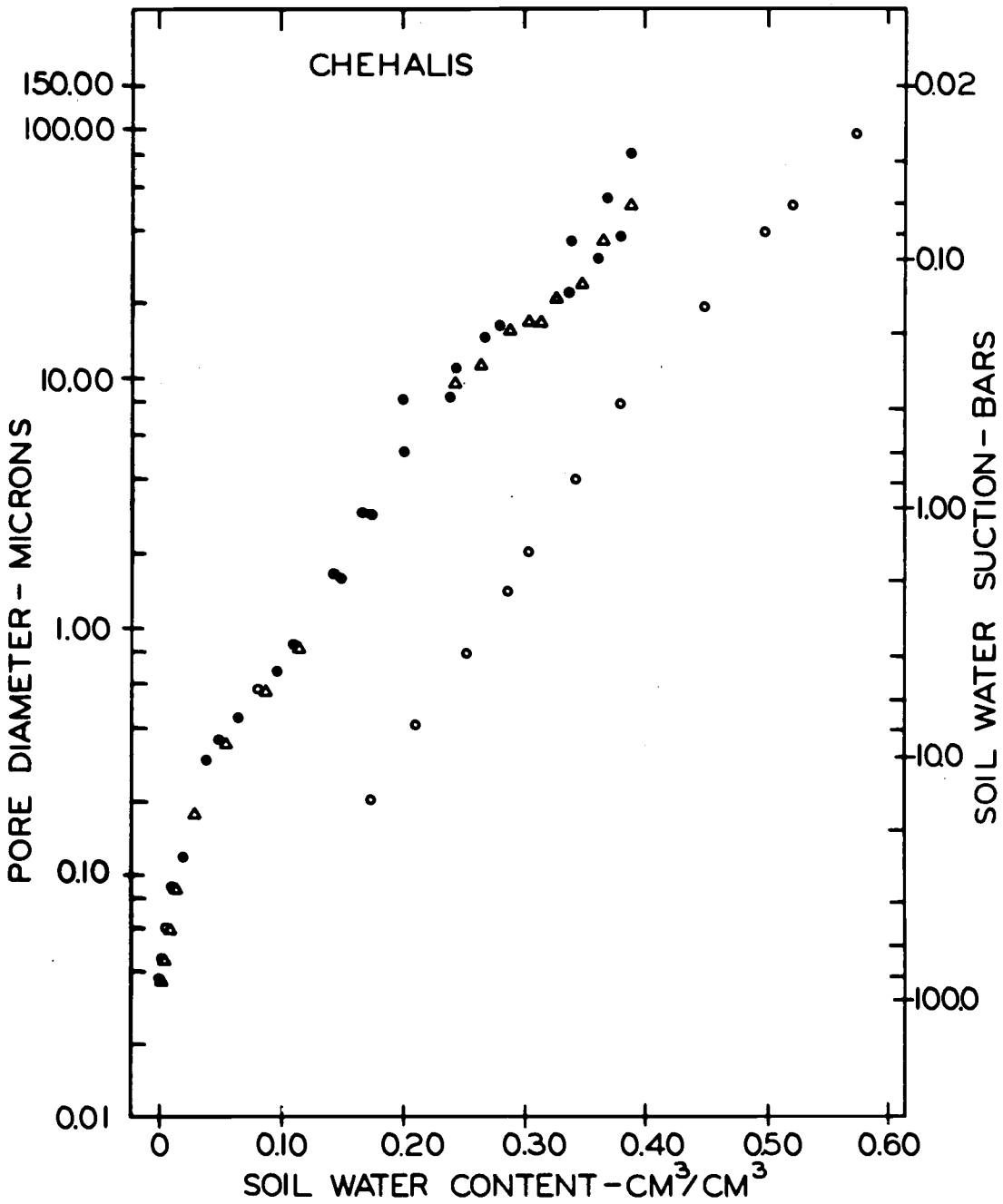

Figure 16. Pore size distribution curves determined by mercury intrusion (● , △) and by the pressure plate apparatus (O). The data obtained by mercury intrusion represent two samples showing the reproducibility of this technique.

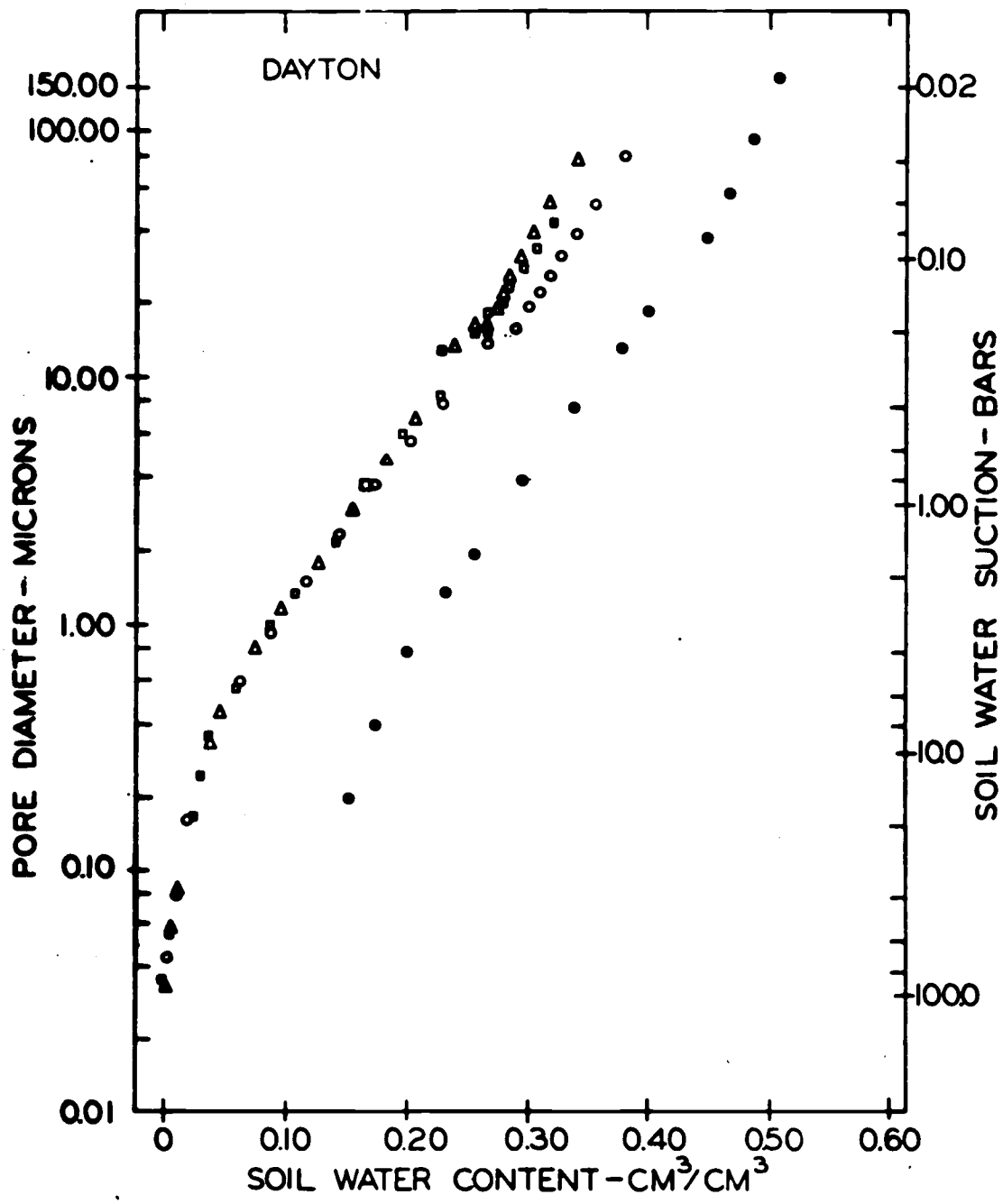

Figure 17. Pore size distribution curves determined by mercury intrusion (○ , □ , and △) and by the pressure plate apparatus (●). The data obtained by mercury intrusion represent three samples showing the reproducibility of this technique.

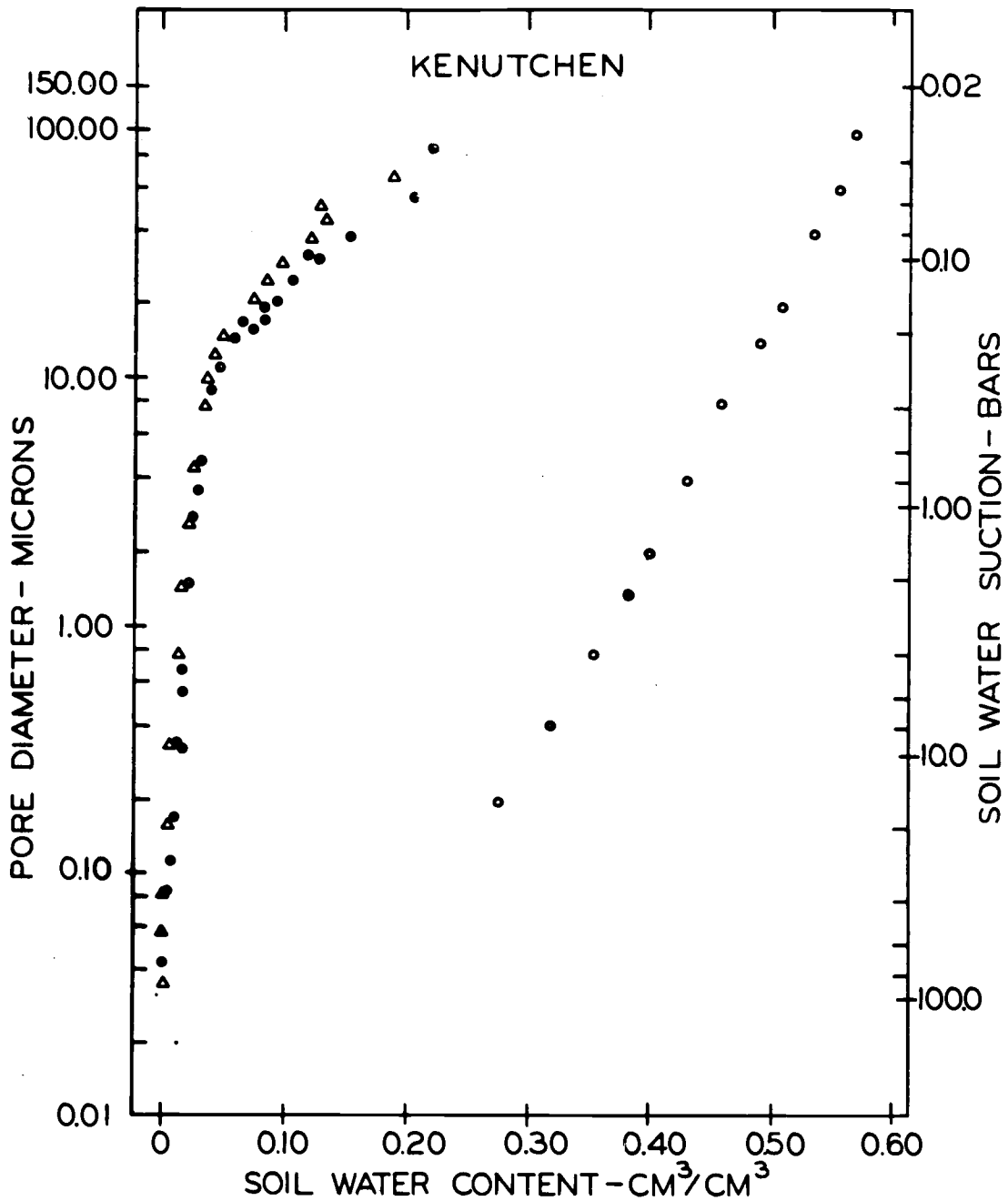

Figure 18. Pore size distribution curves determined by mercury intrusion (● , △) and by the pressure plate apparatus (O). The data obtained by mercury intrusion represent two samples showing the reproducibility of this technique.

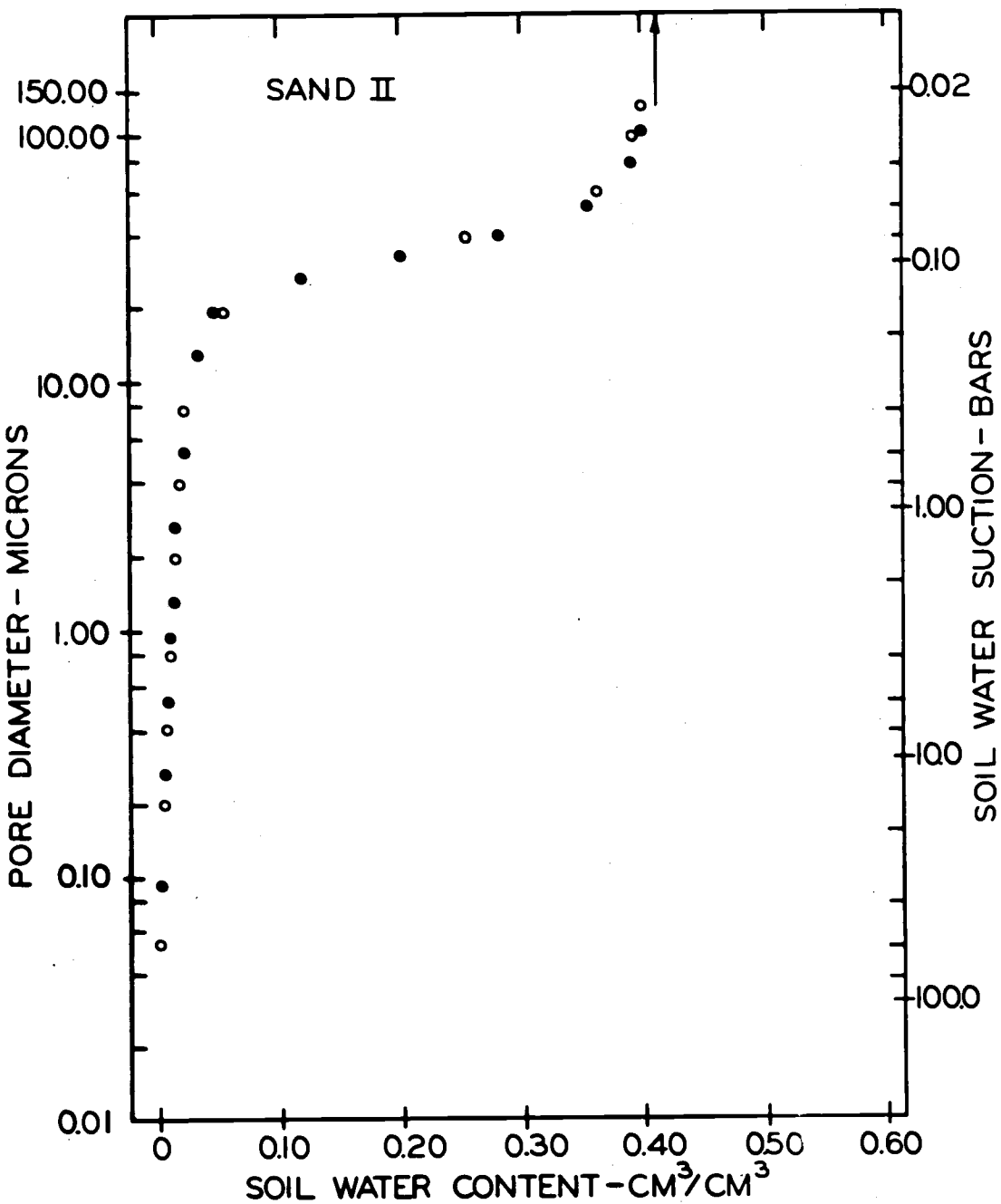

Figure 19. Pore size distribution curves determined by the mercury intrusion porosimeter (●), after correction, and by the pressure plate and the pressure membrane apparatus (○).

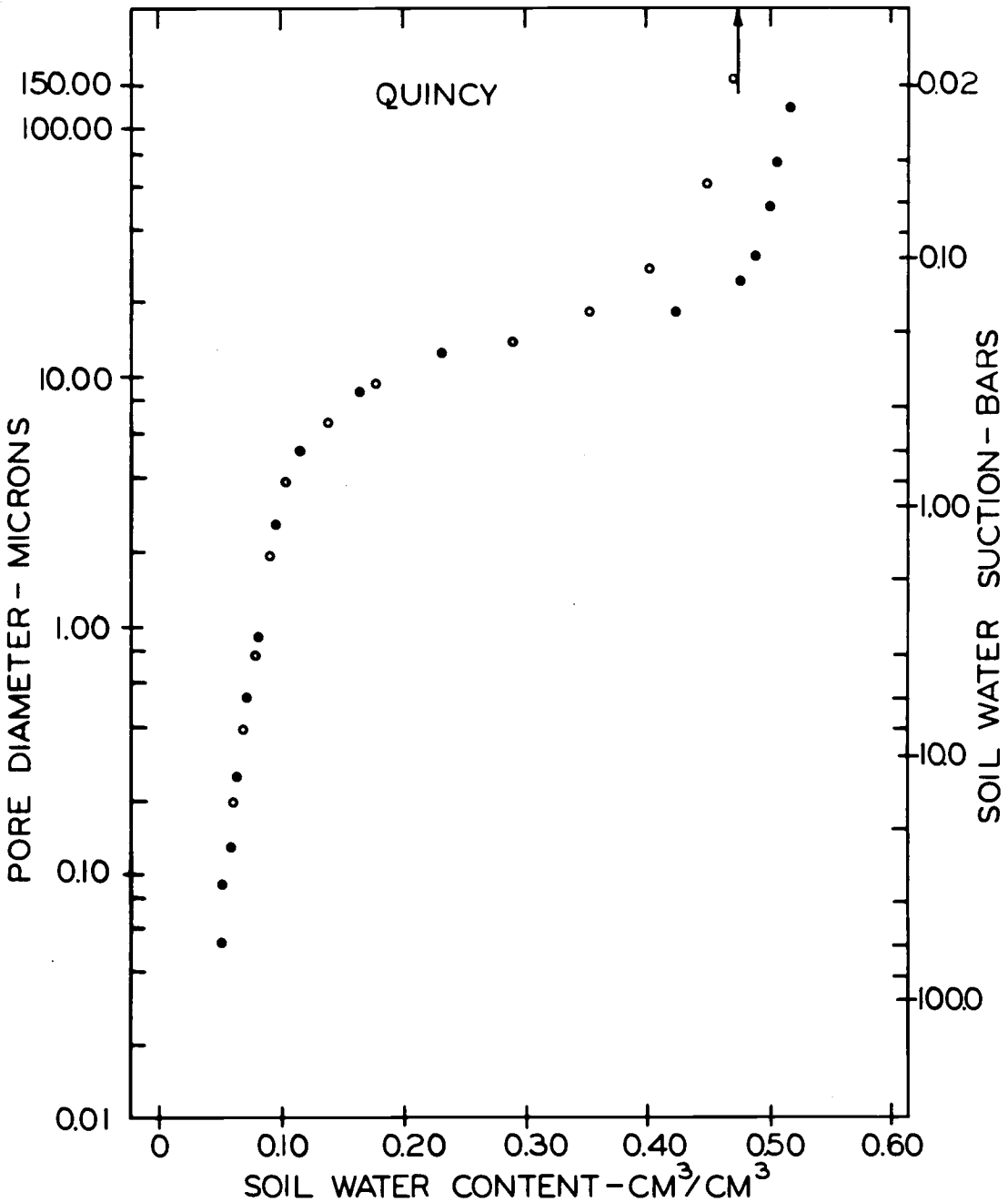

Figure 20. Pore size distribution curves determined by the mercury intrusion porosimeter (●), after correction, and by the pressure plate and the pressure membrane apparatus (○).

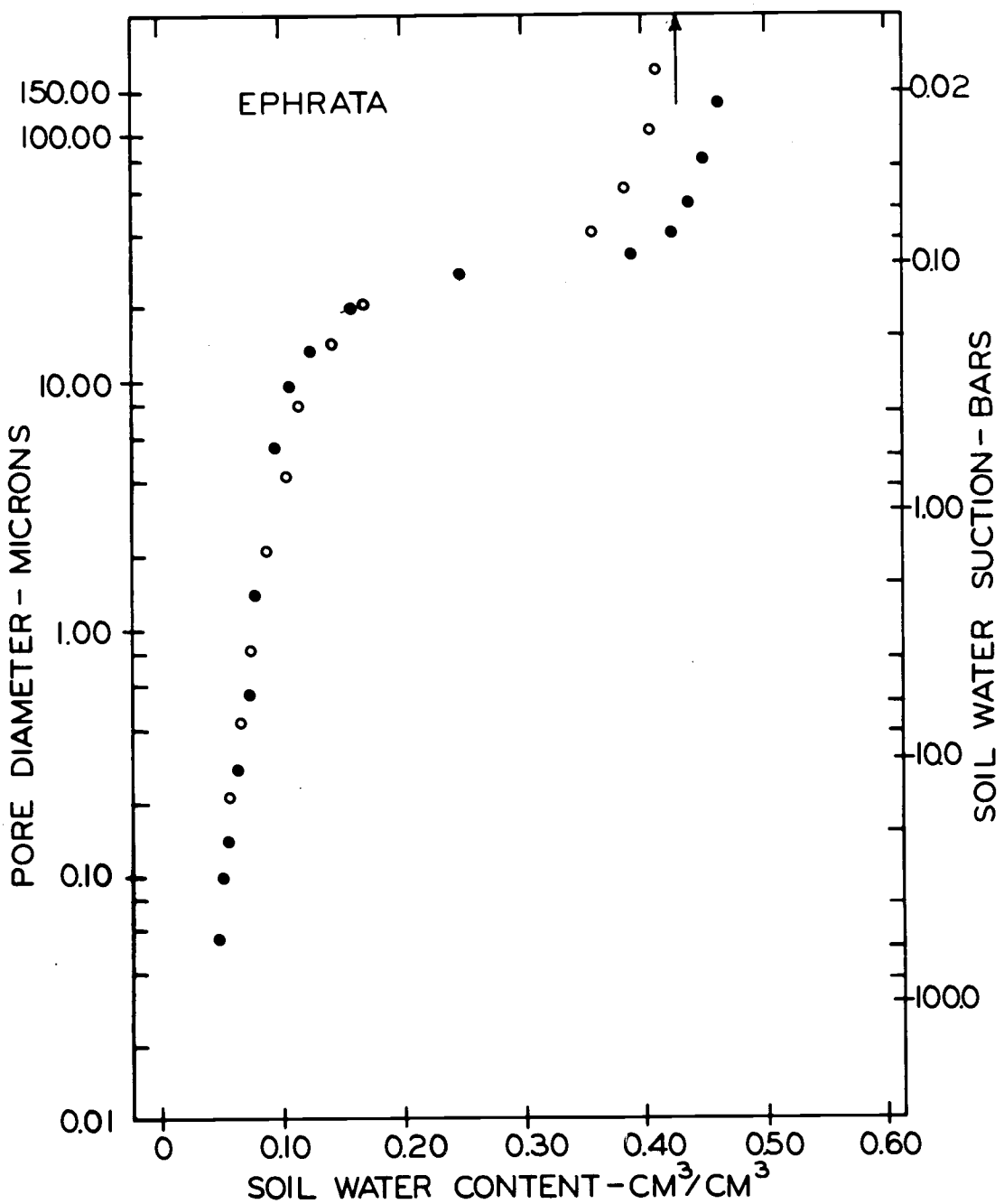

Figure 21. Pore size distribution curves determined by the mercury intrusion porosimeter (●), after correction, and by the pressure plate and the pressure membrane apparatus (○).

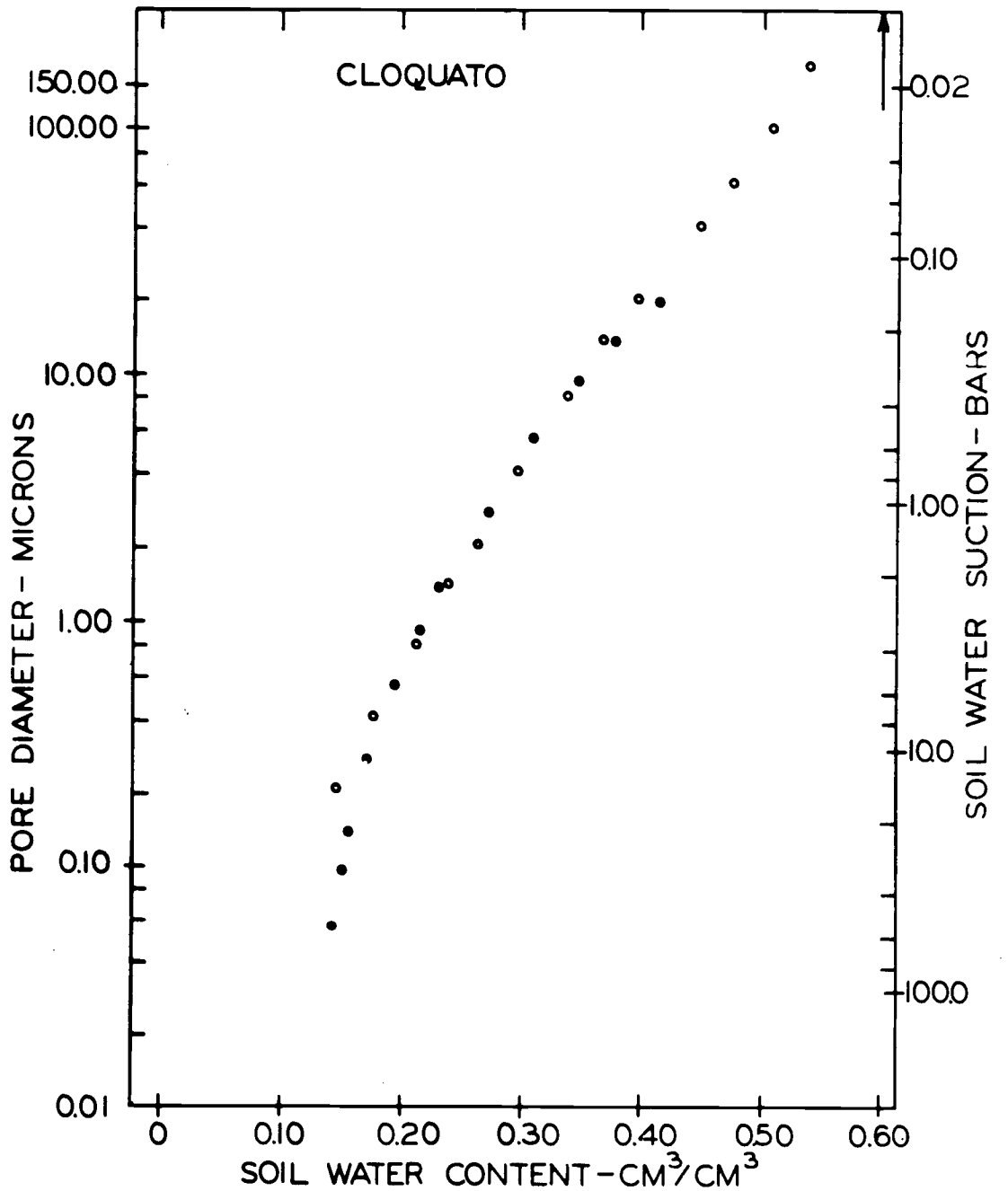

Figure 22. Pore size distribution curves determined by the mercury intrusion porosimeter (●), after correction, and by the pressure plate and the pressure membrane apparatus (○).

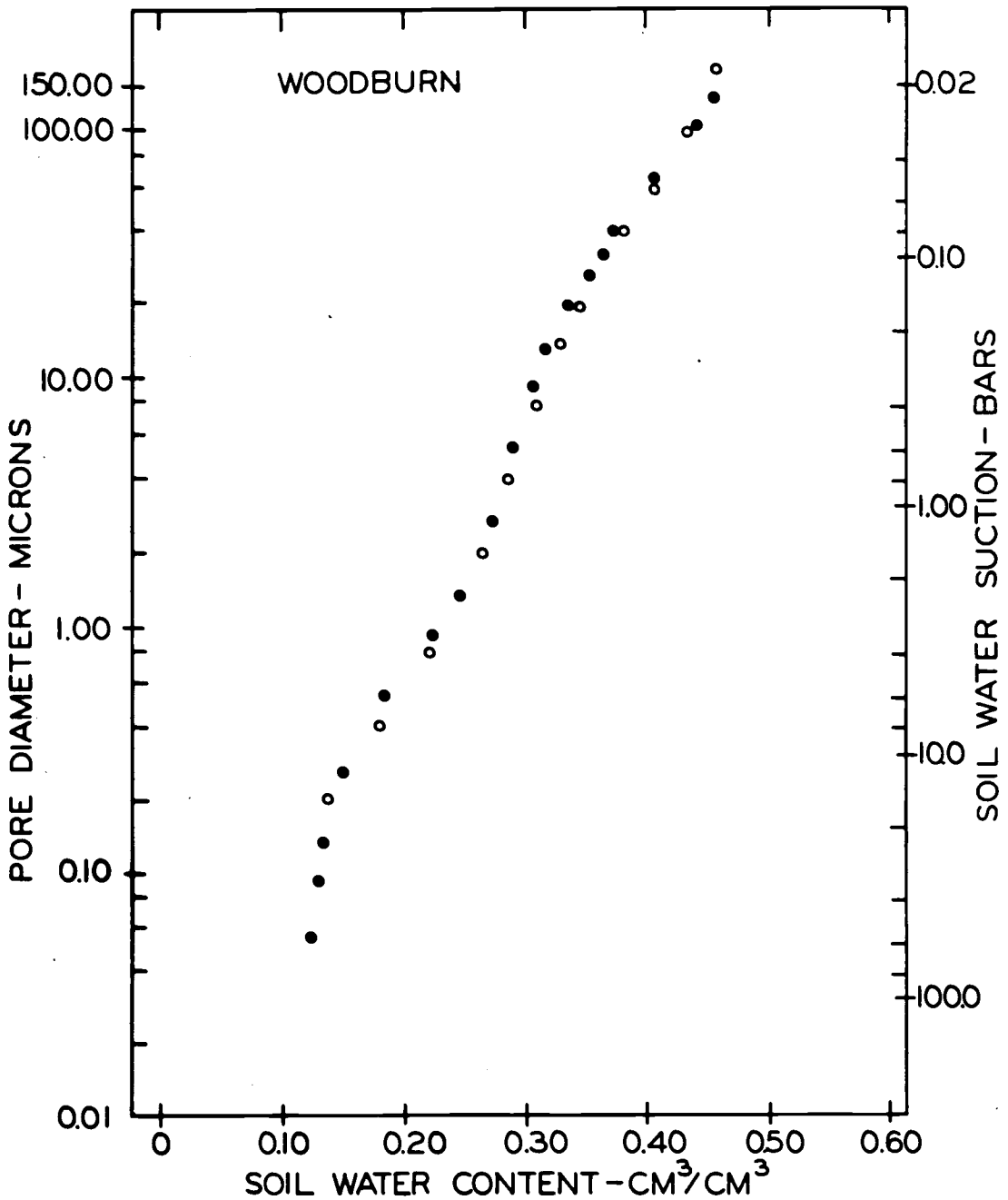

Figure 23. Pore size distribution curves determined by the mercury intrusion porosimeter (●), after correction, and by the pressure plate and the pressure membrane apparatus (○).

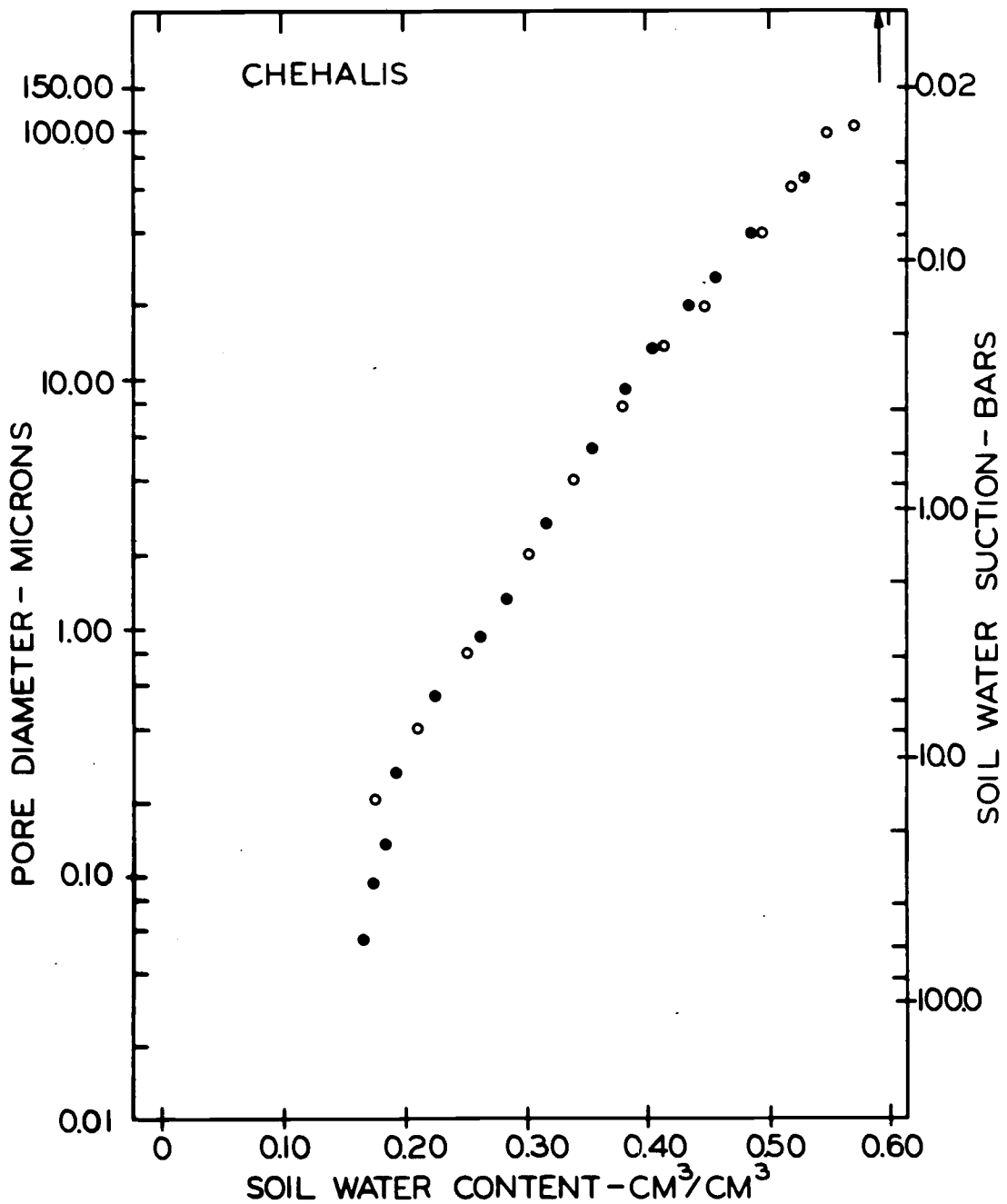

Figure 24. Pore size distribution curves determined by the mercury intrusion porosimeter (●), after correction, and by the pressure plate and the pressure membrane apparatus (○).

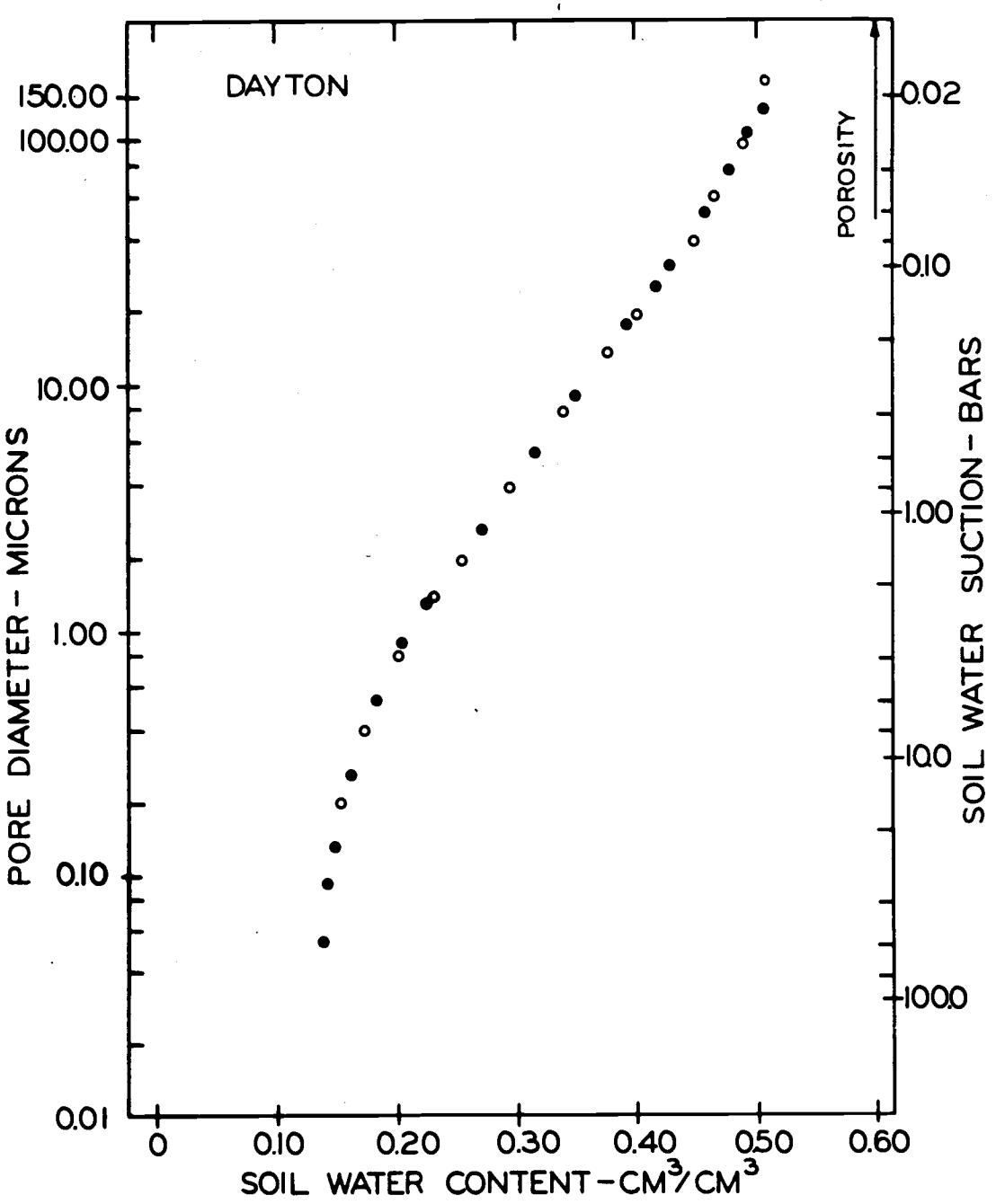

Figure 25. Pore size distribution curves determined by the mercury intrusion porosimeter (●), after correction, and by the pressure plate and the pressure membrane apparatus (○).

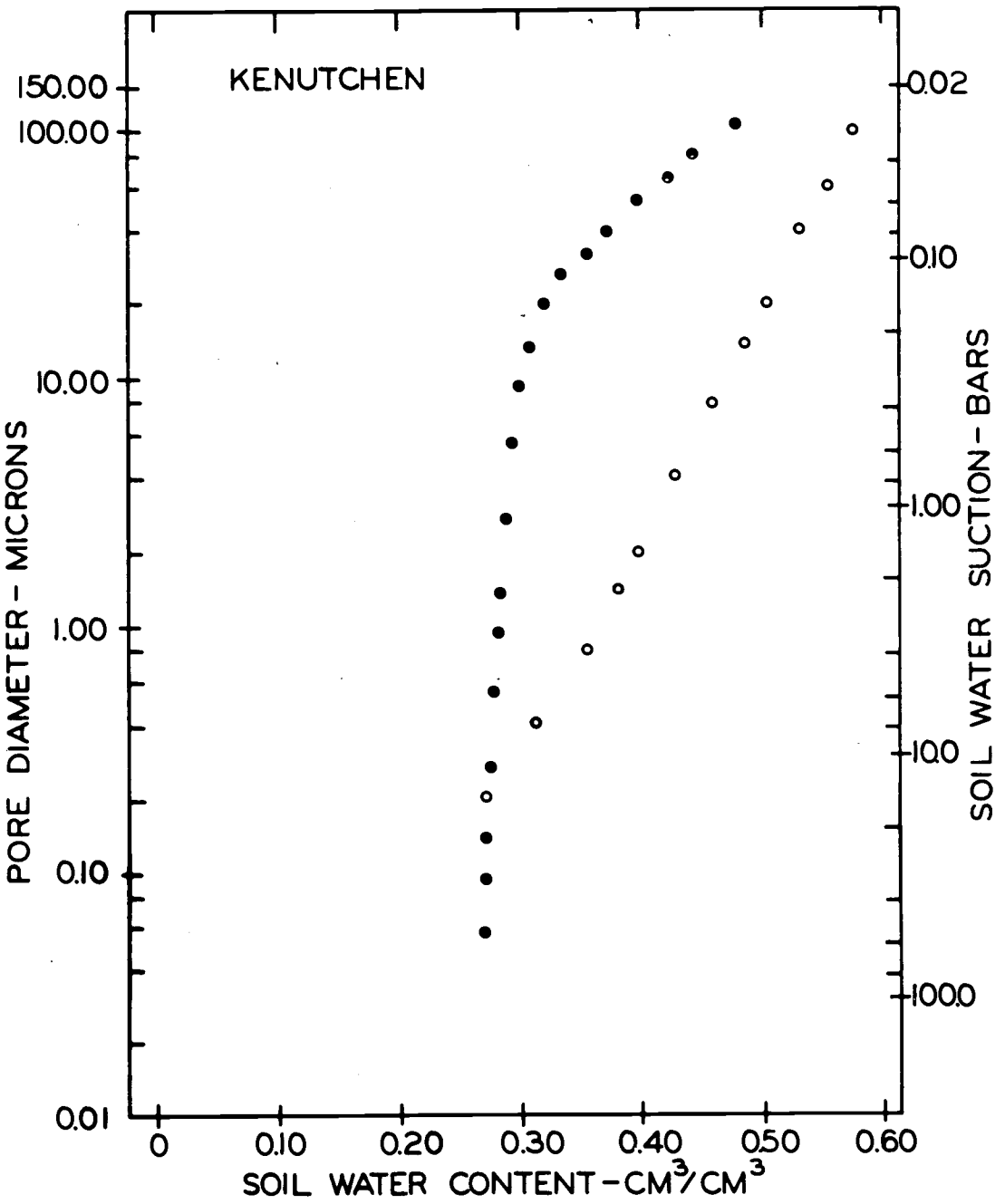

Figure 26. Pore size distribution curves determined by the mercury intrusion porosimeter (●), after correction, and by the pressure plate and the pressure membrane apparatus (○).

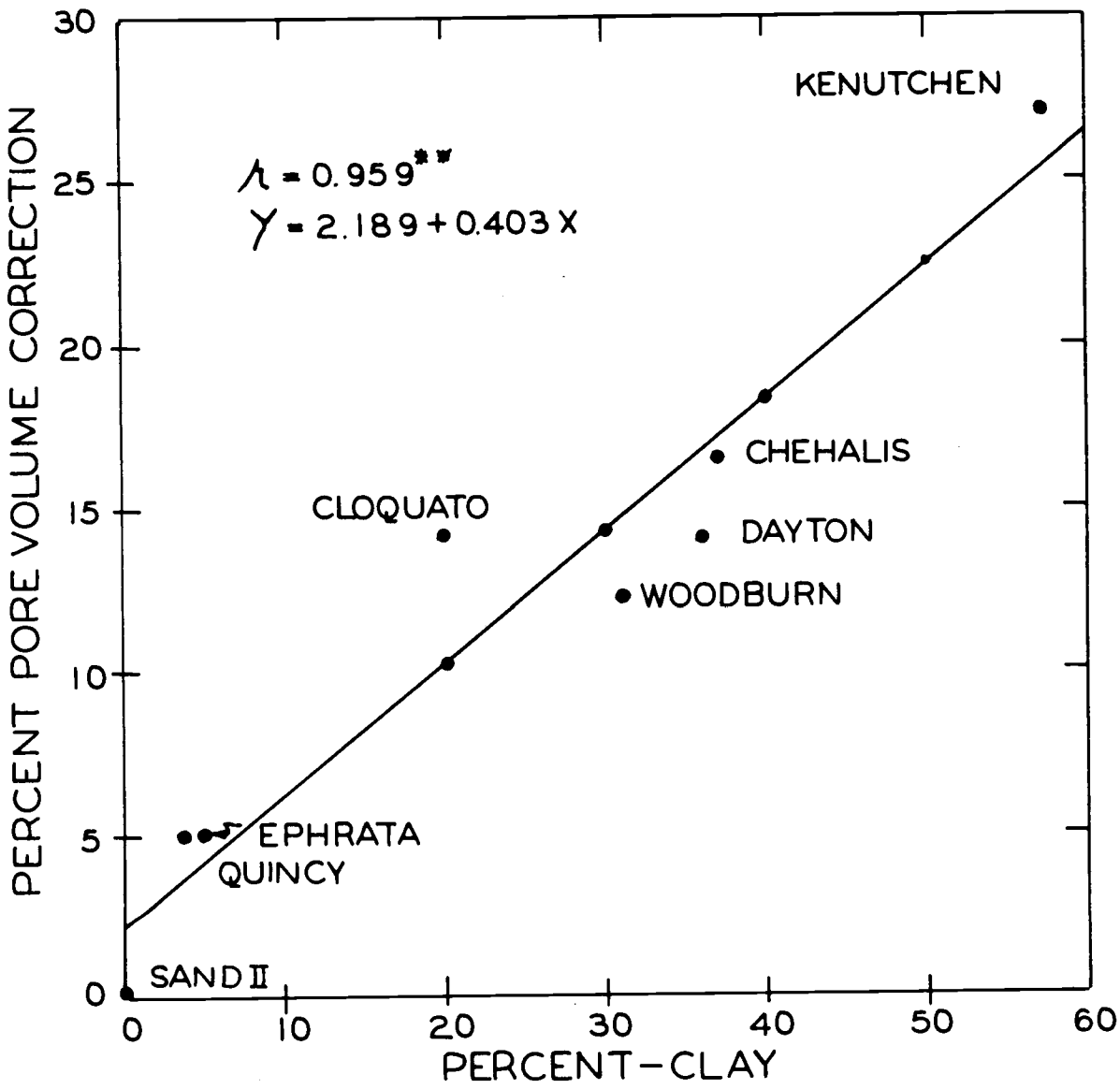

Figure 27. The percent pore space correction required to make the mercury intrusion and the pressure plate determined pore size distribution curves coincide, as a function of clay content of the soil.

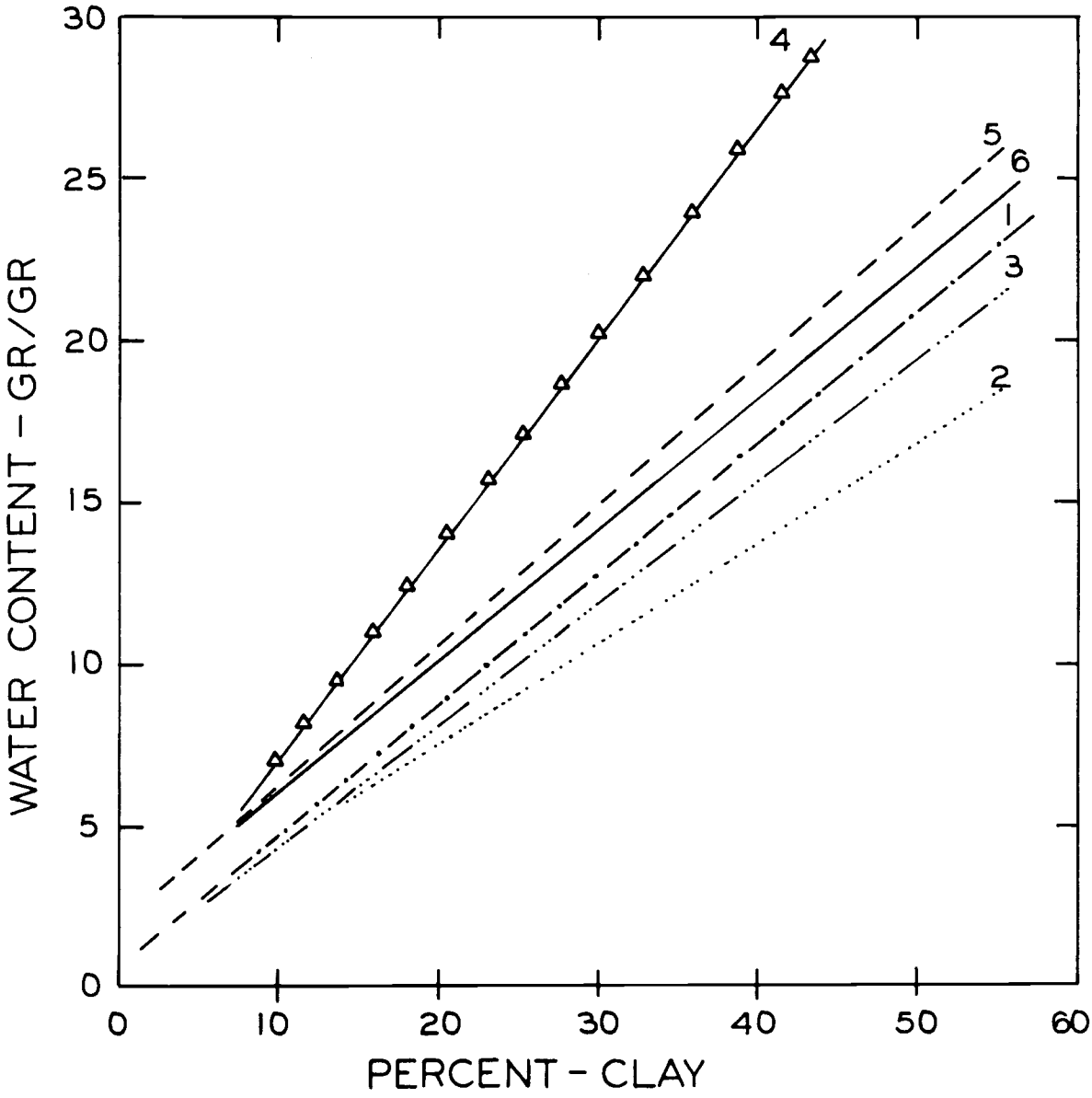

Figure 28. Correlation between clay content and water content at 15.0 bars for clay soils from various geographic regions. (1) Latosols, Nigeria and Brazil; (2) Clay soils, Sweden; (3) Clay soils, Illinois, USA; (4) Marine clay, West-Friesland, Netherland; (5) River clay, Betuwe, Netherland; (6) Clay soils, Willamette Valley, Oregon, USA.

THERMAL CONDUCTIVITY

Introduction

Thermal conductivity is an important parameter in the study of heat transfer. In a porous medium thermal conductivity is a function of the properties of the solid material but also depends on texture, pore space, and water content.

Thermal Conductivity of Dry Soils

Smith and Byers (1938) examined the relationship between thermal conductivity and various soil parameters. Using soils of various morphological characteristics they demonstrated the importance of texture in regulating the thermal conductivity of a soil. Sandy soils had higher thermal conductivities than soils with high clay content. A linear decrease in thermal conductivity with increase in pore space was observed. Nakshabandi and Kohnke (1965) made similar observations. The difference in thermal conductivities was attributed to the soil aggregation. Sandy soils are poorly aggregated and, therefore, have less pore space and better contact between particles than well aggregated soils. Working with glass beads and washed sands, it was further suggested that texture had only a small effect upon the thermal conductivity of dry single grain materials with constant bulk

density.

In their experiments with Maury silt loam soil, Skaggs and Smith (1967) demonstrated a direct relationship between thermal resistance and pore space. The resistance to heat transfer decreases with a decrease in pore space.

Thermal Conductivity of Wet Soils

Smith (1939) observed an increase in heat transport with an increase in water content of soils. The increase per unit water added was larger in coarse textured soils than in soils with high clay content. No attempts were made to explain this behavior. These measurements were made under constant thermal gradients (hot plate method). A significant movement of water vapor from the hot to the cold end was also observed.

Working with fine sand, silt loam, and clay and examining the influence of water content and texture, Nakshabandi and Kohnke (1965) observed an increase in thermal conductivity with water content. The increase was more gradual in fine textured soils than in coarse textured soils. However, no significant textural effects were observed when thermal conductivities were compared at the same soil water suction. This similarity of the conductivity curves of the extremely different soils was attributed to the fact that the thickness and geometry of water shells around the particles determine the conductivity of

the soil-air-water system.

Using the model presented by de Vries (1952) to predict thermal conductivities of soils, Skaggs and Smith (1967) calculated a relationship between thermal conductivity, porosity, and water content. Their results showed that the thermal conductivities of soils decrease with an increase in pore space regardless of initial water content. As compared to dry soils, a sharp decrease in thermal conductivity with increasing pore space was predicted in wet soils.

Calculation of Thermal Conductivity

Several investigators (Gement, 1950; Webb, 1956; Woodside, 1958) attempted to predict the thermal conductivity of granular or porous materials by considering the different elements of the conducting system. It was considered to consist of spherical solid material dispersed in a continuous medium of air and/or water. Equations were derived assuming that the heat flow, at all points in the material, is parallel to the direction of a mean temperature gradient.

The assumptions employed by these investigators do not hold true for a porous medium such as soils and, therefore, may be expected to yield incorrect results. Gement's (1950) results, for instance, indicated that the agreement between experimental and calculated thermal conductivities is good from 5% to 25% of soil water content. Below 5% soil water content, the experimental values were

higher. Webb (1956) observed that the calculated thermal conductivity of dry soil was one-third of the observed value. This discrepancy was attributed to the assumption that the particles were ideally packed spheres. Woodside's (1958) results indicated that the equations derived are not applicable to moist porous materials due to the complexity of the system.

De Vries (1952) developed a model that can be used to predict the thermal conductivity of a system made up of non spherical solid particles. The simplified assumption made in his derivation of equations used to calculate the above parameter was that the temperature distribution in a given particle is independent of the temperature distribution in surrounding particles.

In a porous medium, not completely saturated with water, the heat transfer is complicated by the movement of water in vapor form under the temperature gradient modifying the thermal conductivity of dry air. De Vries (1952) tried to account for this by considering the apparent thermal conductivity of air-filled pores, which is given by

$$\lambda_{apparent} = \lambda_a + \lambda_v , \tag{5}$$

where

λ_a = thermal conductivity of dry air (cal/cm sec°C), and

λ_v = thermal conductivity due to vapor movement (cal/cm sec°C).

This model has been tested by several investigators (Cochran

et al., 1967; Skaggs and Smith, 1967; Woodside and Cliffe, 1959; and de Vries, 1952) and found to give in general reliable results.

The model takes the vapor transfer into account. The hypothesis was made that water vapor transfer may occur more easily in a few large pores with little tortuosity than in many small pores with a great deal of tortuosity when the same total pore volume is considered. This hypothesis could in part explain the observation that the increase in thermal conductivity per unit water added was larger in coarse textures soils than in fine textured soils (Smith, 1939; Nakshabandi and Kohnke, 1965).

The thermal conductivity of beds made up of three size classes of glass beads was measured to evaluate the influence of particle size on thermal conductivity at various water contents.

Materials and Methods

Experimental Measurement of Thermal Conductivity

To study the influence of particle size and water content on thermal conductivity, three classes of glass beads with particle sizes ranging from 210 microns to 149 microns, 105 microns to 74 microns, and 74 microns to 53 microns, were selected. The glass beads were spherical in shape and each class had a pore space of 40 percent.

Thermal conductivity was determined with a thermal conductivity

probe. The method is based on a principle which states that the rate of temperature rise of a cylindrical probe, embedded in an infinite medium and heated at a constant rate, is directly proportional to the logarithm of time and inversely proportional to the thermal conductivity of the surrounding medium. Samples were contained in large glass jars, representing an infinite medium. Details of this method are given by Cochran, Boersma, and Youngberg (1967).

The samples were prepared by mixing the amount of water required to bring a sample to the desired water content. The moist sample was packed in a glass jar that was tapped thrice on the top of the table with each scoop of sample poured into it. The number of scoops per jar was the same for each sample. To avoid evaporative loss of water, the container was covered with a polyethylene sheet secured with a rubber band. The container was capped with a lid having a hole in the middle to receive the conductivity probe. The lid and the lid hole were masked by tape. The containers were kept in a constant temperature cabinet at 26°C for a week to insure uniform distribution of water and temperature throughout the samples before the measurements were made.

The temperature increase of the thermal conductivity probe was recorded with a Heath strip chart recorder. In order to facilitate reading of the probe temperature to the third decimal place, the recorder was adjusted to read 1°C for the full span of the chart. The

probe was inserted through the lid hole. An electric current of 0.004 amperes was passed through the probe. Temperature increase as a function of time was recorded on the chart for seven to eight minutes. A chart trace is shown in Figure 29. Thermal conductivity (λ) was calculated with Equation (6),

$$\lambda = 0.0000956k \frac{\log (t_1/t_2)}{T_2-T_1} \quad \frac{\text{cal}}{\text{sec cm°C}}, \tag{6}$$

where t is time in seconds, T is the temperature of the probe in °C, and k is the instrument constant. The value of k is 1.80 and was estimated by calibrating the probe against dry and saturated samples of sand of known thermal conductivities.

The water content of each sample was determined gravimetrically immediately after thermal conductivity measurements were completed.

Theoretical Calculation of Thermal Conductivity

The model presented by de Vries (1966) was used to calculate theoretical values of the thermal conductivity of the glass beads. In this model, water, air, or the solid phase can be taken as the continuous medium in a porous material, with the remaining two components dispersed in it. In this analysis water was considered to form the continuous medium, except at very low water contents where air was

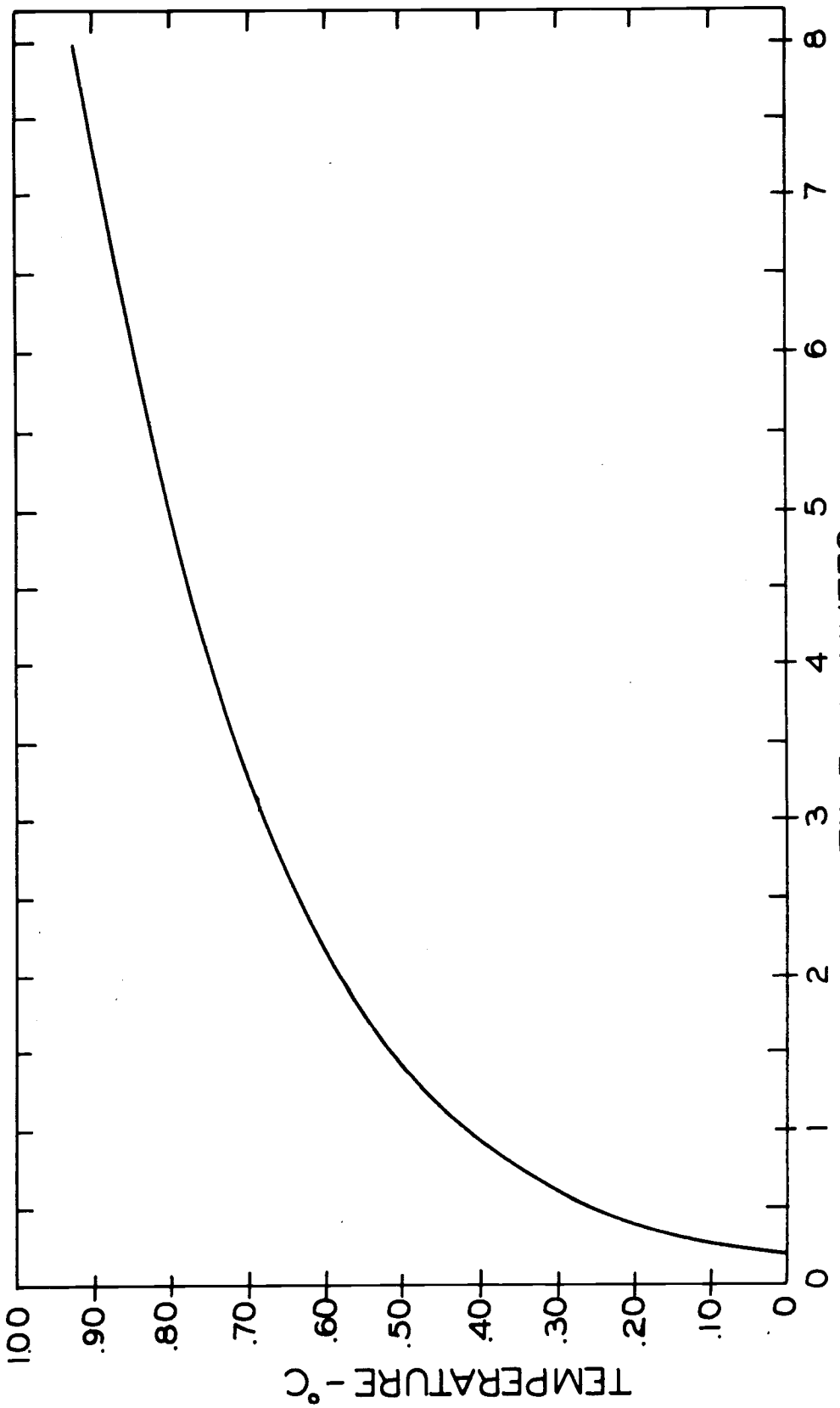

Figure 29. Rise in temperature of the thermal conductivity probe inserted in a sample as a function of time.

regarded to be the continuous medium.

When water is considered to be the continuous phase, thermal conductivities are calculated as follows:

$$\lambda = \frac{x_w \lambda_w + k_s x_s \lambda_s + k_a x_a \lambda_a}{x_w + k_s x_s + k_a x_a}, \tag{7}$$

where x_w, x_a, x_s, are the volume fractions occupied by water, air and the solid material respectively; λ_w, λ_a, λ_s are the thermal conductivities in cal/cm sec°C of water, air and the solid material respectively, and the quantity k is the ratio of the average temperature gradient in the granules and the corresponding quantity in the medium.

The value of k depends on the ratio of thermal conductivities, size and shape of the granules and their relative positions. Under certain limiting assumptions the k value can be calculated:

$$k_s = \frac{2}{3} \frac{1}{1 + (\frac{\lambda_s}{\lambda_w} - 1) g_a} + \frac{1}{3} \frac{1}{1 + (\frac{\lambda_s}{\lambda_w} - 1) g_c}, \tag{8}$$

and

$$k_a = \frac{2}{3} \frac{1}{1 + (\frac{\lambda_a}{\lambda_w} - 1) g_a} + \frac{1}{3} \frac{1}{1 + (\frac{\lambda_a}{\lambda_w} - 1) g_c}, \tag{9}$$

where g_a, g_b, and g_c are the depolarization factors in the a,

b, and c axes. They satisfy the relationship

$$g_a + g_b + g_c = 1 \tag{10}$$

and hence $g_b = 1 - (g_a + g_c)$. Thus for spherical granules $g_a = g_b = g_c = 1/3$.

In general, it is assumed that g_a varies linearly with x_a and x_w between the values $1/3$ at $x_a = 0$ (for spherical solid particles) and 0.035 at $x_w = 0$. Thus, in unsaturated samples with water as continuous medium

$$g_a = 0.33 - 0.697\, x_a . \tag{11}$$

When air is considered to be the continuous medium, g_a is given by,

$$g_a = 0.013 + 0.944\, x_w \tag{12}$$

and for this condition, equations for thermal conductivities are identical to Equations (7), (8), and (9) except that the position of subscripts 'a' and 'w' is interchanged, and k_a becomes k_w. For completely saturated ($x_a = 0$) and completely dry ($x_w = 0$) media, the beads being solid spheres

$$g_a = g_b = g_c = \frac{1}{3},$$

which reduces Equation (7) to

$$\lambda = \frac{x_w \lambda_w + k_s x_s \lambda_s}{x_w + k_s x_s} , \qquad (13)$$

where

$$k_s = \frac{1}{1+\frac{1}{3}\left(\frac{\lambda_s}{\lambda_w}-1\right)} . \qquad (14)$$

Again, for air to be a continuous phase, identical equations can be written by replacing subscript 'w' with 'a' in Equations (13) and (14).

Results and Discussion

Thermal conductivity as a function of moisture content for the three size classes of glass beads is shown in Figure 30. The solid line indicates the theoretical values of thermal conductivity calculated using the model presented by de Vries (1966).

Examination of the diagram indicates that the experimental data fit closely to the theoretical values of thermal conductivity. A sharp increase in the heat conductivity with a small increase in moisture content of dry samples can be observed. Further increase in water content brings a rather slow increase in thermal conductivity.

Since glass is mostly quartz, it was speculated that thermal properties of glass beads were comparable with quartz. The results of Figure 30 when compared with those of de Vries (1966, Fig. 7.5)

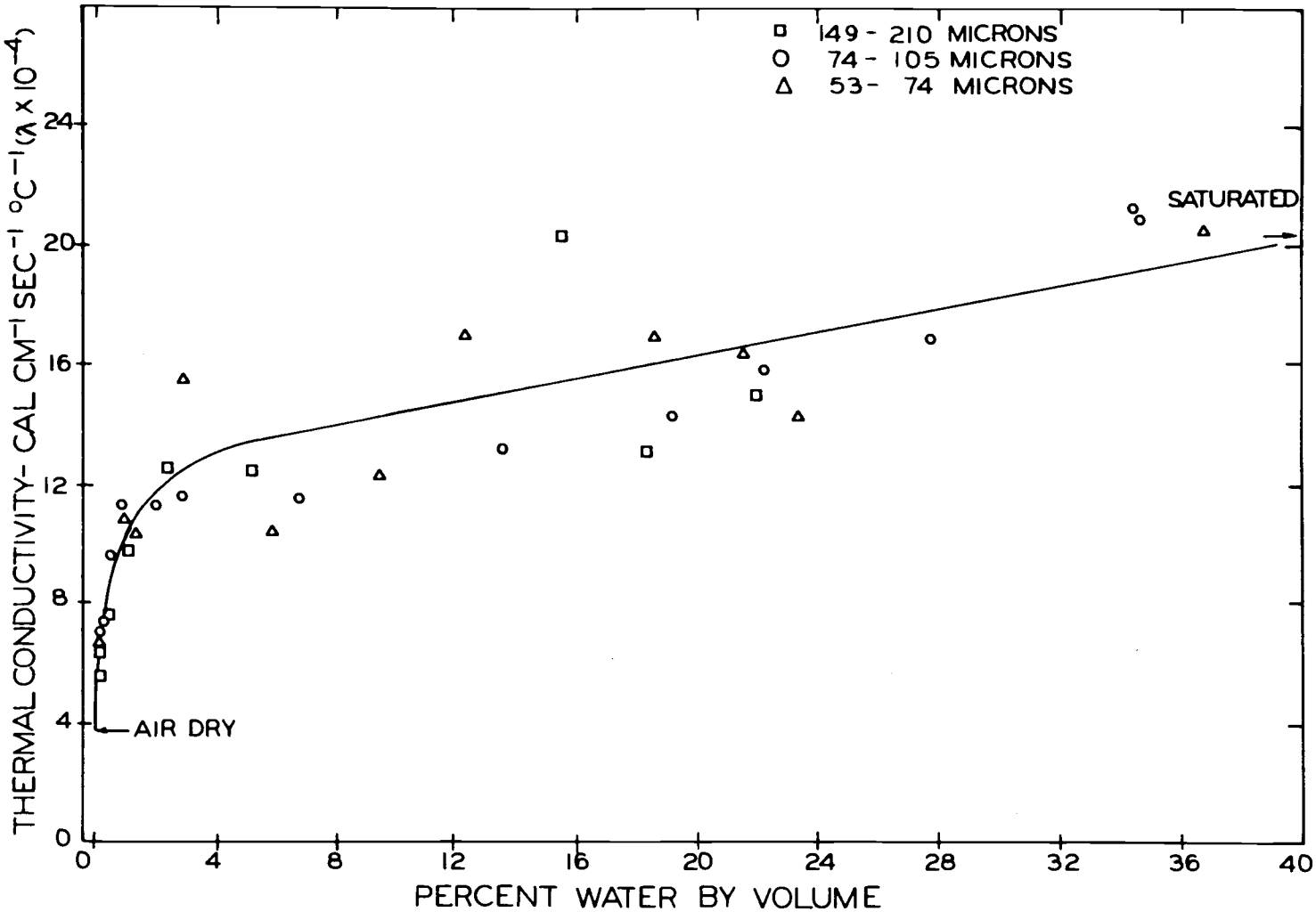

Figure 30. The thermal conductivity of three samples of glass beads as a function of water content. The solid line represents the thermal conductivity calculated according to the procedure proposed by de Vries (1966).

obtained with quartz sand, however, indicate lower values of thermal conductivity for glass beads. This is due to the fact that the glass bead material is amorphous in nature and has smaller thermal conductivity, λ_s in Equation (14), than crystalline quartz material. The glass beads used in these experiments were manufactured from high grade crown glass, soda lime type, with a silica content of more than 60%. In comparison to 21.0 mcal/cm sec°C for quartz, the manufacturer's value of thermal conductivity of the glass bead material is 2.5 mcal/cm sec°C.

The data suggest that for the range of sizes considered, particle size and therefore also pore size, had no influence on the thermal conductivity of the glass beads porous medium. When the same thermal conductivities are plotted against water suction however a dissimilarity due to particle size differences appears (Figure 31). Textural differences are quite striking at low suctions but tend to disappear as the suction increases. Results shown in Figure 31 are best understood by considering Figure 32. There the water characteristic curves derived from mercury intrusion data for the three porous media are shown. These graphs show that most of the water in these media is withdrawn over a very narrow suction range. This range corresponds to the suction range over which the thermal conductivity decreased. The rapid decrease in thermal conductivity shown in Figure 31 is the result of a rapid water loss over this

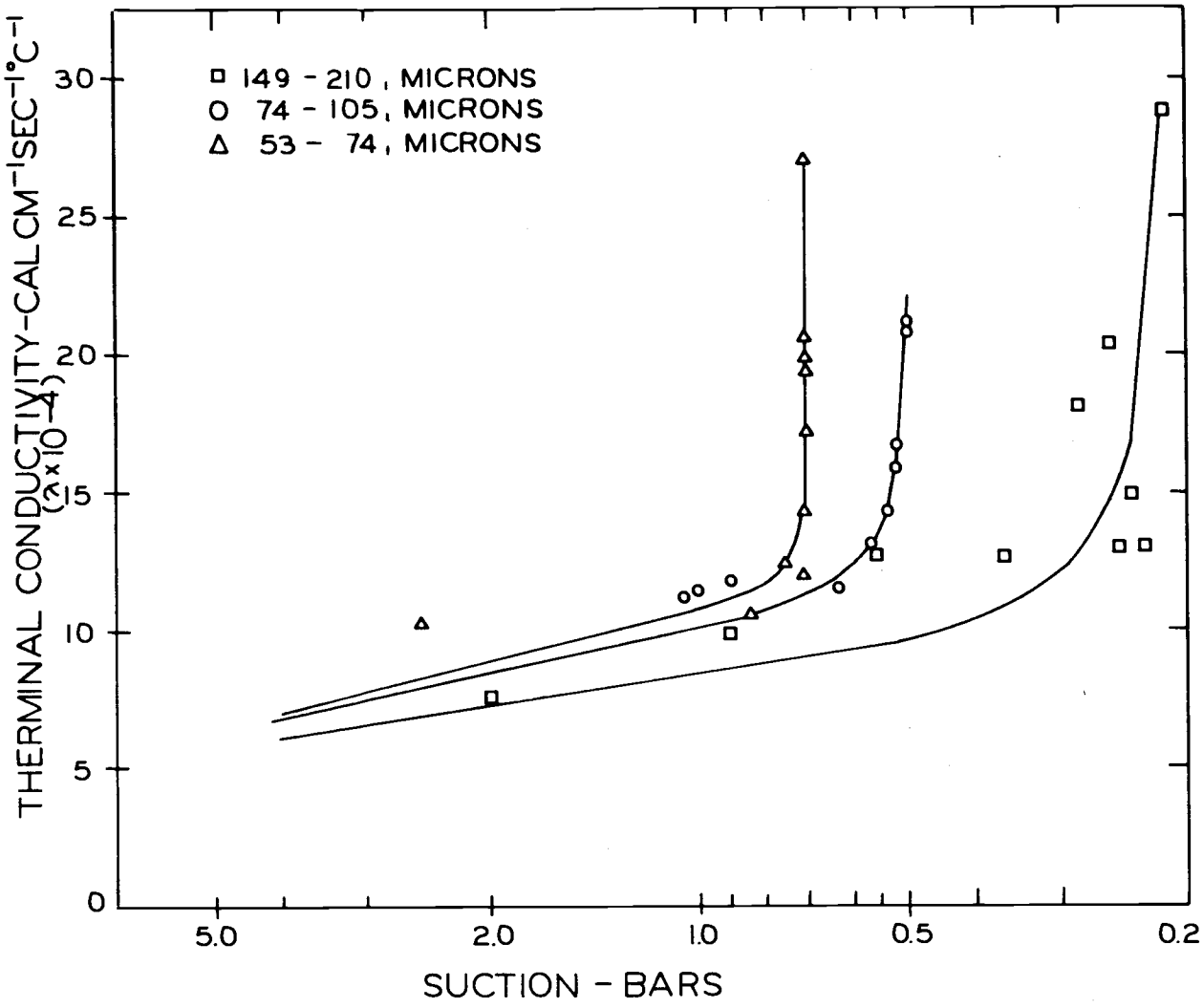

Figure 31. The thermal conductivity of three samples of glass beads as a function of water suction. The samples were considered to contain no water at a suction of 15.0 bars and to have the same thermal conductivity at zero water content.

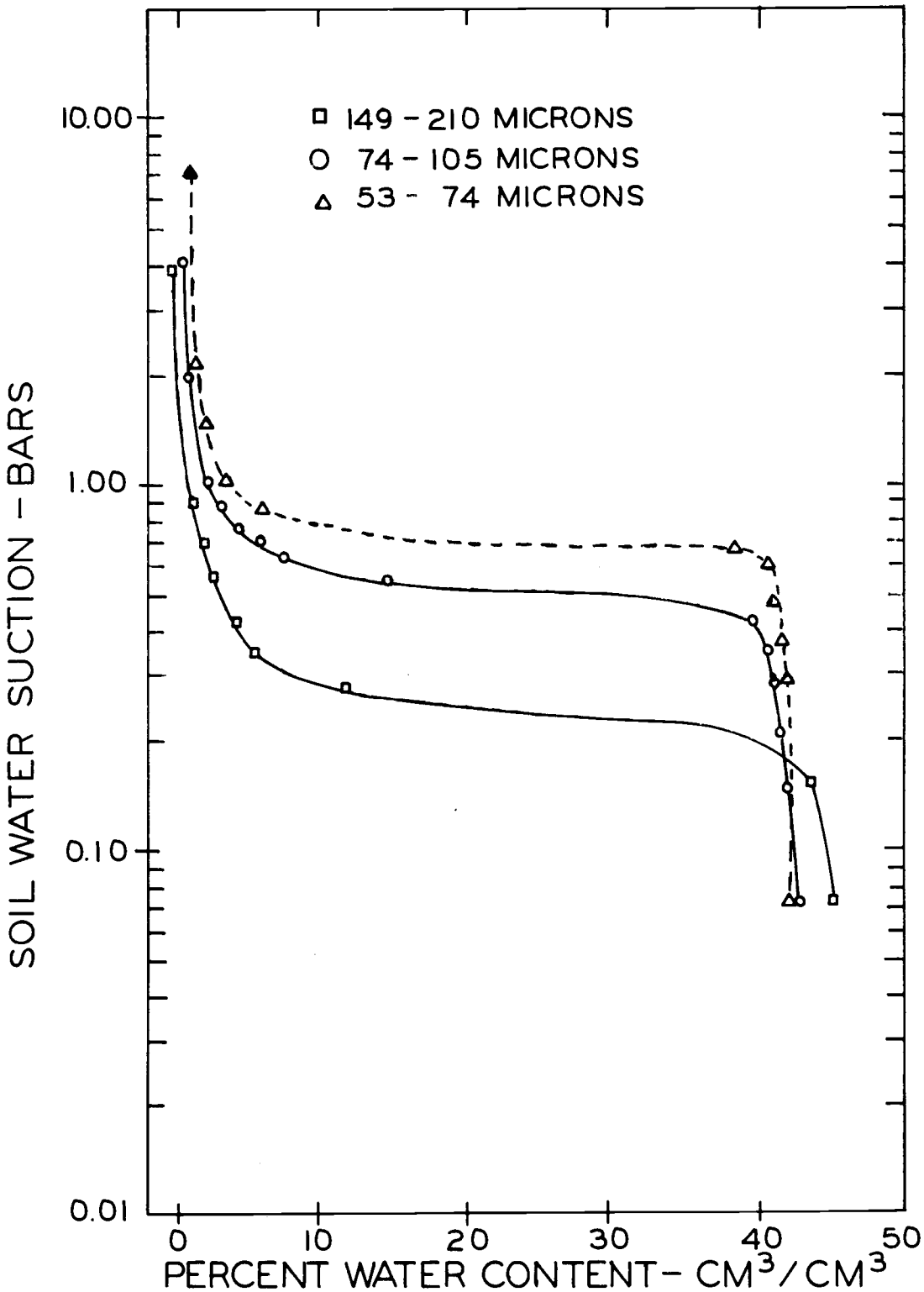

Figure 32. Soil water characteristic curves for three samples of glass beads as obtained with the mercury intrusion porosimeter.

suction increment. Most of the water of all three classes has been withdrawn at a suction of 1.0 bar. At suctions greater than 1.0 bar little water is left and the thermal conductivities of the three materials should be nearly the same. This was confirmed by the experimental results shown in Figure 31. The curves shown in Figure 31 for suction values greater than 1.0 bar were drawn on the basis of the following assumptions: (1) the water content at 15.0 bars is zero, (2) the relation between suction and thermal conductivity is linear at suctions greater than 1.0 bar, and (3) the thermal conductivity at 15.0 bars (dry beads) is 3.68×10^{-4} cal/cm sec°C.

Contrary to the observation of Smith and Byers (1938) in dry soils, the data (Figure 30) do not suggest textural differences on the conductive properties of the glass beads. The contrary conclusion must be explained on the basis of soil aggregation and thermal conductivity of the constituent components. Textural difference is not synonomous with particle size difference. Smith and Byers used soils which varied in clay content. The thermal conductivity for quartz sand is given as 21.0 mcal/cm sec°C and for clay as 7 mcal/cm sec°C by de Vries (1966). Sandy soils are poorly aggregated and therefore have less pore space and better contact between particles than well aggregated clayey soils. On the other hand the three classes of glass beads used in these experiments had the same total pore space and simulate a structureless soil. Since the bulk density of glass beads

(1.45 g/cm^3) is also the same, no textural differences are expected. A similar observation for samples of glass beads and washed sand was made by Nakshabandi and Kohnke (1967).

In moist soils heat transfer is complicated by water movement, both in liquid as well as in vapor form. Thermal conductivity increases with increase in soil moisture. As the arrangement of water molecules in the soil is linked with moisture tension, it was postulated that thermal conductivity of soils should be a function of moisture tension (Nakshabandi and Kohnke, 1965). These investigators observed that the relationship between thermal conductivity and suction was the same for fine sand, silty clay, and clay, but the relationship between thermal conductivity and water content was different for each material. Exactly opposite results are indicated by Figures 30 and 31. Here the thermal conductivity recorded as a function of water content was independent of size class, but different curves resulted when the thermal conductivity was plotted as a function of suction.

The disagreement between the observations made by Nakshabandi and Kohnke (1965) and those of the present investigation can in part be explained on the basis of soil porosity. Using Equation (4), Skaggs and Smith (1967) calculated the thermal conductivity of a soil as a function of pore space and water content. Their results showed an increasing resistance to heat flow at identical water contents with an increase in the pore space. The effect of total pore space on thermal

conductivity was most pronounced at the highest soil water contents. In the experiments reported by Nakshabandi and Kohnke, the three soils used were fine sand with 40%, silt loam with 48%, and clay with 58% of total pore space. The observed textural differences in thermal conductivity-soil water content relationship reported by these investigators could be the result of differences in air filled pore space at identical water contents. Had the total pore space been the same probably no differences would have been found. Since each fraction of glass beads had a total pore space of 40%, no influence of the size of the glass beads on thermal conductivity was apparent within the range of water contents studied.

With regard to the relationship between thermal conductivity and soil water suction it must be realized that the glass beads represent porous media with a narrow range of pore sizes. This is demonstrated by the water characteristic curves shown in Figure 32. The soils used in the experiment by Nakshabandi and Kohnke probably had a much wider range of pore sizes. In this case the relation between thermal conductivity and water suction would not have the sharp change observed for the glass bead samples. The more gradual change might be expected to obscure at least in part any difference between soil material. Probably more careful analysis of the results would show a difference as suggested by Figure 31.

Conclusions

The measurements indicate that the thermal conductivity of a wet porous material at a given total air filled pore space is independent of the size of the air filled pores (Figure 30). It had been hypothesized that the vapor transfer component of heat transfer in the medium would be pore size dependent. Results shown in Figure 30 do suggest a trend indicating the pore size effect. The data points for the smaller fractions constitute the lower part of the points shown on the graph. It was expected that the diffusion coefficient through the smaller pores would be lower. That the pore size effect was not observed experimentally in a more clear cut manner can be due to several circumstances. Vapor transfer is not a major component of heat transfer. Any large variations in this component due to pore size would still only cause a relatively small variation in the total thermal conductivity. The experimental errors involved in the use of the probe method for measuring thermal conductivity are probably greater than the real variation caused by differences in pore size.

The results obtained suggest that the theoretical model presented by de Vries (1966) can be used to predict the thermal conductivity of a wet porous material and that a pore size correction factor in the vapor transfer component is not required.

SIMULTANEOUS TRANSFER OF HEAT AND WATER

Introduction

Pronounced seasonal and diurnal temperature fluctuations in soils have long been recognized. Seasonal fluctuations affect the soil temperature to a depth greater than the rooting zones of most crops while diurnal fluctuations influence approximately the surface 30 cm of bare soil (Smith, 1932). The variation of temperature with depth gives rise to thermal gradients which tend to move water in both vapor and liquid phases. Lebedeff (1927) conducted a field experiment over the winter months in Russia and concluded that more than 6 cm of soil water moved upward into the soil profile in response to seasonal thermal gradients. Many investigators (Maclean and Gwatkin, 1946; Gurr et al., 1952; and others) demonstrated this phenomenon in laboratory studies.

Attempts have been made to describe water transfer under a temperature gradient. Although the fact that the flow of water is non-isothermal in nature was well recognized, the influence of thermal gradients was not taken into account when equations were written to describe the flow until recent years. Considering evaporation as an isothermal process, Gardner and Hillel (1962) compared cumulative evaporation curves under different evaporation potentials with solutions

to equations derived for isothermal conditions. Their results showed a poor fit of the curve under non-isothermal conditions. Hanks and Gardner (1965) used the isothermal diffusion equation to investigate the influence of variation of the diffusivity function on evaporation of soil water. They found that changes in diffusivity at water contents of less than 10%, had no significant effect on the cumulative evaporation. Variation of the diffusivity function at water contents greater than 10% gave large differences in cumulative evaporation.

Phillip and de Vries (1957) advanced a theory describing soil water movement in response to temperature gradients. It includes the contributions of vapor and liquid phases in response to both soil-water pressure and vapor pressure gradients. The validity of this approach was supported by earlier experimental results of Gurr et al. (1952) and Jones and Kohnke (1952) among others. Dirksen (1964) showed the analysis to be valid for water movement into frozen soil.

More recently, Taylor and Cary proposed a theory of water movement based on irreversible thermodynamics and developed it extensively (Taylor and Cary, 1960, 1964, 1965; Taylor, 1962, 1963; Cary, 1963, 1964, 1965, 1966). Their approach can be used to describe certain types of water flow that might exist under both isothermal and non-isothermal conditions. The theory is not limited to water and heat flow but can be extended to include the flow of any constituent of the system.

Simultaneous heat and water flow has an important implication in the evaporation of water from soils. Weigand and Taylor (1962), studying the temperature distribution in drying soil columns, demonstrated that evaporative drying of moist soil is a non-isothermal process, and indicated that the analysis of drying as an isothermal process may contain appreciable error. Heat and water vapor are both transferred across the soil-air interface during this process. Working with soil columns subjected to temperature gradients, Gardner and Hanks (1966) observed that heat flux measurements give a good indication of the evaporation zone which extends deeper into the soil as the surface dries out.

It was postulated in the previous chapter that pore sizes and pore size distributions might be important parameters in heat flow considerations. According to the results reported there the size of the pores is not important when the contribution of vapor transfer to heat transfer is considered.

The hypothesis that pore size, pore size distribution and tortuosity is important to vapor transfer in the soil still needs to be considered with respect to evaporations from a soil surface. If indeed pore size is an important parameter among those which determine rates of water loss from a porous material it would have profound effects on the total heat budget. The heat used to change water from the liquid to the vapor state is an important part of the heat budget.

Experiments were conducted in which the heat budget and rate of water loss from two glass bead beds made up of different size classes of beads were measured.

Materials and Methods

Experimental Configuration

Simultaneous transfer of heat and water resulting from a diurnal temperature cycle imposed on a column of glass beads was monitored using the experimental arrangement shown in Figure 33. With some modifications, this experimental arrangement is similar to the one employed by Kowsar (1968).

A sample of glass beads was contained in a box 40 cm deep, 25 cm wide, and 4 cm thick on the inside. The box was made of 1/4-inch plywood, sealed on the inside with epoxy paint and covered on the outside with thermal insulating material. Changes in water content were measured with a gamma beam attenuation system, at predetermined depths and at regular intervals of time. The gamma beam was manipulated with an automatic scanning drive. Diurnal temperature fluctuations at the surface of the sample were obtained with a resistance heating element positioned above the surface. The heat flux was regulated with a sinusoidal power controller. Temperatures were measured at regular intervals with thermistors and were

1. Stepping switch selector
2. Strip-chart recorder for thermistor
3. Stepping switch logic and power supply
4. Gamma attentuation system control box
5. Vertical motion program cam
6. Horizontal motion program cam
7. Am-241 source
8. Heater assembly
9. Sample cell
10. Pulse height analyzer, scaler-timer
11. High voltage power supply
12. Digital printer
13. Heater power supply
14. Heater sinusoidal programmer
15. Scintillation detector

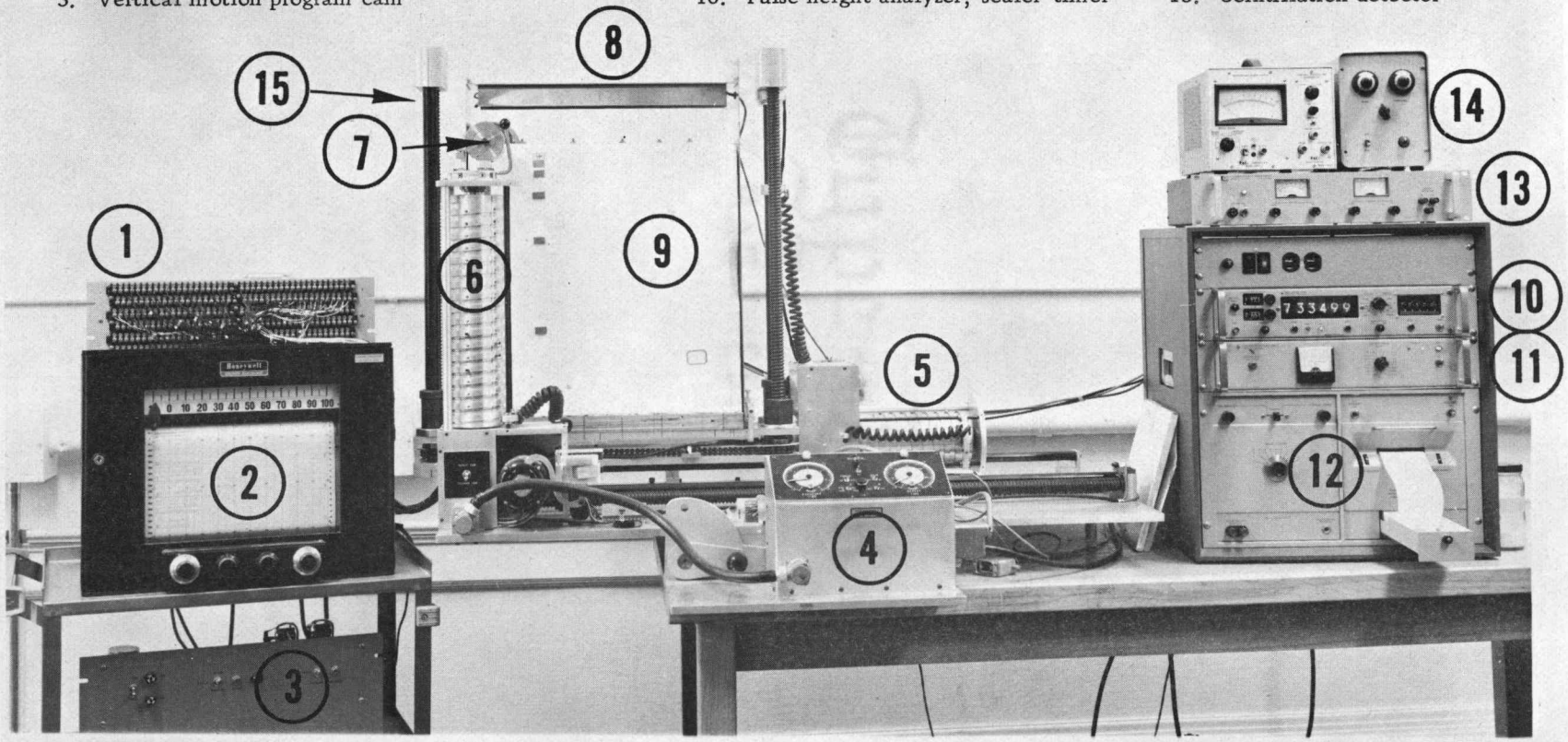

Figure 33. Experimental arrangement used for the study of simultaneous transfer of heat and water in glass bead beds. The sample holder (9) consists of a box with inside dimensions of 40 x 25 x 4 cm. Insulation provided around the box prevented all heat exchange except at the soil surface.

recorded on a strip chart recorder. The experiments were conducted in an air conditioned laboratory.

Several experiments were conducted in which changes in water content and temperature brought about by the diurnal heat load were measured. Table 5 shows a summary of the experiments.

Table 5. List of experiments conducted for the study of simultaneous transfer of heat and water in glass bead beds.

Experiment No.	Size Class	Initial Water Content
	microns	percent by volume
I	53- 74	Air dry (0%)
II	53- 74	Saturated (40%)
III	53- 74	Initially saturated (40%)
IV	53- 74	Initially unsaturated (34%)
V	149-219	Air dry (0%)
VI	149-210	Saturated (40%)
VII	149-210	Initially saturated (40%)
VIII	149-210	Initially unsaturated (30%)

Heating of the Sample

The heating system consisted of a heater, a programmed power supply, and a sinusoidal power controller.

The resistance heating element was made up of number 22 helically wound nichrome wire with a total resistance of 48 ohms. The wire coils were stretched slightly to fit three parallel rows 45 cm long, 2.5 cm between centers and supported by 9 porcelain insulators.

Additional resistance wire was used for series connections between the rows to avoid an abrupt cool end effect. A U-shaped polished stainless steel reflector and auxilliary aluminum foil end pieces directed the heat energy downwards. An aluminum frame held the heater assembly 10 cm above the sample surface.

Power for the heating element was derived from a Hewlett-Packard 6443B 300 watt direct current power supply with a capacity of 2.5 amperes at 120 volts. The instrument was slightly modified for remote voltage programming by use of a variable external voltage.

A controller was constructed to provide an approximate sinusoidal power input to the sample. The time base was selected so that the positive half cycle (0-180 degrees) was 12 hours. No power was applied to the sample during the negative half cycle. During this time conductive and radiative cooling of course continued. Heat output as a function of time is shown in Figure 34. Maximum heat input occurred six hours (90 degrees) after initiating the sinusoidal wave. The basic sinusoidal voltage was derived from a continuous rotation sine function potentiometer driven by a synchronous motor. An appropriate resistance-voltage network was calculated to transform the sinusoidal resistance function into a shaped voltage to program the power supply for a sinusoidal output. The peak power was adjustable, but during these experiments was left at a 75 volt maximum into the 48 ohm heater, or 115 watts.

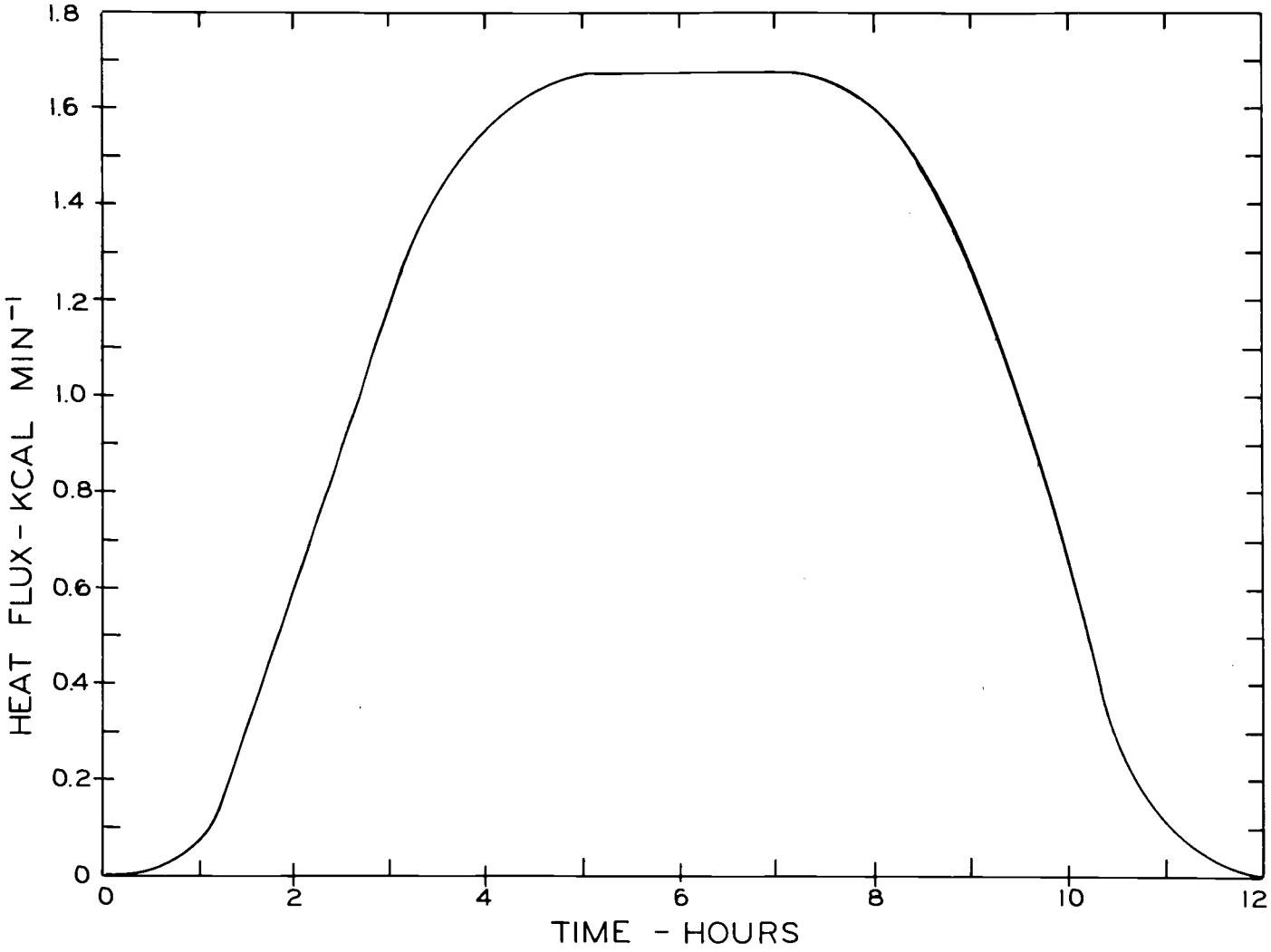

Figure 34. Heat input from the heat source as a function of time. The maximum voltage obtained was 75 volts.

Temperature Measurements

The temperature sensors (thermistors) were inserted through holes drilled in the side of the soil container. Temperature measurements were made at depths of 2, 4, 7, 11, 18, 28, and 38 cm. At each depth four thermistors were placed some distance apart from one another. Figure 35 indicates the placement of the thermistors in the box. The thermistors penetrated about 2 cm into the sample. Fenwall GB 41P8 glass probe thermistors were used. Each thermistor was calibrated individually, against a Hewlett-Packard 2801A quartz thermometer, in terms of its resistance as a function of temperature.

A single channel strip chart recorder was employed to record the temperature measurement for each thermistor. The chart readings were calibrated in terms of resistance with a resistance box. A plot of the chart reading as a function of resistance is shown in Figure 36. For each group of thermistors, a relation was drawn between chart reading and temperature. A table was prepared showing the temperature corresponding to a given chart reading. Part of such a table is shown in Table 6.

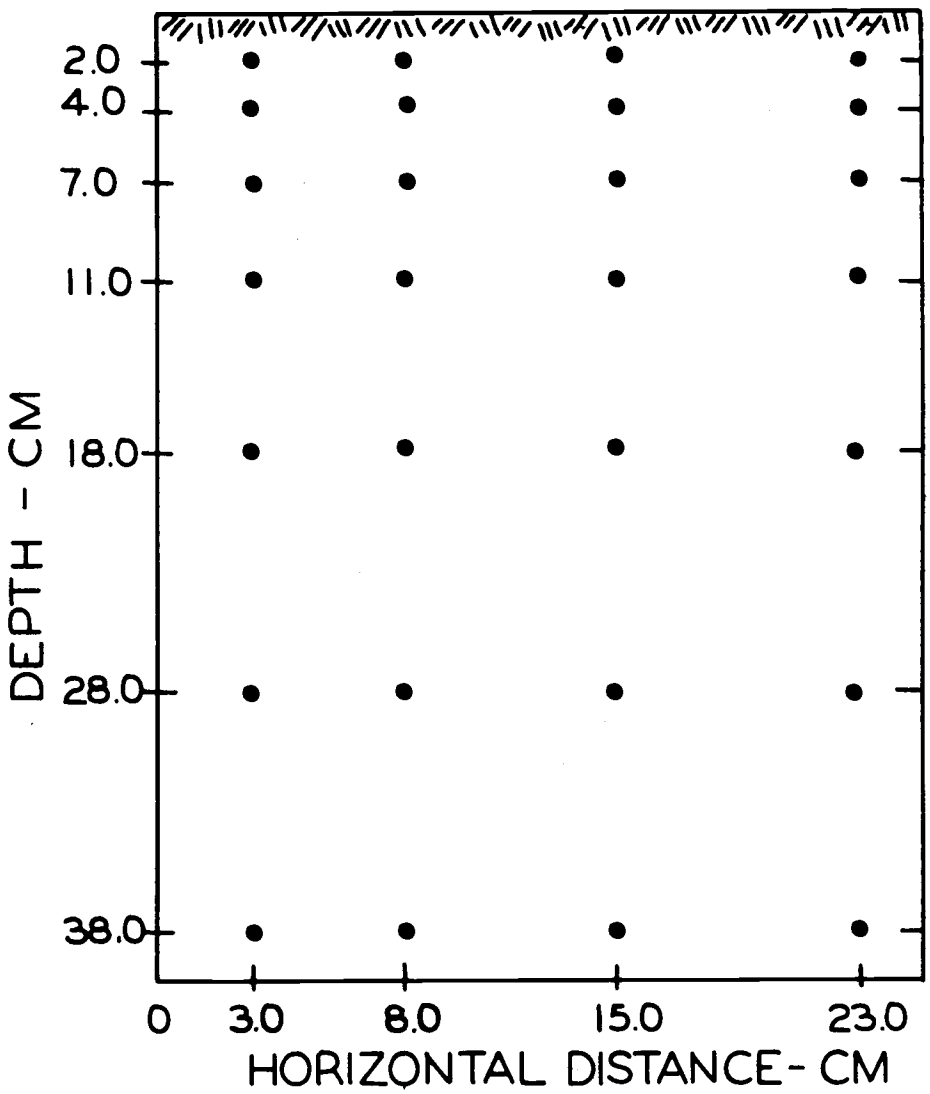

Figure 35. Positions at which temperature measurements in glass bead samples were made. The sample was contained in a box of dimensions 40 x 25 x 4 cm.

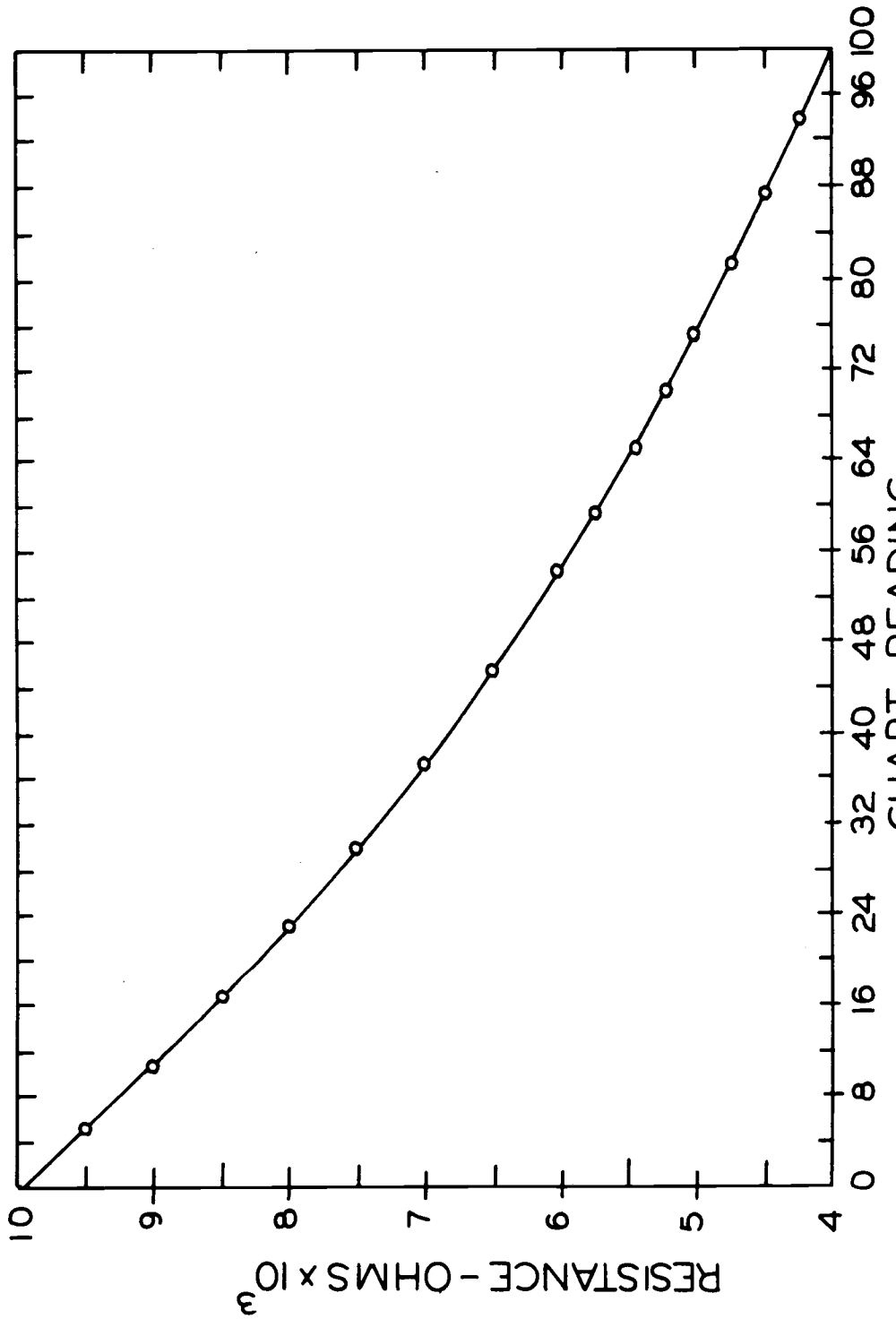

Figure 36. The calibration curve for the temperature recorder, showing the relation between chart reading and resistance.

Table 6. A sample of tables prepared for each group of thermistors to convert chart reading to temperature.

Chart Reading	Temperature °C				
	0.00	0.2	0.4	0.6	0.8
0	24.78	24.85	24.92	24.99	25.06
1	25.13	25.20	25.27	25.35	25.42
2	25.49	25.56	25.63	25.70	25.77
3	25.84	25.91	25.99	26.06	26.13
4	26.20	26.27	26.34	26.41	26.48
5	26.55	26.63	26.70	26.77	26.84
6	26.91	26.98	27.05	27.12	27.20
7	27.27	27.34	27.41	27.48	27.55
8	27.62	27.69	27.76	27.84	27.91
9	27.98	28.05	28.12	28.19	28.26
10	28.33	28.41	28.48	28.55	28.62
11	28.69	28.76	28.83	28.90	28.97
12	29.05	29.12	29.19	29.26	29.33
13	29.40	29.47	29.54	29.61	29.69
14	29.76	29.83	29.90	29.97	30.04
15	30.11	30.18	30.26	30.33	30.40
16	30.47	30.54	30.61	30.68	30.75
17	30.82	30.90	30.97	31.04	31.11
18	31.18	31.25	31.32	31.39	31.46
19	31.54	31.61	31.68	31.75	31.82
20	31.89	31.96	32.03	32.11	32.18

Water Content Measurements

Changes in water content were monitored with a gamma beam attenuation system. The method is based on Beer-Lambert's law which states that when a beam of monochromatic radiation, previously rendered plane parallel, enters an absorbing medium at right angles to the plane, the decrease in radiation intensity is an exponential function of the mass absorption coefficient μ, the density ρ, and the

thickness x of the absorbing material. The relation between incident and transmitted radiation intensities in terms of μ, ρ and x is indicated as

$$I = I_0 e^{-\mu\rho x}, \tag{15}$$

where I is the transmitted intensity and I_0 is the incident intensity.

In this experiment where the gamma beam was passed through the box containing moist beads, Beer-Lambert's law becomes

$$I = I_0 e^{-(\mu_w \theta + \mu_s \rho_s)x - \mu_c \rho_c x_c}, \tag{16}$$

where

I = transmitted radiation intensity,

I_0 = incident radiation intensity,

e = base of natural logarithm,

μ_w = mass absorption coefficient for water (cm^2/gm),

μ_s = mass absorption coefficient for dry beads (cm^2/gm),

μ_c = mass absorption coefficient for the container material (cm^2/gm),

θ = moisture content (gm/cm^3),

ρ_s = bulk density of beads (gm/cm^3),

ρ_c = bulk density of the container material (gm/cm^3),

x = sample thickness (cm), and

x_c = thickness of the container (cm).

In Equation (16), the transmitted intensity I is a function of the moisture content θ, since all other parameters are fixed quantities which depend upon the properties of the material and the source. The change in water content, θ, at any point in the column and at any time t, can be obtained, using Equation (16), as follows:

At time $t = t_1$,

$$I_1 = I_0 e^{-(\mu_s \rho_s + \mu_w \theta_1)x - \mu_c \rho_c x_c}, \tag{17}$$

and at any time $t = t_2$,

$$I_2 = I_0 e^{(-\mu_s \rho_s + \mu_w \theta_2)x - \mu_c \rho_c x_c}. \tag{18}$$

Division of Equation (18) by Equation (17) yields

$$\frac{I_2}{I_1} = e^{-(\theta_2 - \theta_1)\mu_w x}, \tag{19}$$

$$\ln \frac{I_2}{I_1} = -\mu_w x(\theta_2 - \theta_1),$$

$$\Delta\theta = \theta_2 - \theta_1 = -\frac{1}{\mu_w x} \ln \frac{I_2}{I_1},$$

and

$$\Delta\theta = \frac{1}{\mu_w x} \ln \frac{I_1}{I_2}, \tag{20}$$

where

I_1 = transmitted radiation intensity at time t_1,

I_2 = transmitted radiation intensity at time t_2, and

$\Delta\theta$ = fractional change in water content (gr/cm^3).

Substituting the value of μ_w for Americium (Am^{241}), which was determined to be 0.1947 cm^2/gm, and $x = 4$ cm, the width of containers, Equation (20) becomes

$$\Delta\theta = 1.351 \ln \frac{I_2}{I_1}. \tag{21}$$

Equipment

The gamma attenuation equipment consisted of a source of low energy γ-radiation, a scintillation detector, a single channel gamma spectrometer, a printer, and an automatic scanner.

The source of low energy gamma radiation employed was Am^{241} (229 mc). Am^{241} emits near monoenergetic gamma rays with approximately 60% of its radiation having an energy of 0.061 Mev. With the low energy output, a minimum of shielding is required. The optimum sample thickness for this energy is four to five centimeters.

The gamma emission was monitored with a scintillation detector

which consists of three parts: a thallium activated sodium iodide crystal three inches in diameter and two inches thick, a photomultiplier tube, and a pre-amplifier. A Hewlett-Packard single channel gamma spectrometer was employed for counting the radiation detected by the scintillation tube. This spectrometer consisted of a high voltage power supply (Model HP5551A) for the scintillation tube (Model HP 10602A) and a scaler, timer, and pulse height analyzer (Model HP 5201L). The output from the scaler was digitized and routed directly to a printer (Model HP 562AR). A digital to analog converter (Model HP 580A) was included which allowed a stripchart recording with a Heathkit (Model EUW-20A) recorder when desired. The pulse height analyzer was set to detect transmitted gamma radiation of 0.061 ± 0.015 Mev.

The automatic scanner was designed to move the source detector assembly in a programmed geometric pattern with relation to the sample box.

The source and the detector were assembled in a rigid frame to maintain the correct orientation of the collimated beam of gamma rays. The assembly was mounted on a movable plate supported by split-bearings and two parallel shafts. This plate could be moved horizontally in either direction by a motor driven lead screw controlled by a helical path pin programmer. By proper placement of program pins, the scanner could be commanded to stop the source-

detector assembly at any desired one cm increment along the horizontal axis of the sample box.

The sample box was mounted on a platform suspended by two vertical lead screws and two shaft and bearing assemblies. This platform could be raised or lowered by a second motor and chain drive connected to the lead screws. The platform position was also controlled by a programmer similar to that described above.

The horizontal and vertical motions were interconnected by limit switches and various relays to automatically scan according to a preset program. A gating circuit was connected to the scaler-timer starting a preset count at the desired positions. Another timer circuit allowed repetition of the scanning pattern at predetermined intervals.

Gamma attenuation readings were taken at predetermined points at regular intervals. The position of these points are indicated in Figure 37.

Results and Discussion

Experiments I and V: Air Dry; 53-74 Microns and 149-210 Microns

The temperature as a function of time for several depths is shown in Figures 38 and 39 for the 53-74 μ size glass beads and in Figures 40 and 41 for the 149-210 μ size glass beads. Results of

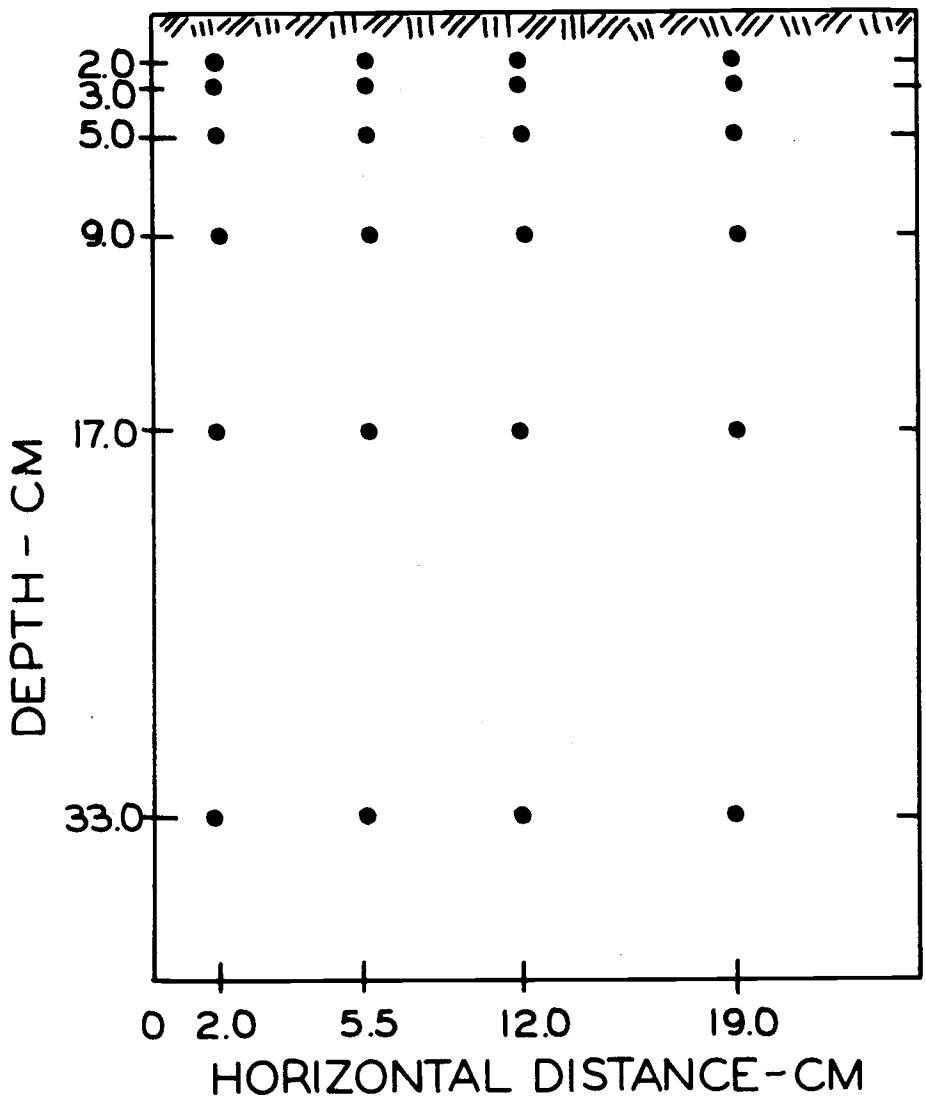

Figure 37. Positions at which water content measurements were made.

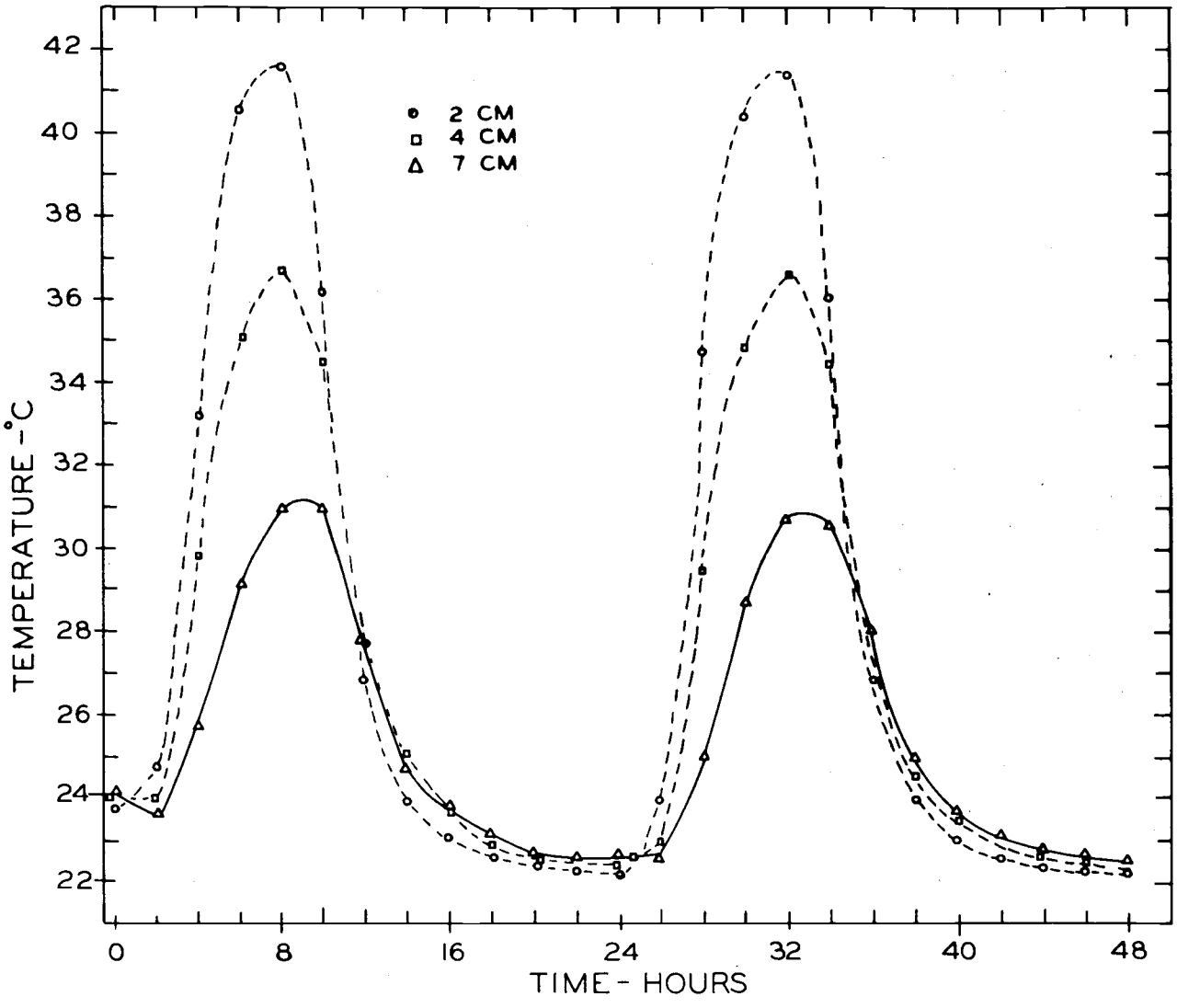

Figure 38. Diurnal temperature variations in air dry column of the 53-74 microns size glass beads at 2 cm, 4 cm, and 7 cm depths. Experiment I.

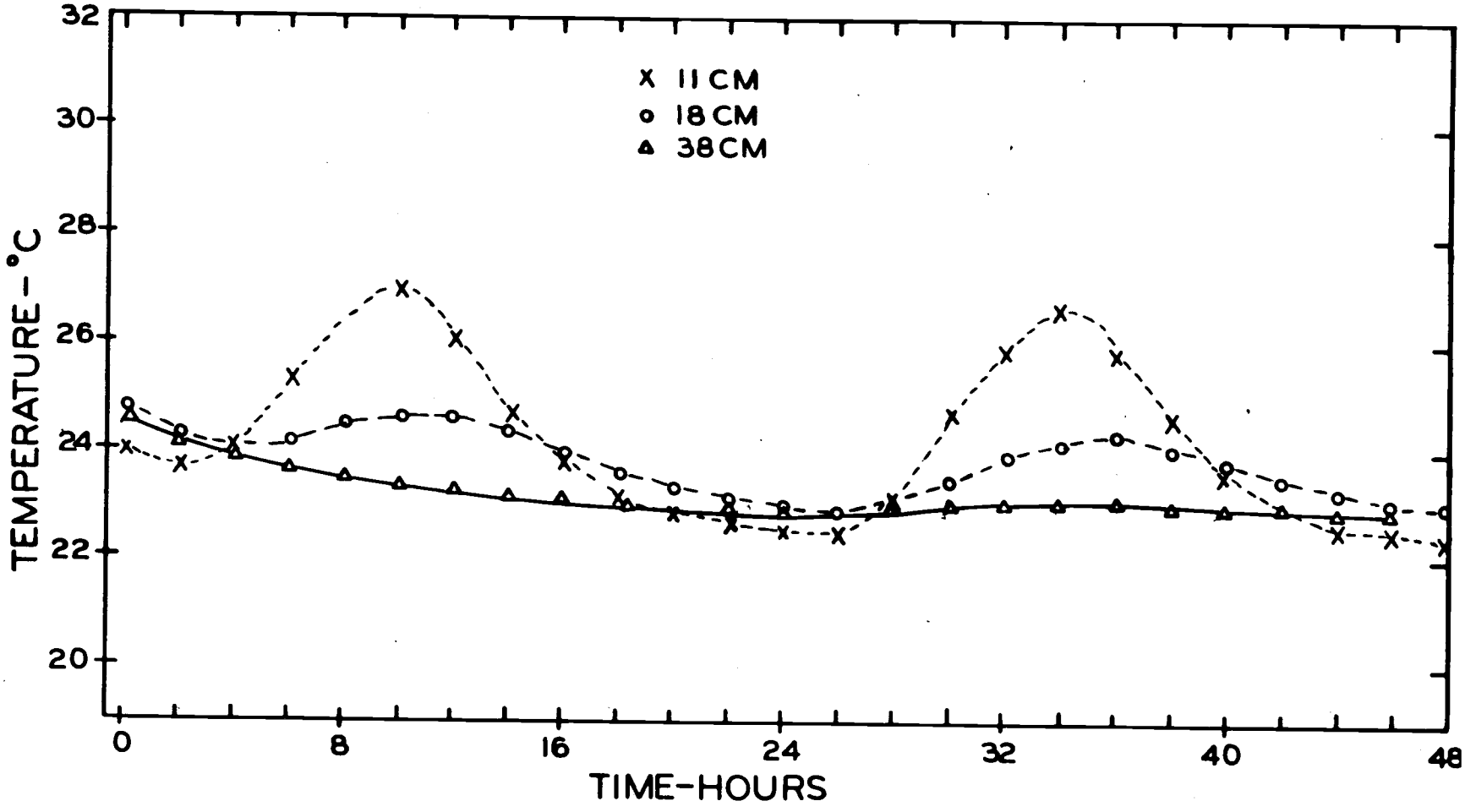

Figure 39. Diurnal temperature variations in air dry column of the 53-74 microns size glass beads at 11 cm, 18 cm, and 38 cm depths. Experiment I.

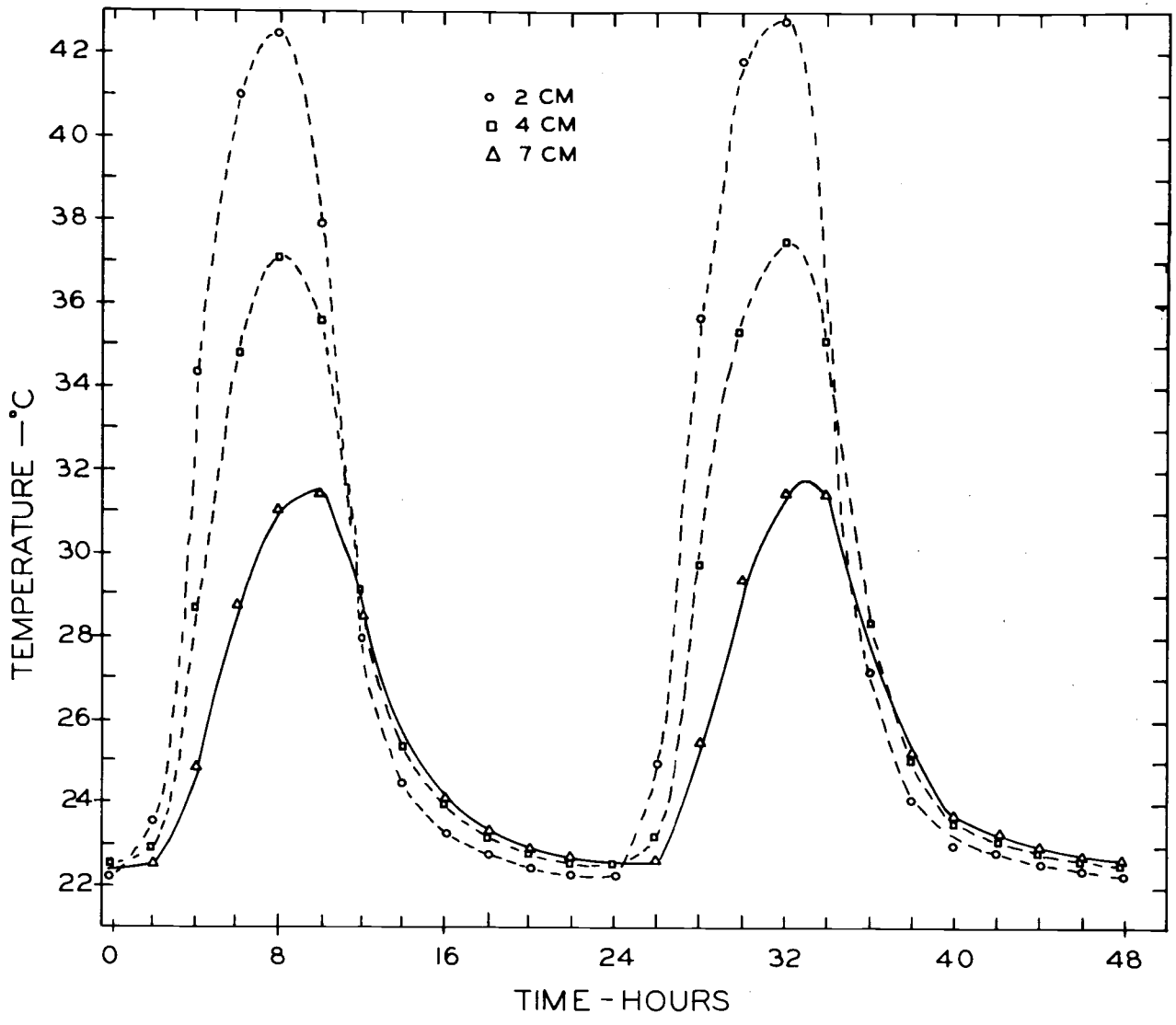

Figure 40. Diurnal temperature variations in air dry column of the 149-210 microns size glass beads at 2 cm, 4 cm, and 7 cm depths. Experiment V.

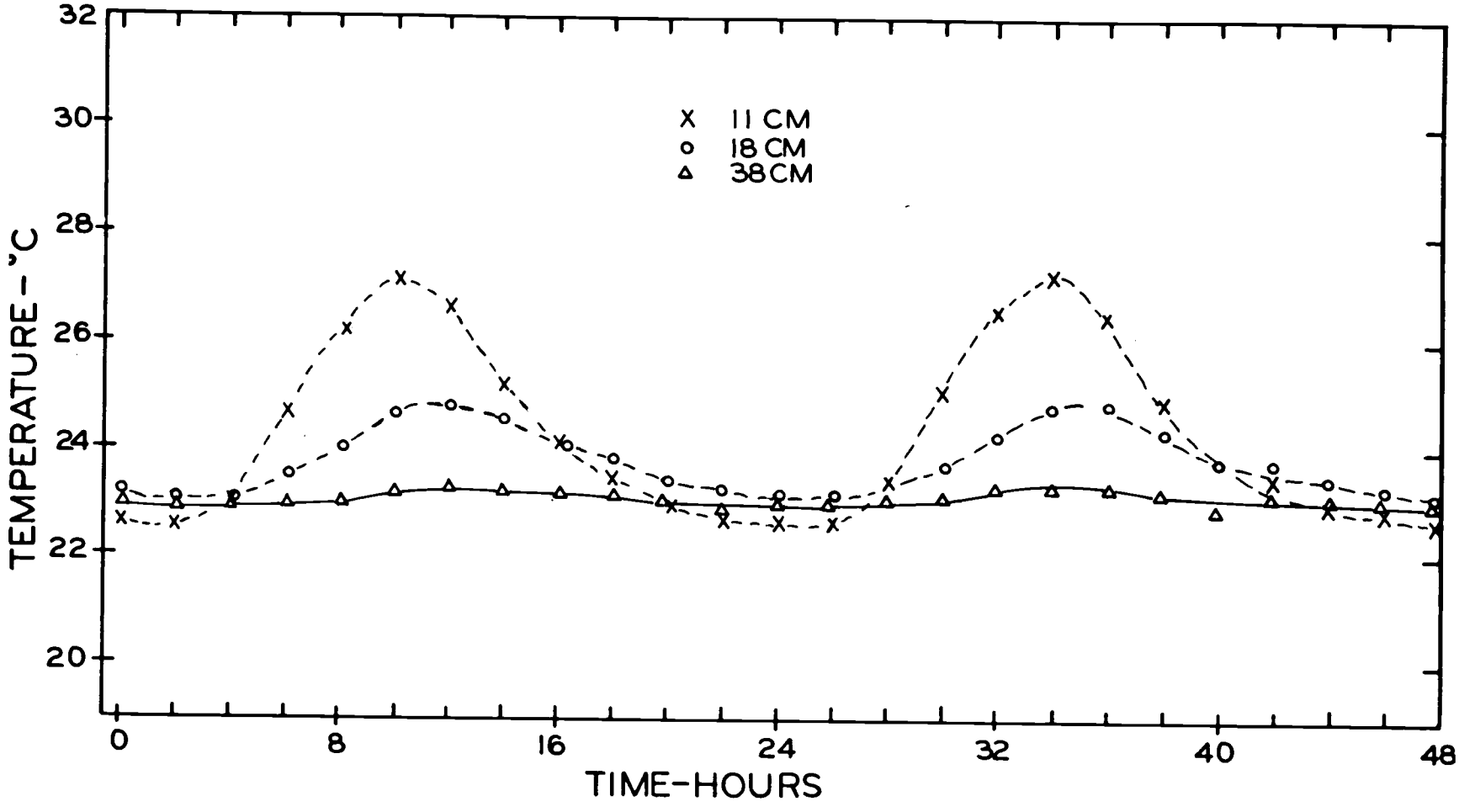

Figure 41. Diurnal temperature variations in air dry column of the 149-210 microns size glass beads at 11 cm, 18 cm, and 38 cm depths. Experiment V.

these experiments are summarized in Table 7. The maximum temperature and the time of its occurrence, at zero depth, were estimated from temperature versus depth and temperature versus time plots.

Table 7. Maximum temperature (°C) and time lag (minutes) observed for air dry samples subjected to a diurnal temperature cycle.

Depth	Maximum Temperature		Time Lag	
	53-74 μ	149-210 μ	53-74 μ	149-210 μ
cm	°C	°C	min	min
0	51.0	52.0		
2	41.6	42.7	33.0	33.0
4	36.6	37.3	57.0	57.0
7	31.2	31.1	129.0	129.0
11	26.9	27.1	189.0	189.0
18	24.5	24.9	270.0	267.0
38	23.0	23.1		

These results show that the two size fractions behave in an identical manner. The explanation of this similarity is that the thermal conductivity of the glass bead beds is the same irrespective of the size of the glass beads (Figure 30). Thermal conductivity as a function of particle size was discussed in an earlier chapter.

Experiments II and VI: Saturated; 53-74 Microns and 149-210 Microns

In these experiments saturated samples of glass beads were used. The columns were kept saturated throughout the experiments by

adding water to the surface as it dried out. The temperature as a function of time for various depths is shown in Figures 42 and 43 for the 53-74 μ size glass beads and in Figures 44 and 45 for the 149-210 μ size glass beads. Table 8 summarizes the results of these experiments. The maximum temperature at the surface of the column and the time of its occurrence were estimated by extrapolating temperature versus depth and temperature versus time curves.

Table 8. Maximum temperature (°C) and time lag (minutes) observed for saturated samples subjected to a diurnal temperature cycle.

Depth	Maximum Temperature		Time Lag	
	53-74 μ	149-210 μ	53-74 μ	149-210 μ
cm	°C	°C	min	min
0	33.0	33.5		
2	29.6	30.3	36	36
7	26.8	27.2	126	126
18	24.0	24.0	300	300
38	22.5	22.8		

These results indicate that the two size fractions behave in an identical manner. Since the thermal conductivity of saturated beads showed no textural differences (Figure 30), no difference in behavior was expected.

The maximum temperatures obtained near the surface were much higher in air dry samples than in saturated samples. This is the result of the high heat capacity and high thermal conductivity of

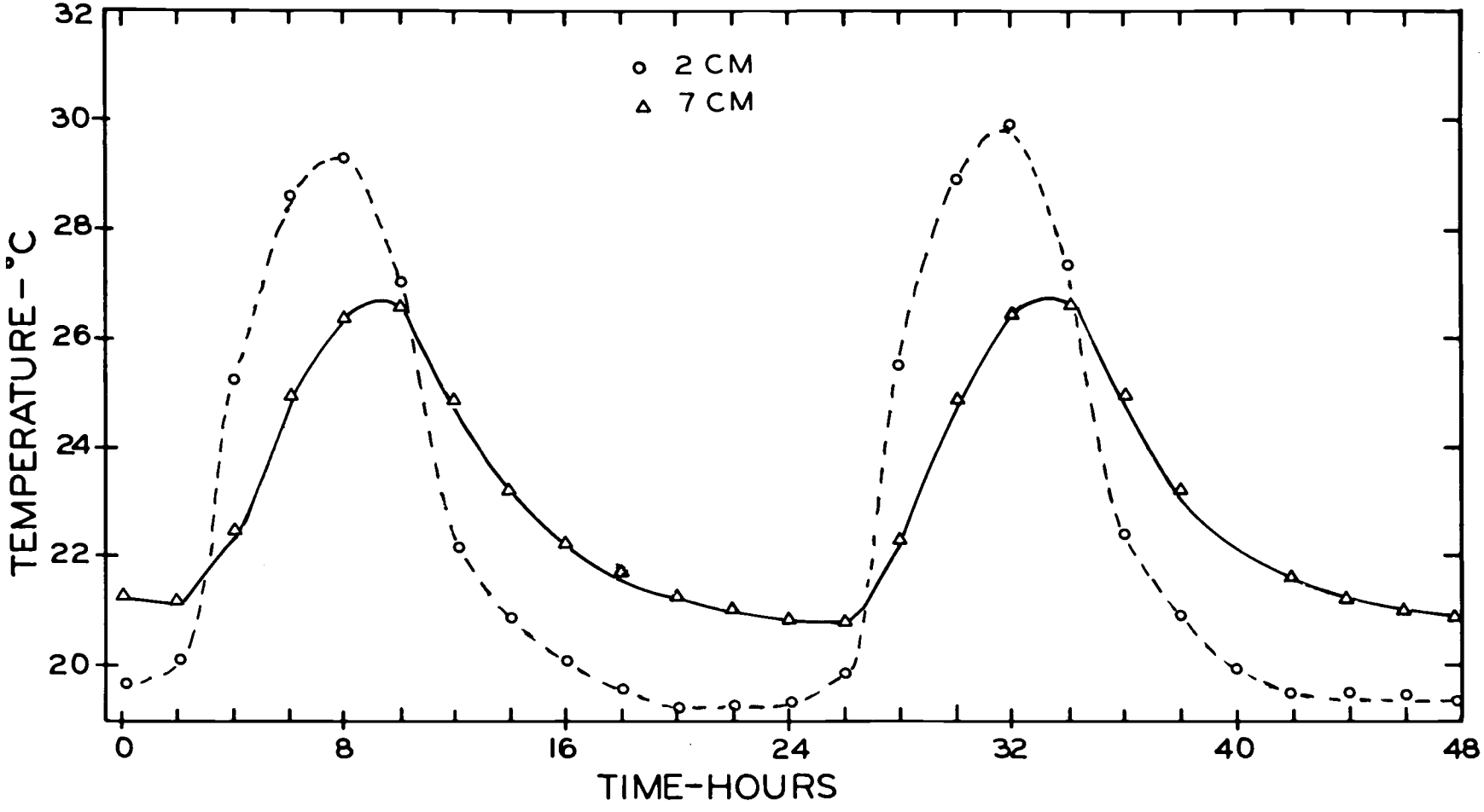

Figure 42. Diurnal temperature variations in saturated column of the 53-74 microns size glass beads at 2 cm, and 7 cm depths. Experiment II.

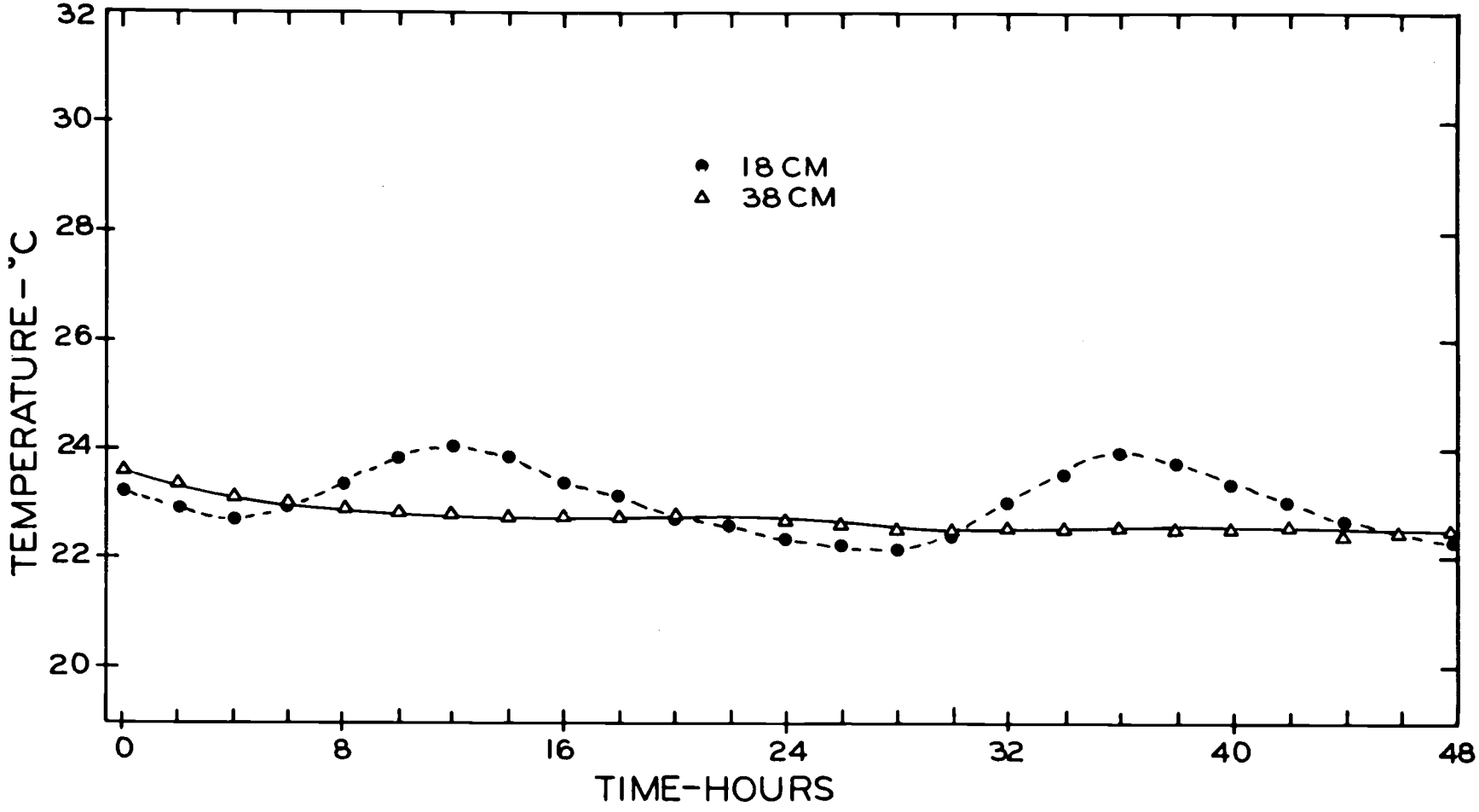

Figure 43. Diurnal temperature variations in saturated column of the 53-74 microns size glass beads at 18 cm, and 38 cm depths. Experiment II.

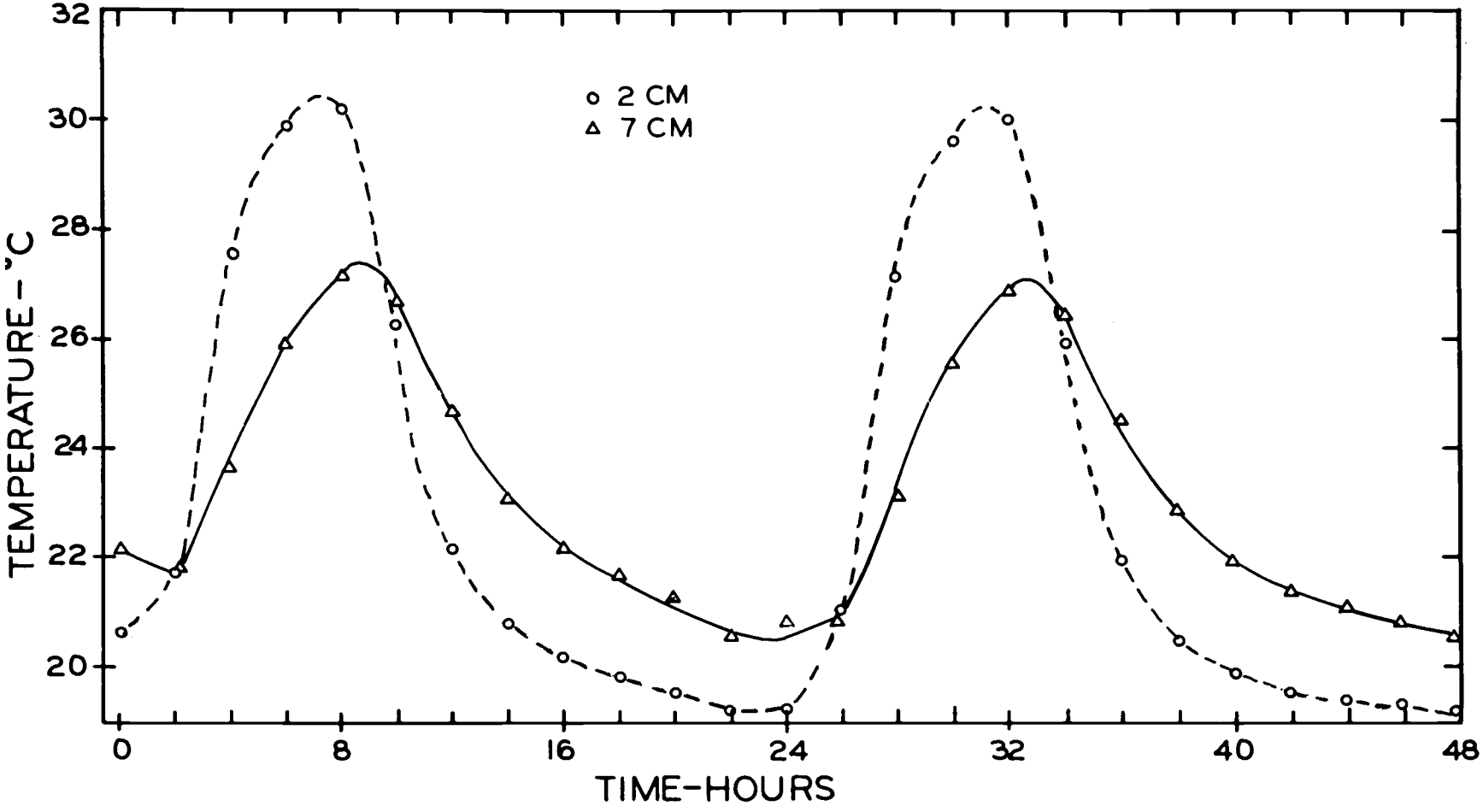

Figure 44. Diurnal temperature variations in saturated column of the 149-210 microns size glass beads at 2 cm, and 7 cm depths. Experiment VI.

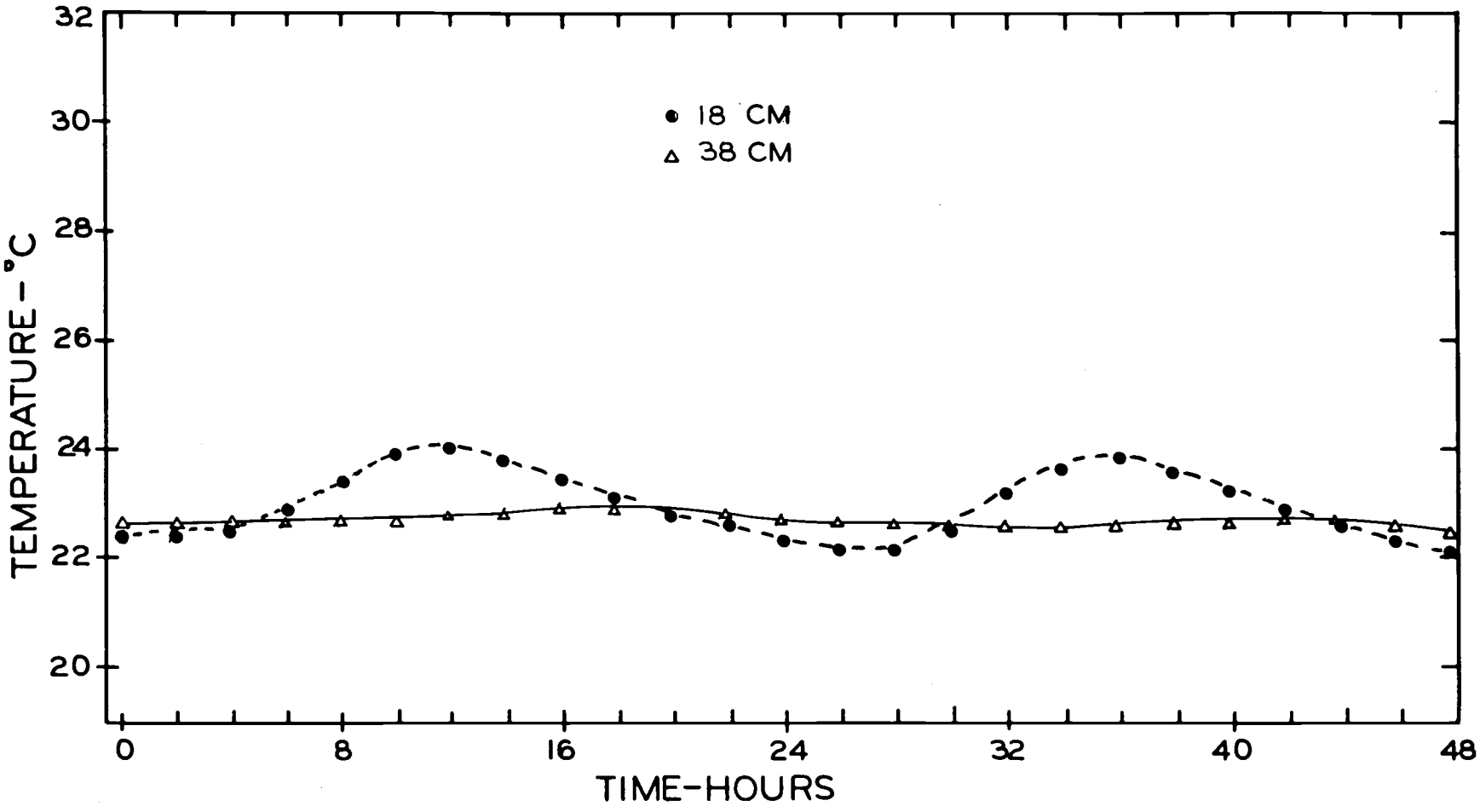

Figure 45. Diurnal temperature variations in saturated column of the 149-210 microns size glass beads at 18 cm, and 38 cm depths. Experiment VI.

moist beads. Heat capacity, C, of soil is given by,

$$C = x_s C_s + x_w C_w + x_a C_a \quad (cal/cm^3\ °C), \tag{22}$$

where x is the volume fraction, C is the heat capacity, and subscripts s, w, and a denote solid, liquid, and gas phases. Since C_a is very small, the term $x_a C_a$ is usually neglected. Heat capacities of dry and wet (saturated) glass beads are listed in Table 9. Thermal conductivities of dry and saturated samples of glass beads, according to the thermal conductivity experiments, are, also, given in this table.

Table 9. Values of parameters used in the calculations of the temperature (°C) at a depth of 2 cm in the 53-74 microns size glass bead beds.

Parameter	Value
λ_{wet}	20.2×10^{-4} cal/cm sec °C
λ_{dry}	3.68×10^{-4} cal/cm sec °C
C_{wet}	0.676 cal/cm^3 °C
C_{dry}	0.276 cal/cm^3 °C
D_{wet}	9.067 cm
D_{dry}	6.056 cm
$\frac{\lambda}{C}$ wet	$.299 \times 10^{-2}$ cm^2/sec
$\frac{\lambda}{C}$ dry	$.133 \times 10^{-2}$ cm^2/sec

The ratio $\frac{\lambda}{C}$ is a measure of time lag. Table 9 indicates that this ratio is higher for saturated samples. This means that the rate of change of temperature at any depth in the column is faster in saturated samples. Therefore, smaller lag times are expected in saturated glass bead beds than in dry beds. The results presented in Tables 7 and 8 do not show this.

Analysis of the Experimental Results

The equation for temperature as a function of time and depth is (Van Wijk and de Vries, 1966)

$$T_{(Z,t)} = T_a + A_0 \exp(-\frac{Z}{D}) \sin(\omega t - \frac{Z}{D}), \qquad (23)$$

where

$T_{(Z,t)}$ = temperature at any depth Z at time t (°C),

T_a = average temperature in the column during a period (°C),

A_0 = surface amplitude (°C),

D = damping depth (cm),

ω = angular frequency = 2π x (frequency of temperature variation) = 7.27×10^{-5}/sec for the diurnal variation,

Z = depth (cm), and

t = time (sec). The zero point of the time scale is chosen such that at t = 0 the surface is at the average temperature.

The constant D is related to the thermal properties of the medium and the angular frequency as follows:

$$D = \left(\frac{2\lambda}{C\omega}\right)^{1/2}, \tag{24}$$

where

λ = thermal conductivity of the medium (cal/cm sec °C), and

C = heat capacity of the medium (cal/cm^3 °C).

The time of occurrence of the maximum temperature at any depth can be obtained from Equation (23). Since T_a, A_0, and D are constant at any depth, the differentiation of Equation (23) with respect to time yields:

$$\frac{dT}{dt} = \exp\left(-\frac{Z}{D}\right)\omega \cos\left(\omega t - \frac{Z}{D}\right). \tag{25}$$

At the maximum temperature, $\frac{dT}{dt} = 0$. Therefore, to satisfy this condition:

$$\cos\left(\omega t_{max} - \frac{Z}{D}\right) = 0,$$

or

$$\omega t_{max} - \frac{Z}{D} = 1.5708, \tag{26}$$

where t_{max} is the time at which the temperature reaches its maximum value at depth Z.

Using Equation (23) and (24), the temperature as a function of

time was calculated for a diurnal cycle at a depth of 2 cm and compared with the experimental results obtained for the two size fractions. Values of A_0 (surface amplitude) used were 8.5°C for the saturated samples and 16.0°C for the air dry samples. Since amplitude, $A_0 e^{-Z/D}$, is a function of depth Z, A_0 was determined by extrapolating amplitude versus depth plots. The temperature amplitude, by definition is the difference between maximum and average temperatures. At any depth Z, the average temperature was taken to be the mean of the observed values of maximum and minimum temperature for 14 hour periods.

For the angular frequency a period of 14 hours was used. The period was chosen larger than the 12 hour cycle used for the heating element to allow for the deviation of the imposed radiation cycle from a true sinusoidal wave. Values of the other parameters used are shown in Table 9. Calculated and observed temperature versus time plots at a depth of 2 cm are shown in Figures 46 (saturated samples) and 47 (air dry samples).

Examination of these figures indicate that estimated temperatures for saturated glass beads agree quite well with the observed values. The temperature versus time plots indicate that observed temperatures are lower than calculated values in air dry samples of either size glass beads. This discrepancy appears to be the result of high surface reflectance of air dry glass bead beds.

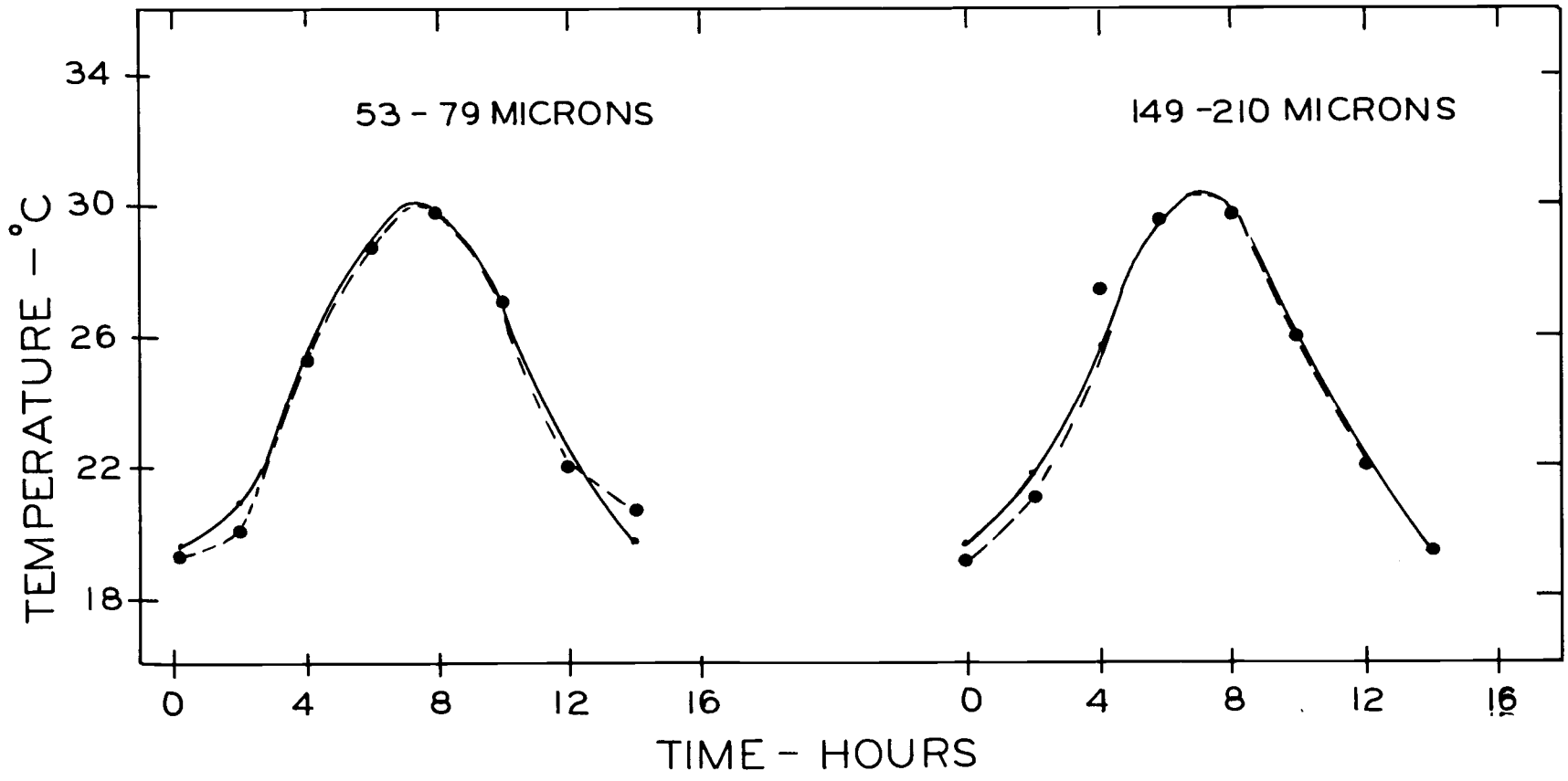

Figure 46. Comparison of the observed (-O-) and the calculated (—) temperature as a function of time at a depth of 2 cm in saturated samples of glass beads. The theoretical temperatures were estimated using a period of 14 hours.

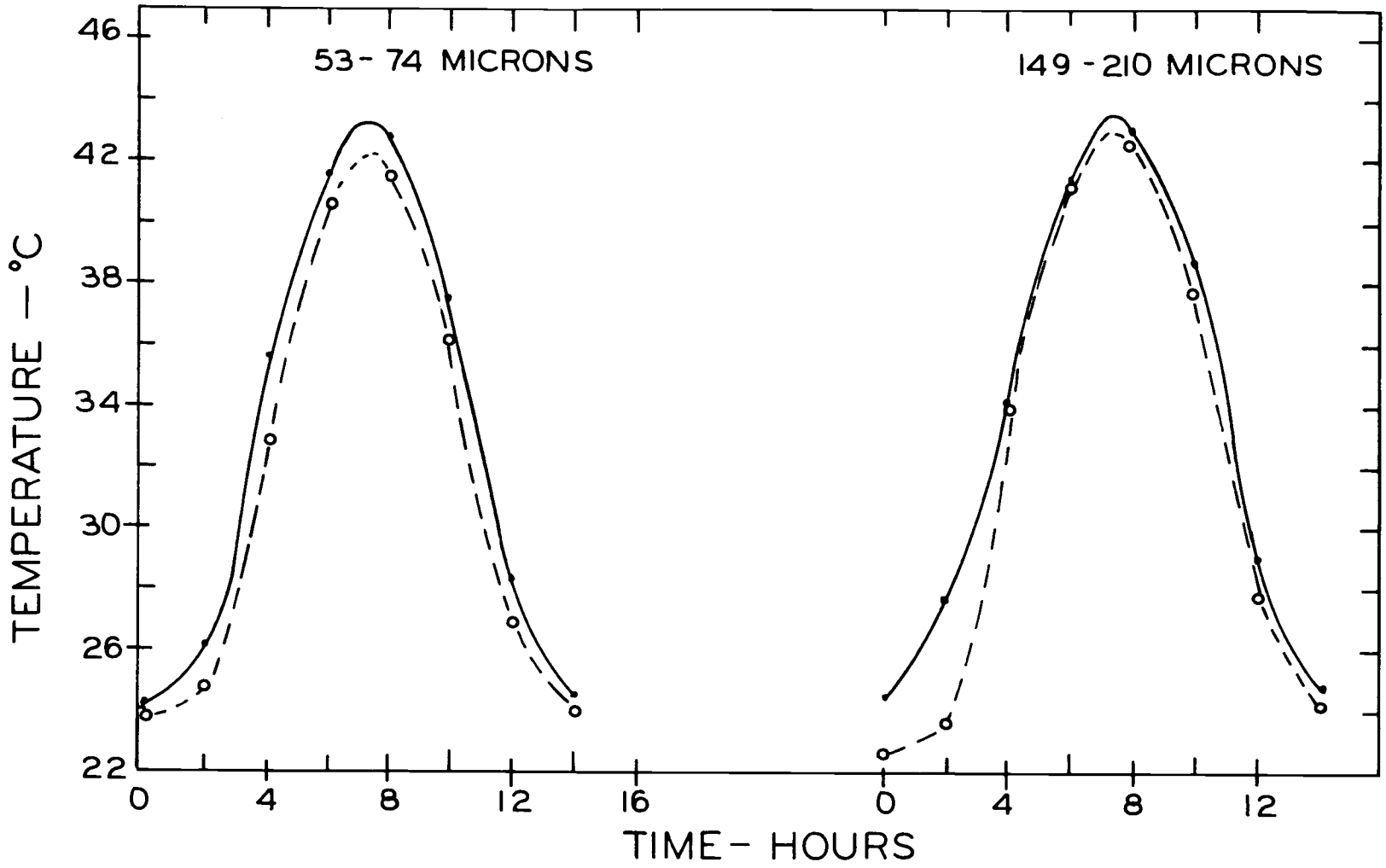

Figure 47. Comparison of the observed (-O-) and the calculated (—) temperature as a function of time at a depth of 2 cm in air dry samples of glass beads. The theoretical temperatures were estimated using a period of 14 hours.

Since the reflection coefficient of a material increases with temperature, this difference in estimated and observed temperatures tend to increase near the maxima. The fact that heat loss is determined by surface temperature and thermal gradients accounts for the discrepancy in temperature versus time plots during cooling cycles.

The saturated glass beads have a low coefficient of reflection and high heat capacity. Both of these factors result in an increased influx at the surface and low net heat loss.

Using angular frequency based on a 14 hour period, maximum temperatures and time lags for each size fraction were computed at various depths with Equations (23), (24), and (26). The values obtained are listed in Tables 10 and 11.

Table 10. Calculated maximum temperature (°C) and time lag (minutes) for air dry samples, based on a 14 hour period.

Depth	Maximum Temperature		Time Lag	
	53-74 μ	149-210 μ	53-74 μ	149-210 μ
cm	°C	°C	min	min
0	53.6	53.7		
2	42.6	43.0	58	58
4	37.2	37.4	116	116
7	31.7	31.9	203	203
11	26.9	27.0	319	319
18	24.3	24.3	522	522
38	23.0	23.0		

Table 11. Calculated maximum temperature (°C) and time lag (minutes) for saturated samples, based on a 14 hour period.

Depth	Maximum Temperature		Time Lag	
	53-74 μ	149-210 μ	53-74 μ	149-210 μ
cm	°C	°C	min	min
0	32.8	33.2		
2	30.1	30.3	38	38
7	26.3	26.9	135	135
18	23.8	23.9	346	346
38	22.7	22.7		

The results in Tables 10 and 11 when compared with that of the observed data (Tables 7 and 8) indicate that estimated peak temperatures obtained at shallow depths for air dry samples are higher than experimental values. Deep in the sample beds, where surface temperature fluctuations are not felt, the observed and the calculated peak temperatures are nearly the same. At 18 cm depth and below the maximum temperature tend to approach an average value of room temperature.

The difference in time lag for air dry samples can be clearly explained with Equations (24) and (26). Solving for t_{max}, these equations yield:

$$t_{max} = \frac{1.5708}{\omega} + \frac{Z}{(\frac{2\lambda\omega}{C})^{1/2}} . \qquad (27)$$

Time lag is calculated according to time of occurrence of the

maximum temperature. This means that the value of the sine function in Equation (23) should be constant and equal to 1.5708. Different values, however, were obtained for the sine function when observed values of parameters Z, λ, ω, and D were substituted. This, results in the above observed discrepancy in time lags for air dry glass beads.

In saturated beds the observed time lags and the maximum temperatures agree closely with the calculated values for the obvious reasons of high heat capacity of moist beads and low net loss of heat at the surface of the beds.

Experiment III and VII: Initially Saturated; 53-74 Microns and 149-210 Microns

These experiments were conducted with initially saturated samples, which were allowed to dry. No water was added during the course of the experiments. The temperature profiles for the 52-74 μ size glass beads are shown in Figures 48 and 49 and for the 149-210 μ size glass beads in Figures 50 and 51. The general trend of the temperature profiles is similar to that discussed earlier. A summary of daily maximum temperature and time lag is shown in Tables 12 and 13.

Table 12 shows that maximum temperatures at any depth during the first day are nearly the same as in experiments II and VI (Table 8). The maximum temperature obtained during each cycle increased during the course of the experiment. The two size fractions used, did

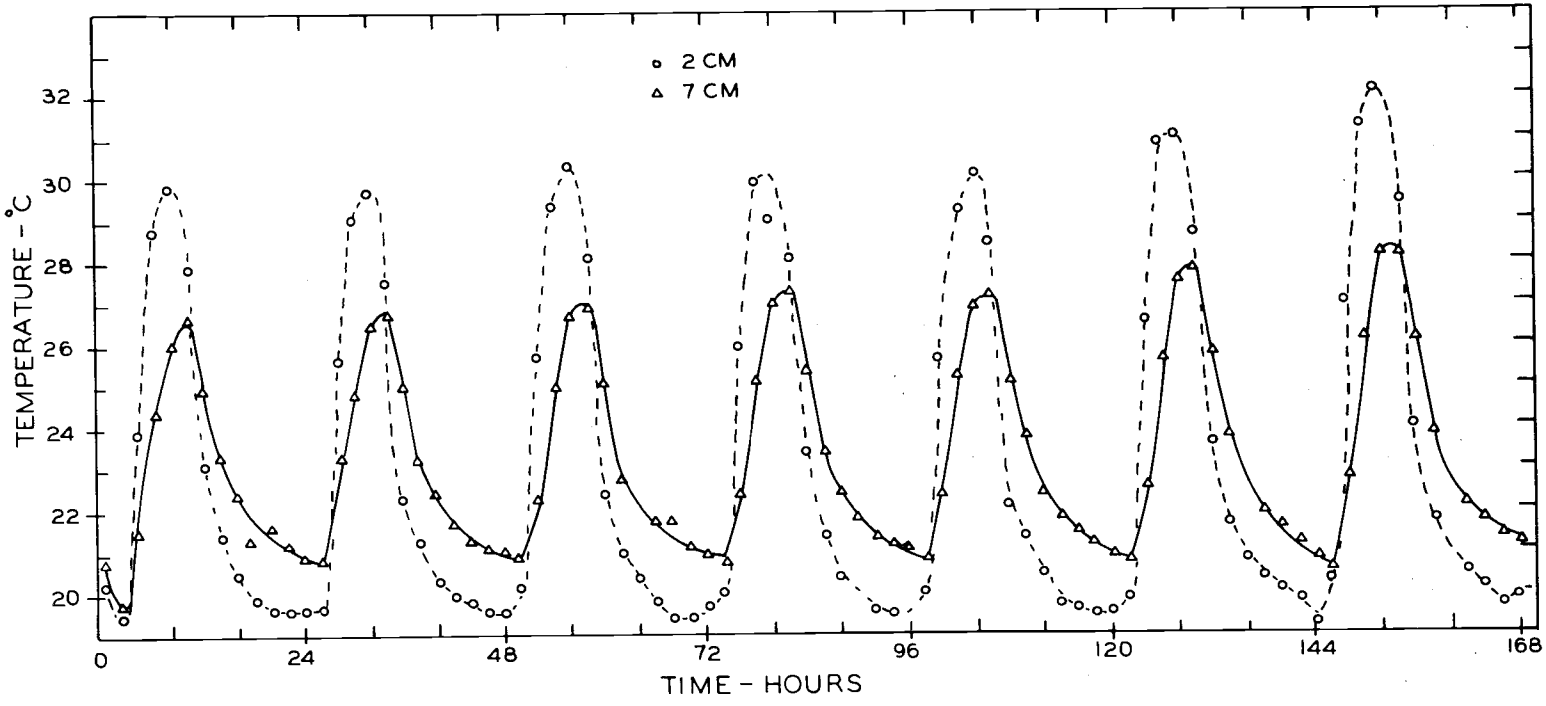

Figure 48. Diurnal temperature variations in initially saturated column of the 53-74 microns size glass beads at 2 cm, and 7 cm depths. Experiment III.

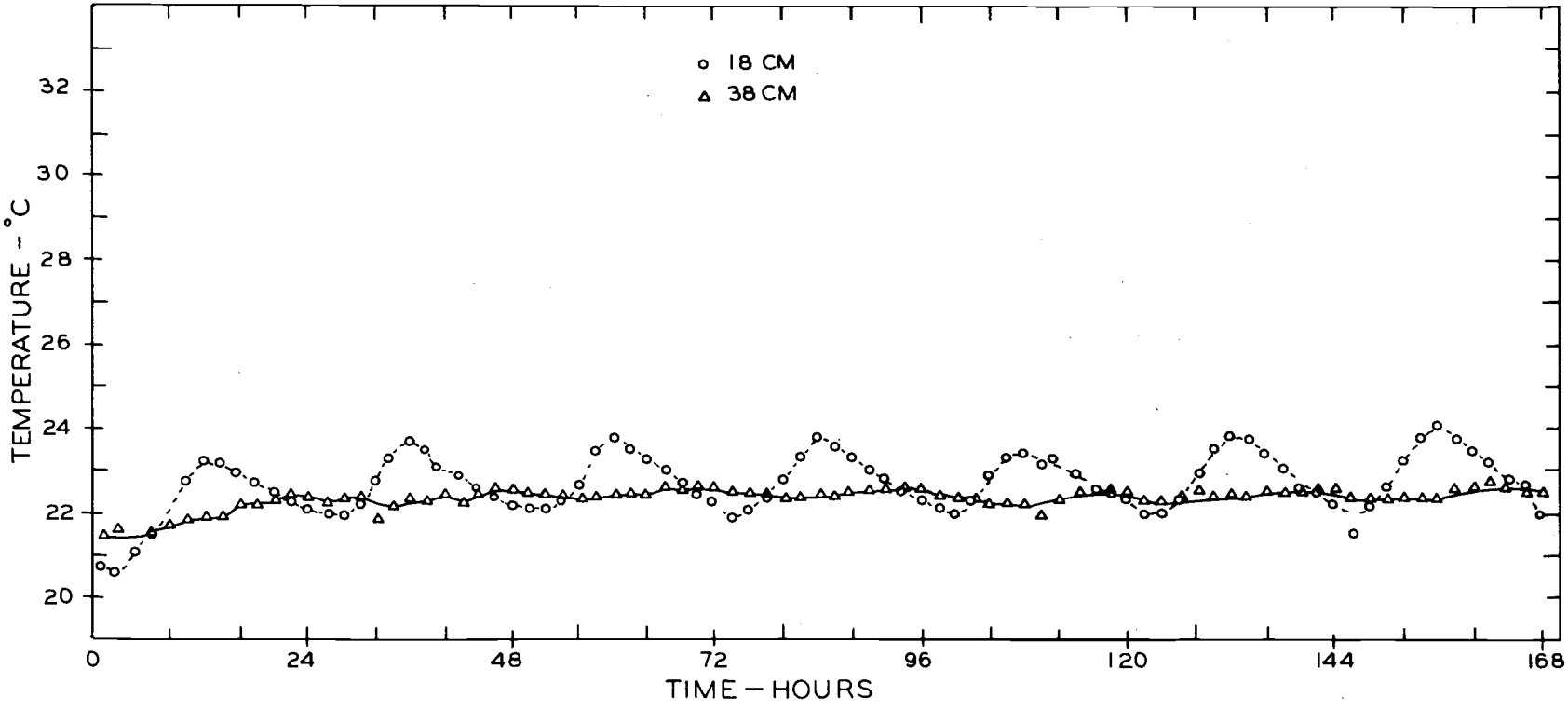

Figure 49. Diurnal temperature variations in initially saturated column of the 53-74 microns size glass beads at 18 cm, and 38 cm depths. Experiment III.

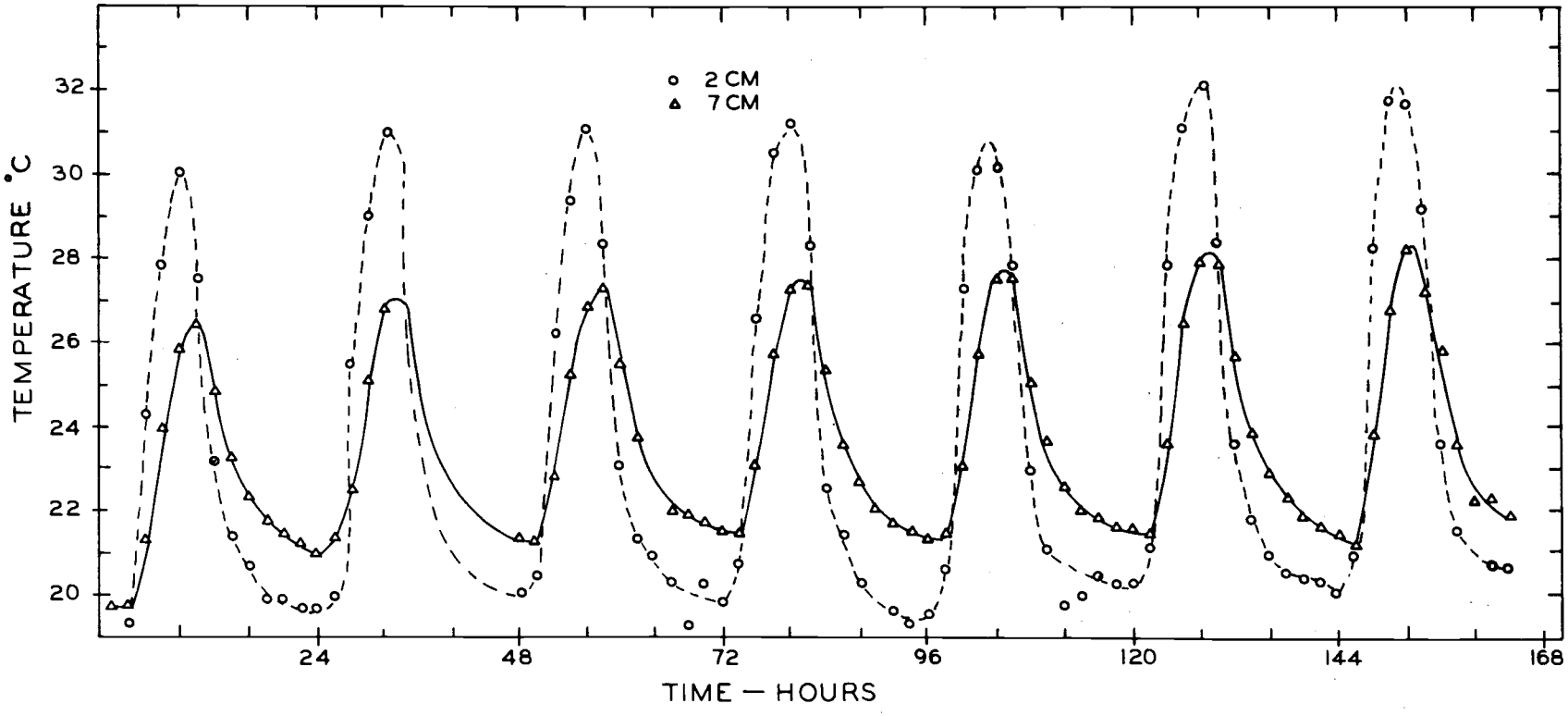

Figure 50. Diurnal temperature variations in initially saturated column of the 149-210 microns size glass beads at 2 cm, and 7 cm depths. Experiment VII.

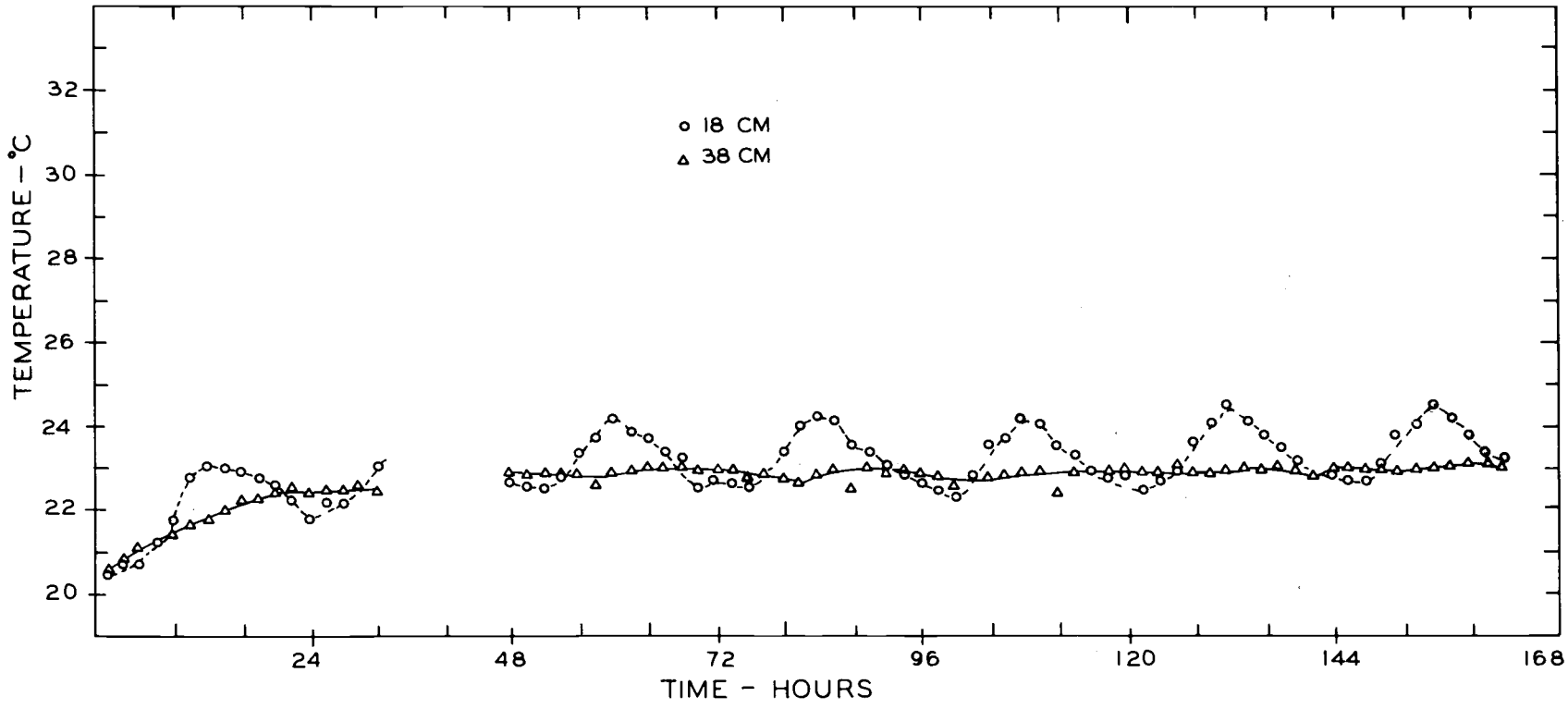

Figure 51. Diurnal temperature variations in initially saturated column of the 149-210 microns size glass beads at 18 cm, and 38 cm depths. Experiment VII.

not behave entirely the same. For the 149-210 μ material an increase in maximum temperature could be observed on the second day at a depth of 2 cm whereas for the 53-74 μ material an increase in maximum temperature was not observed until the sixth day.

Table 12. Maximum temperature in °C observed for the initially saturated columns subjected to a diurnal radiation cycle.

Day No.	Material	Depth (cm) 2	7	18	38
		°C	°C	°C	°C
1	53-74 μ	29.8	26.5	23.2	22.3
2		29.8	26.7	23.5	22.5
3		30.3	27.1	23.7	22.5
4		30.2	27.3	23.8	22.5
5		30.0	27.3	23.4	22.5
6		31.1	27.9	23.7	22.5
7		32.1	28.4	24.0	22.6
1	149-210 μ	30.0	26.5	23.0	22.5
2		31.1	27.3	---	23.0
3		31.1	27.3	24.1	23.0
4		31.2	27.6	24.2	23.0
5		31.0	27.8	24.2	22.9
6		32.1	28.2	24.4	23.0
7		32.2	28.4	24.5	23.0

The time lag (Table 13) shows a behavior identical to that observed in the first four experiments. The results show no effect of drying of the sample on the time lag in either size fraction.

Table 13. Time lag in minutes observed for the initially saturated columns subjected to a diurnal radiation cycle.

Day No.	Material	Depth (cm) 2	7	18
		min	min	min
1	53-74 μ	36	126	336
2		36	96	321
3		39	120	309
4		30	114	306
5		36	114	276
6		30	120	324
7		39	105	294
1	149-210 μ	36	126	306
2		--	---	---
3		36	126	291
4		24	99	294
5		30	105	321
6		30	120	324
7		39	104	324

Water content measurements were made at three hour intervals at depths of 2, 3, 5, 9, 17, and 33 cm. The percent change in amount of water present was calculated with Equation (21). Results of these measurements are shown in Figures 52 and 53 for the 53-74 μ size fraction and in Figures 54 and 55 for the 149-210 μ size fraction. These figures indicate an initially rapid decrease in water content at shallow depths. As the material dried the rate of water loss was slower for the finer material. The water content at the 17 cm depth and below remained essentially constant. This is more clearly demonstrated by Table 14 where the information on water loss is

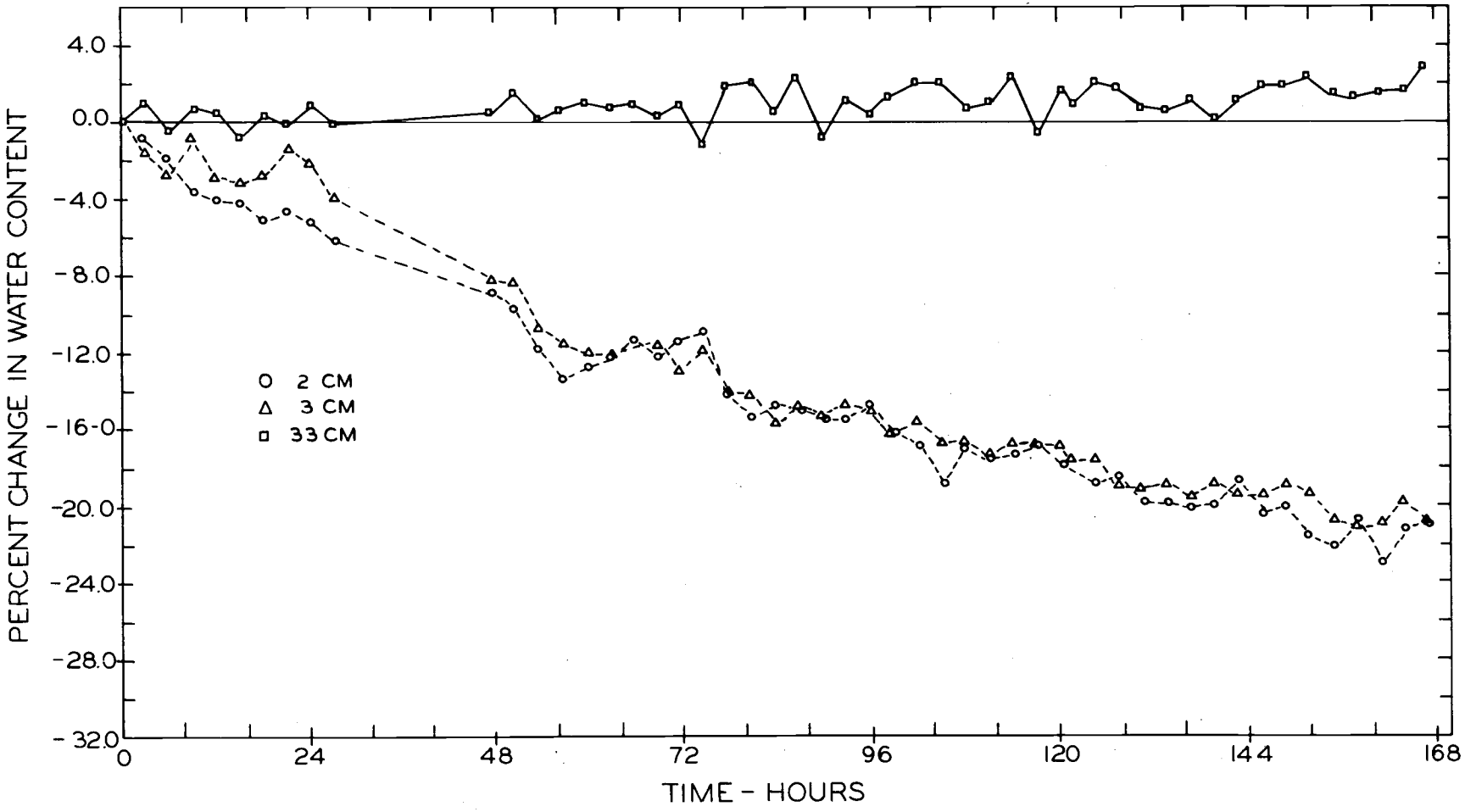

Figure 52. Percent change in water content as a function of time in initially saturated column of the 53-74 microns size glass beads at 2 cm, 3 cm, and 33 cm depths. Experiment III.

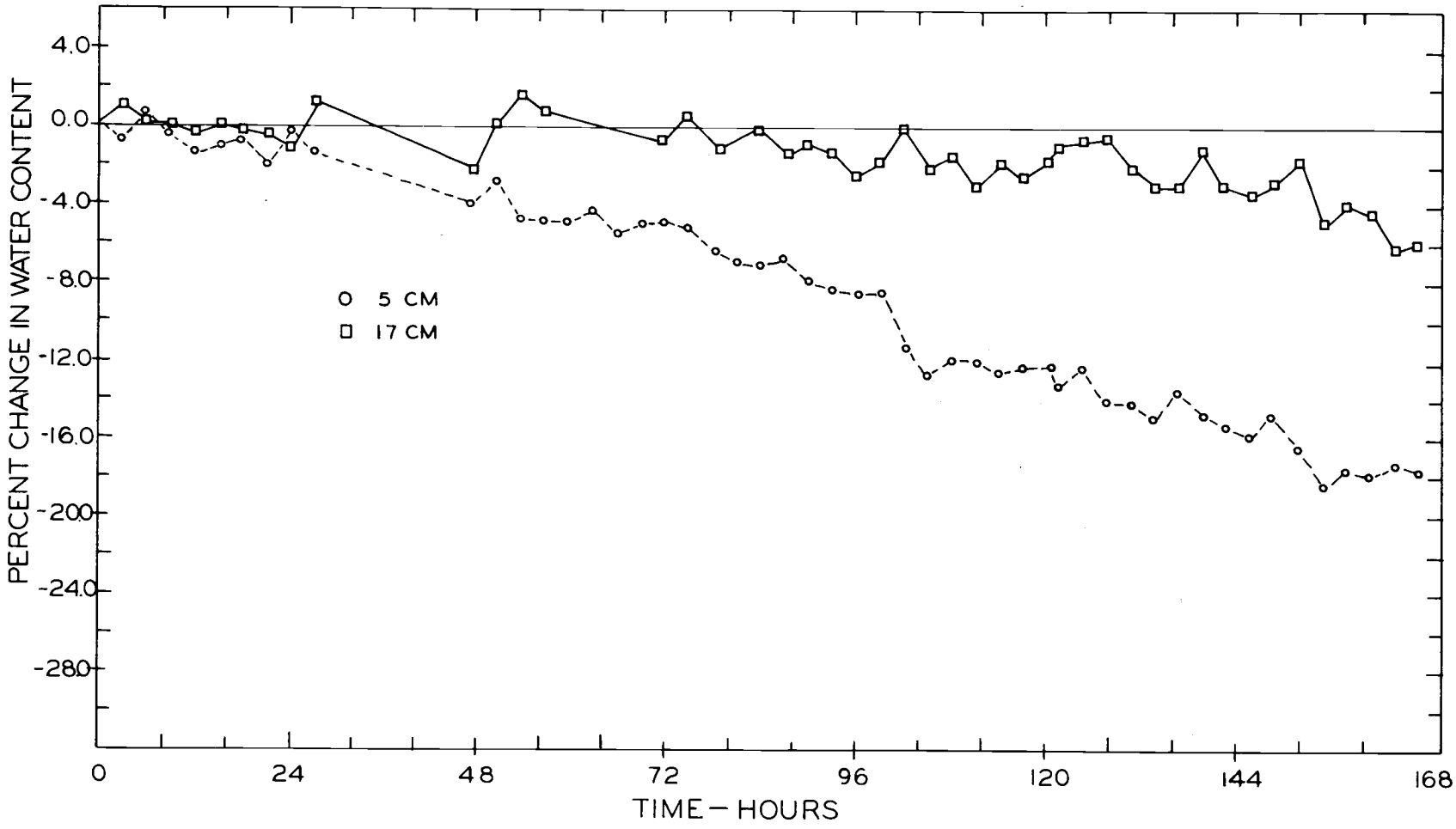

Figure 53. Percent change in water content as a function of time in initially saturated column of the 53-74 microns size glass beads at 5 cm, and 17 cm depths. Experiment III.

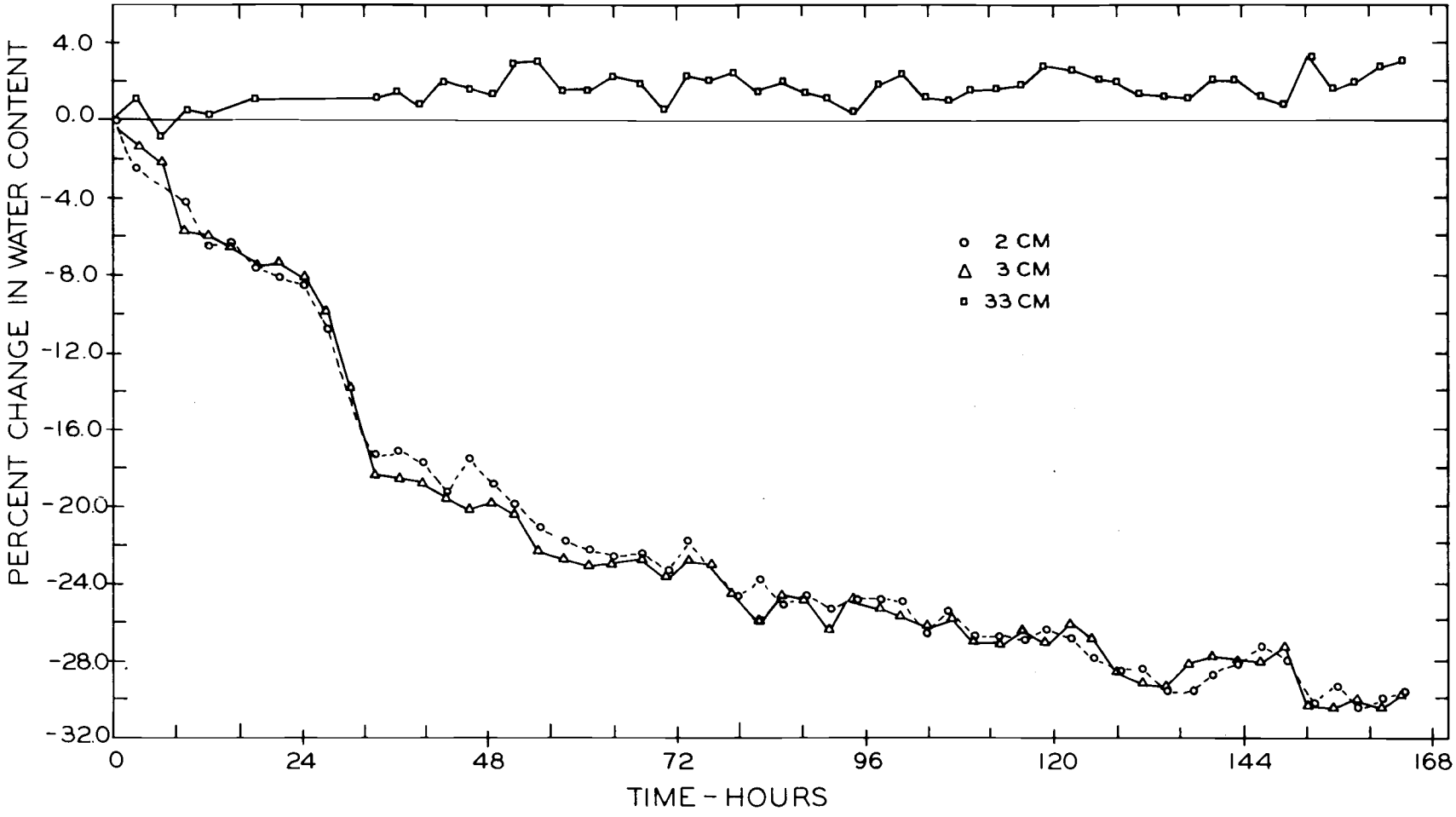

Figure 54. Percent change in water content as a function of time in initially saturated column of the 149-210 microns size glass beads at 2 cm, 3 cm, and 33 cm depths. Experiment VII.

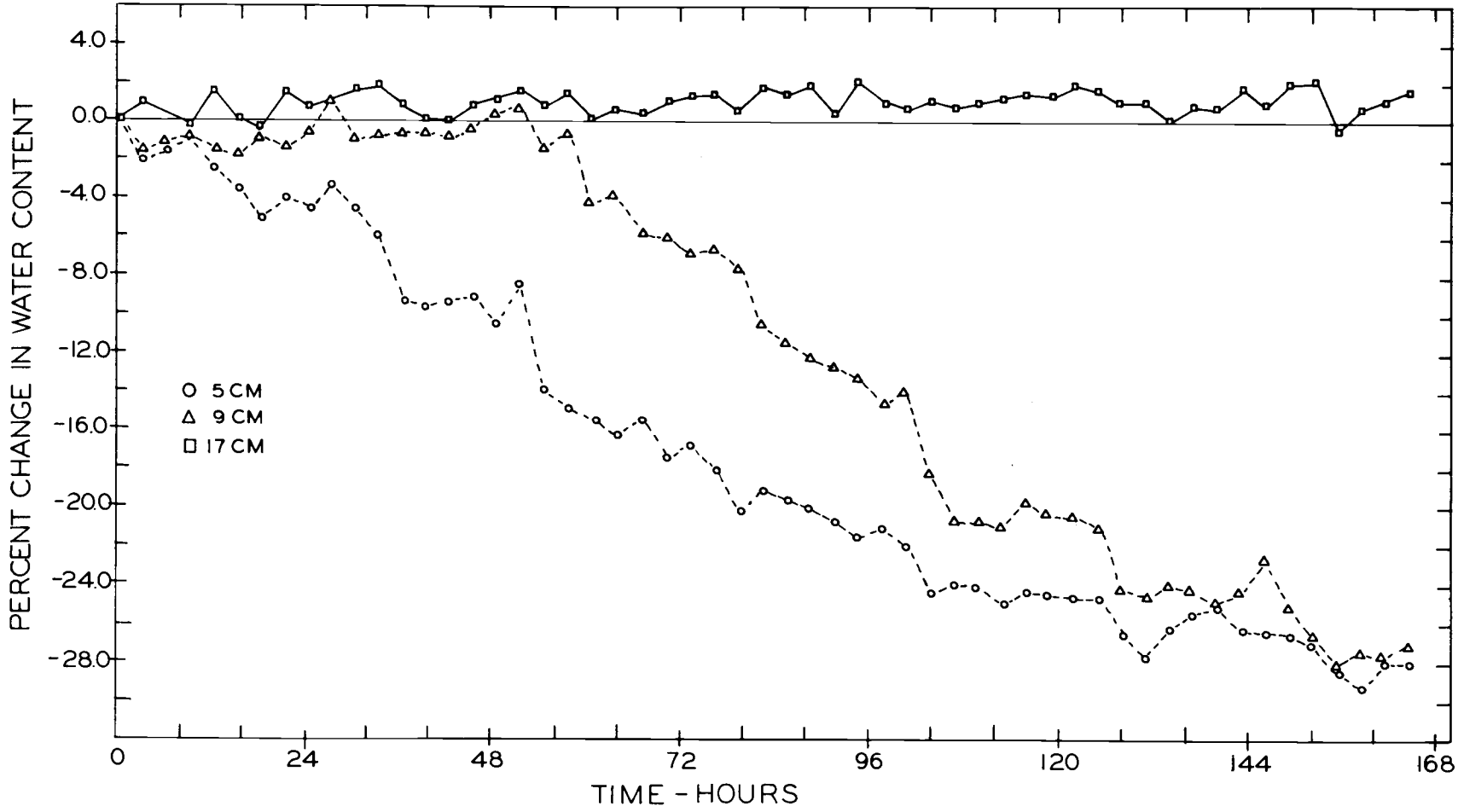

Figure 55. Percent change in water content as a function of time in initially saturated column of the 149-210 microns size glass beads at 5 cm, 9 cm, and 17 cm depths. Experiment VII.

summarized.

Table 14. Percent change in water content at the end of each day for initially saturated samples subjected to a diurnal temperature cycle.

Day No.	Material	Depth (cm)					
		2	3	5	9	17	33
		%	%	%	%	%	%
1	53-74 μ	- 5.2	- 2.1	- 0.4		-1.2	+0.8
2		- 9.0	- 8.1	- 3.8		-2.1	+0.7
3		-11.4	-13.0	- 5.0		-0.6	+0.8
4		-14.7	-14.9	- 8.6		-2.6	+0.3
5		-17.9	-16.9	-12.3		-2.0	+1.5
6		-19.5	-19.4	-15.5		-3.2	+1.4
7		-20.9	-20.9	-17.6		-6.0	+2.7
1	149-210 μ	- 8.4	- 8.1	- 4.6	- 0.7	+0.8	+1.1
2		-18.6	-19.8	-11.3	+ 0.3	+1.0	+1.4
3		-22.7	-23.4	-17.2	- 6.5	+1.2	+1.4
4		-24.8	-25.0	-21.4	-13.9	+1.6	+1.0
5		-26.6	-26.8	-24.6	-20.5	+1.5	+2.7
6		-28.0	-28.0	-26.4	-24.0	+1.6	+2.8
7		-29.7	-29.7	-28.0	-26.9	+1.6	+3.0

These results show that at shallow depths the coarse fraction lost water at a much faster rate. At the 2 cm depth, a loss of 18.6% in the amount of water present initially was observed at the end of the second day for the 149-210 μ fraction, whereas the 53-74 μ fraction had lost about the same amount of water at the end of the sixth day. This clearly explains why an increase in the maximum temperature, at the 2 cm depth, was observed on the second day of the experiments in the coarse fraction, and on the sixth day in the fine fraction.

The data also indicate that the zone of evaporation extended downward faster in the coarse material. During the third day of the experiment, the evaporation zone reached a depth of 5 cm in the 149-210 μ size fraction, whereas little change in water content was observed for the 53-74 μ fraction at this depth. This is the result of the fact that the 53-74 μ size fraction consists of small size pores as compared to the 149-210 μ size fraction (Figure 31), and the resistance offered by the small pore to vapor flow is larger. In other words, the rate with which water evaporated from fine textured glass beads was low and the evaporation zone extended downward slower.

Experiment IV and VIII: Initial Water Content 34% for 53-74 Microns and 30% for 149-210 Microns Glass Beads

These experiments were conducted with initially unsaturated samples. No water was added during the course of the experiments. The temperature profiles for the 53-74 μ material are shown in Figures 56 and 57 and for the 149-210 μ material in Figures 58 and 59. A summary of daily maximum temperature and time lag is shown in Tables 15 and 16.

Table 15 indicates that the two size fractions behave in a manner similar to that observed in experiments III and VII. The peak temperatures at shallow depths suggest the influence of initial water content. Again, the maximum temperature obtained during each cycle

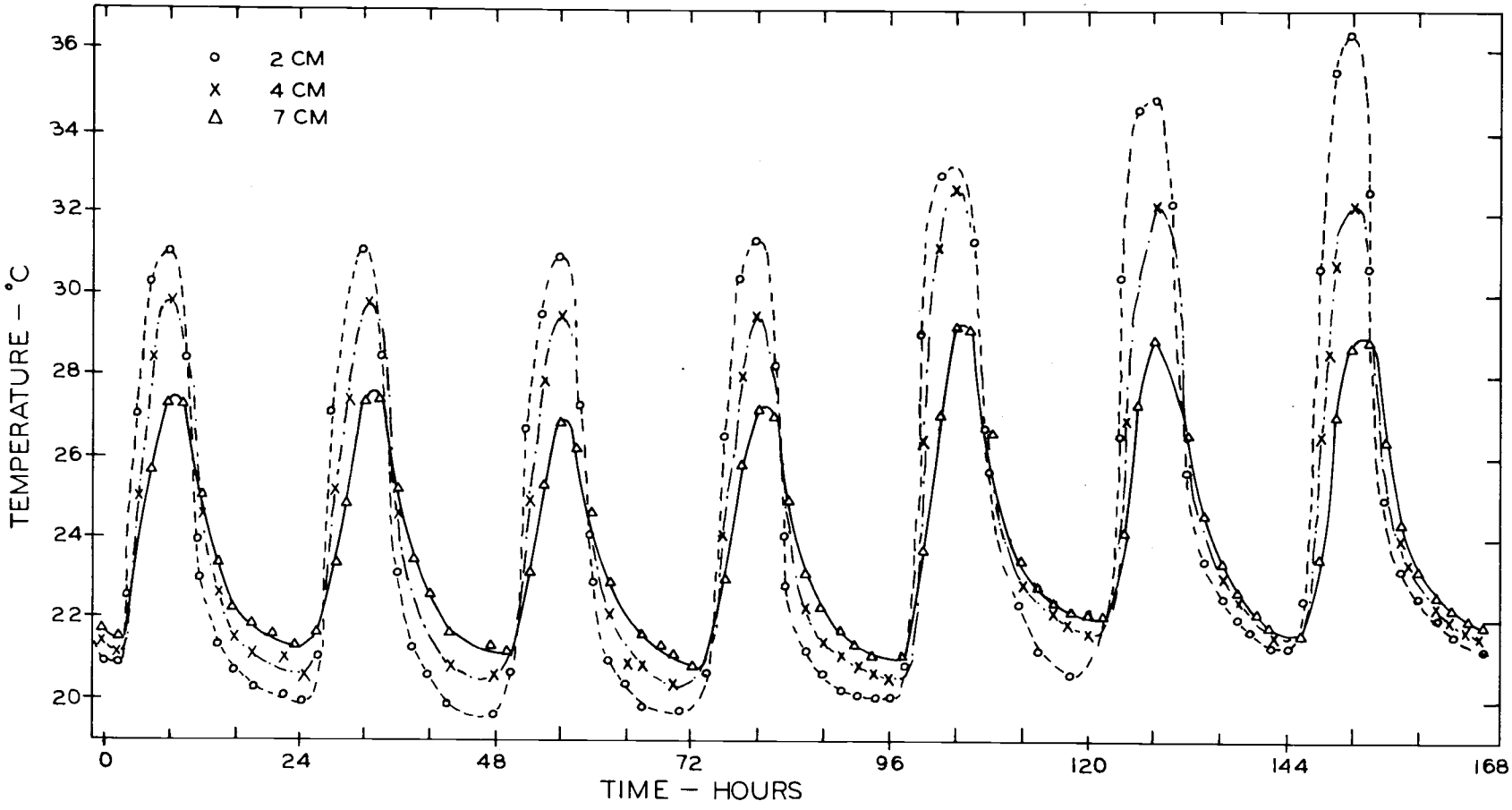

Figure 56. Diurnal temperature variations in initially unsaturated column of the 53-74 microns size glass beads at 2 cm, 4 cm, and 7 cm depths. Experiment IV.

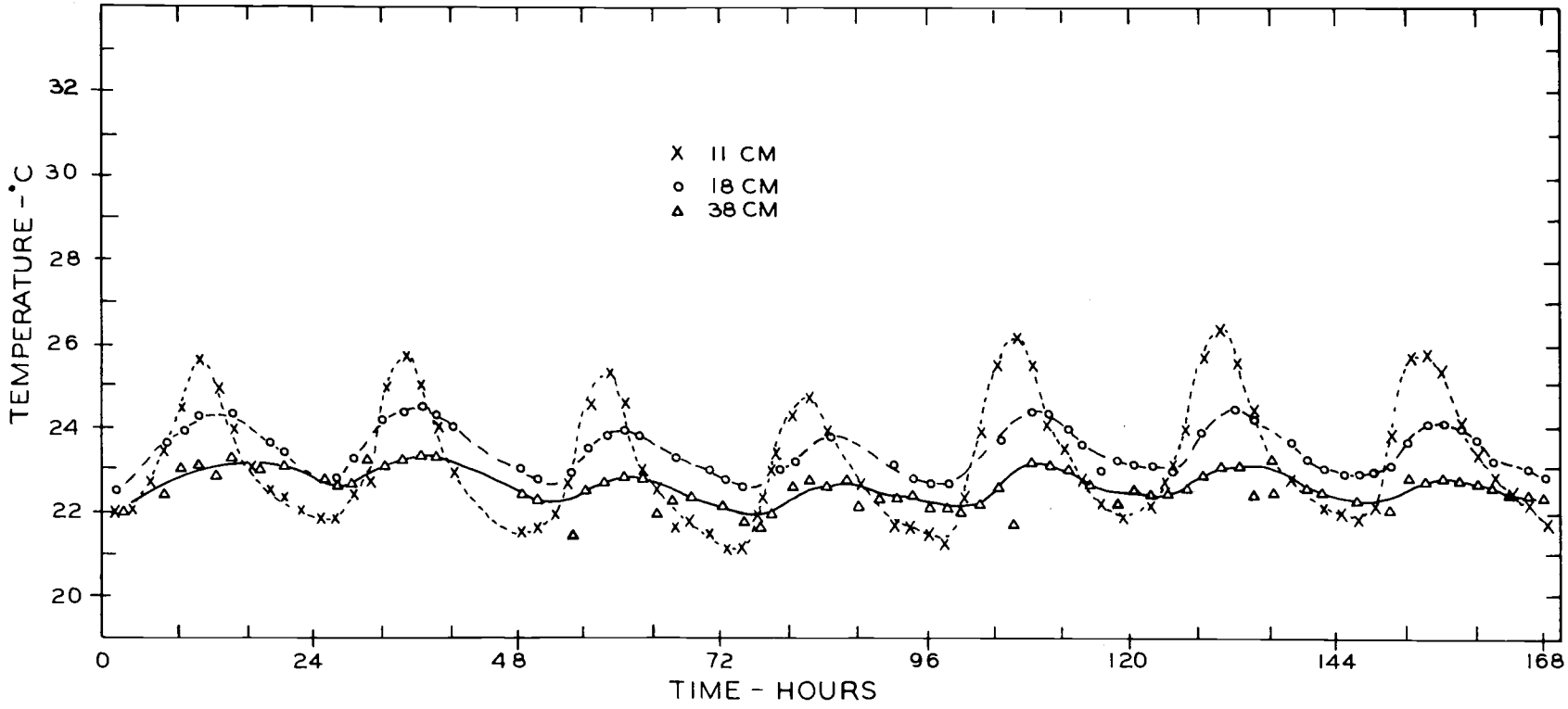

Figure 57. Diurnal temperature variations in initially unsaturated column of the 53-74 microns size glass beads at 11 cm, 18 cm, and 38 cm depths. Experiment IV.

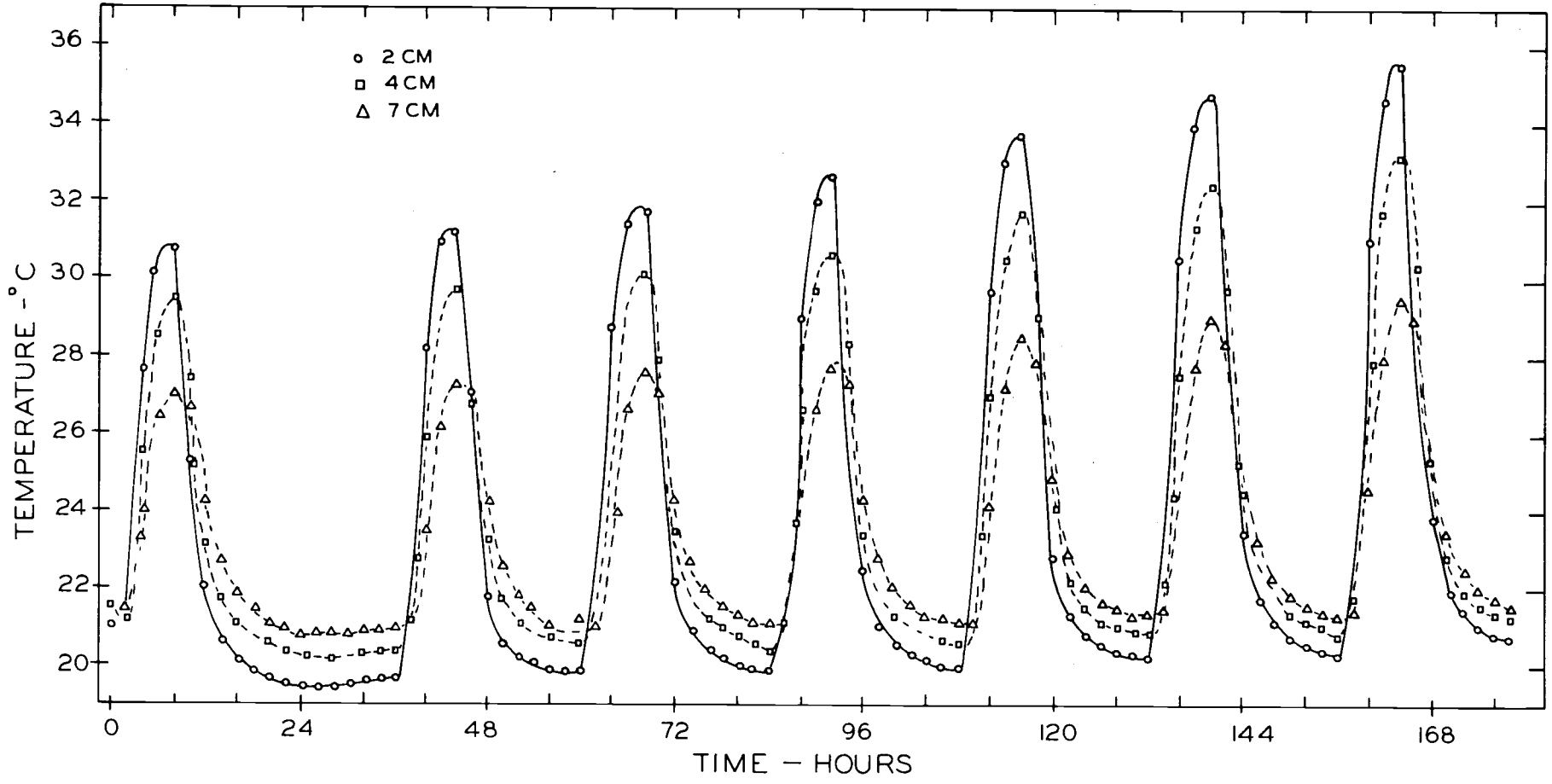

Figure 58. Diurnal temperature variations in initially unsaturated column of the 149-210 microns size glass beads at 2 cm, 4 cm, and 7 cm depths. Experiment VIII.

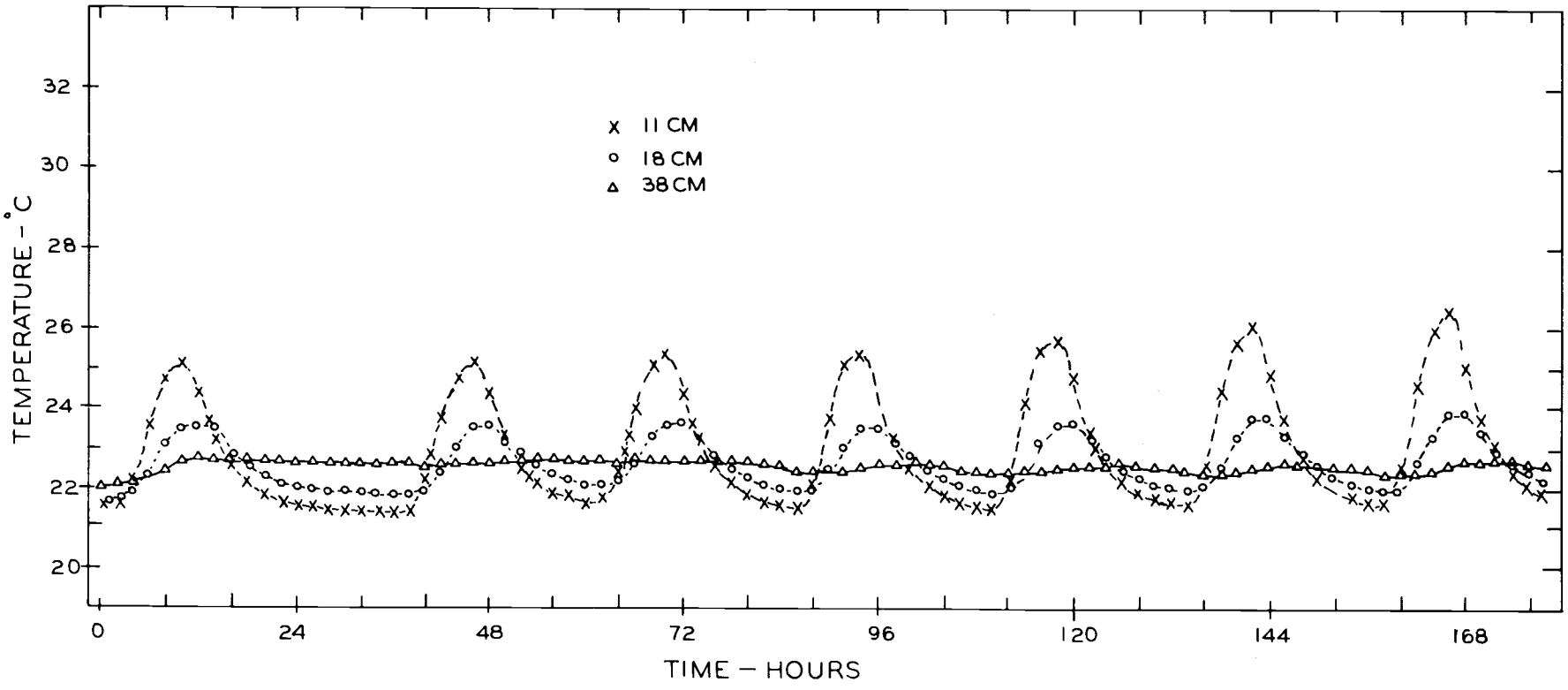

Figure 59. Diurnal temperature variations in initially unsaturated column of the 149-210 microns size glass beads at 11 cm, 18 cm, and 38 cm depths. Experiment VIII.

Table 15. Maximum temperature in °C observed for initially unsaturated columns subjected to a diurnal temperature cycle.

Day No.	Material	Depth (cm) 2	4	7	11	18	38
		°C	°C	°C	°C	°C	°C
1	53-74 μ	31.0	29.9	27.5	25.7	24.4	23.3
2		31.1	29.8	27.6	25.8	24.5	23.3
3		29.9	29.4	26.9	25.4	24.0	22.9
4		31.4	29.5	27.3	24.9	23.9	22.9
5		33.2	32.6	29.3	26.3	24.5	23.3
6		34.9	32.3	29.2	26.5	24.5	23.2
7		36.5	32.3	29.1	25.9	24.2	22.9
1	149-210 μ	30.9	29.5	27.0	25.1	23.6	22.7
2		31.3	29.8	27.4	25.2	23.6	22.7
3		31.8	30.2	27.7	25.4	23.7	22.7
4		32.7	30.8	27.9	25.4	24.6	22.6
5		33.7	31.8	28.6	25.7	23.7	22.6
6		34.7	32.5	29.1	26.0	23.8	22.6
7		35.7	33.2	29.6	26.4	24.0	22.7

increased during the course of the experiment. For the 149-210 μ size glass beads, the increase in the maximum temperature could be observed during the third day of the experiment whereas for the 53-74 μ fraction the increase in the maximum temperature was not observed until the fifth day.

As before the time lag, as shown in Table 16, indicated no effect of drying of the sample.

Table 16. Time lag in minutes observed for initially unsaturated columns subjected to a diurnal temperature cycle.

Day No.	Material	Depth (cm) 2	4	7	11	18
		min	min	min	min	min
1	53-74 μ	30	54	90	180	318
2		30	60	108	186	282
3		24	30	90	186	360
4		24	42	84	132	312
5		18	42	90	120	300
6		18	36	84	180	288
7		30	54	102	150	306
1	149-210 μ	30	54	78	162	324
2		36	66	138	186	288
3		24	66	90	168	264
4		36	69	129	189	288
5		30	76	100	166	276
6		30	57	78	183	270
7		30	63	99	180	276

Water content measurements were made at three hour intervals at depths of 2, 3, 5, 9, 17, and 33 cm. Results of these measurements are shown in Figures 60 and 61 for the 53-74 μ material and in

Figures 62 and 63 for the 149-210 μ material. A summary of the results is given in Table 17.

Table 17. Percent change in water content at the end of each day in initially unsaturated columns subjected to a diurnal temperature cycle.

Day No.	Material	Depth (cm) 2	3	5	9	17	33
		%	%	%	%	%	%
1	53-74 μ	- 2.7	- 1.8	- 1.9	-0.6	-1.7	+0.1
2		- 4.7	- 4.3	- 3.6	-2.5	-3.7	-1.2
3		- 6.2	- 6.2	- 3.8	-2.6	-3.8	-2.6
4		-19.9	-10.4	- 4.6	-2.7	-4.2	-2.4
5		-23.8	-12.3	- 4.4	-2.7	-3.6	-3.0
6		-25.6	-11.8	- 5.0	-3.4	-4.5	-3.3
7		-25.5	-12.5	- 6.1	-3.4	-5.1	-3.0
1	149-210 μ	- 9.8	- 9.2	- 6.7		-0.9	-0.4
2		-12.8	-11.3	- 9.4		-0.8	+0.2
3		-14.2	-14.2	-12.3		-0.3	+0.8
4		-14.5	-14.7	-12.8		-3.6	+0.8
5		-14.9	-15.8	-13.8		-7.8	+1.0
6		-15.1	-15.2	-14.4		-10.6	+2.2
7		-16.1	-16.1	-15.2		-12.5	+1.8

These results show that the two size fractions behave in a manner similar to the one observed for experiments III and VII. A rapid loss in water content was observed at shallow depths. For the coarse material (149-210 μ), an initial rapid loss could be observed. At the end of the third day, the 149-210 μ fraction indicated a loss of 14.2% in the amount of water present initially at 2 cm depth, whereas for the 53-74 μ fraction a loss of only 6.2% was observed. This resulted in the observed increase in the maximum temperature for the

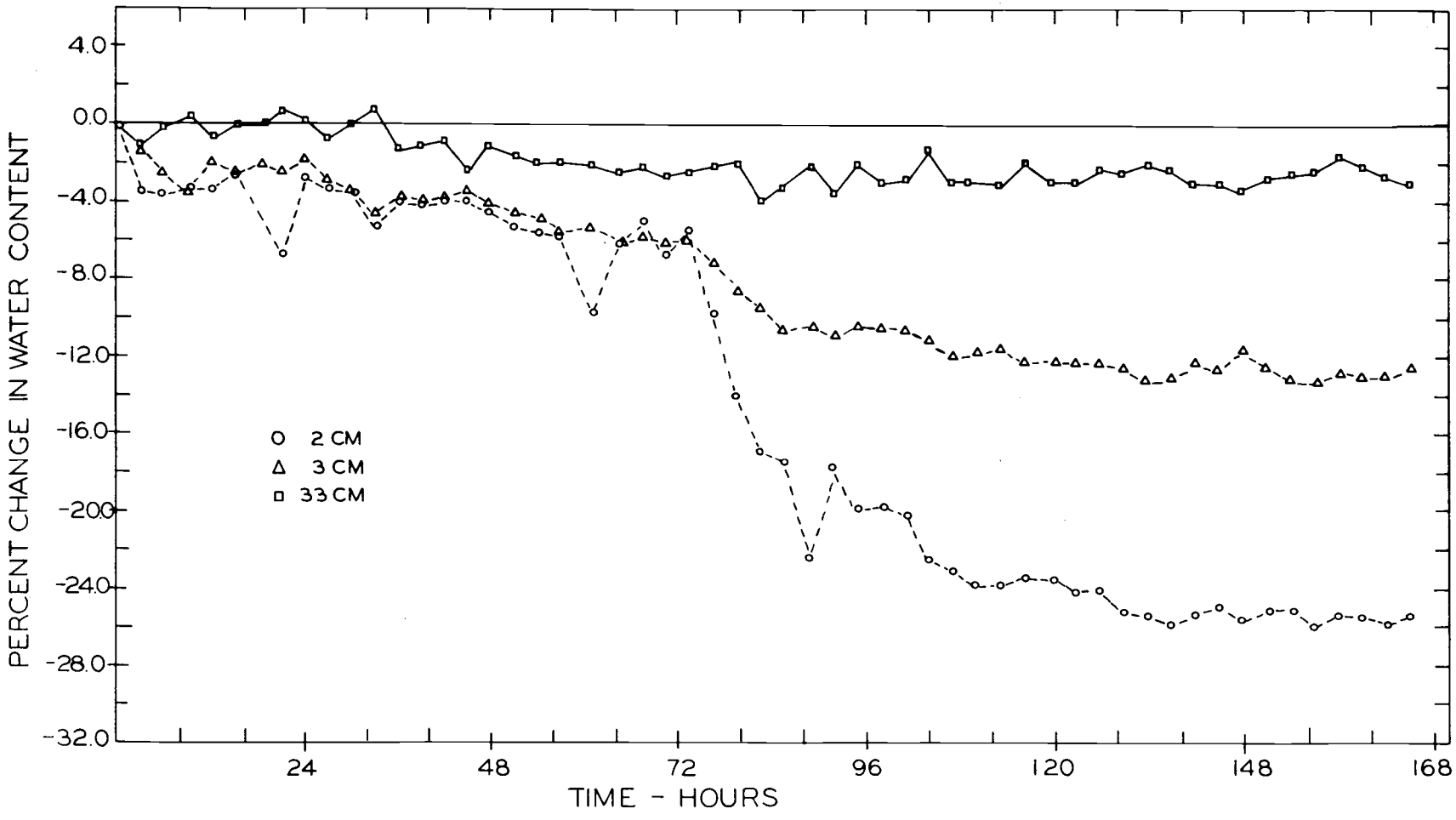

Figure 60. Percent change in water content as a function of time in initially unsaturated columns of the 53-74 microns size glass beads at 2 cm, 3 cm, and 33 cm depths. Experiment IV.

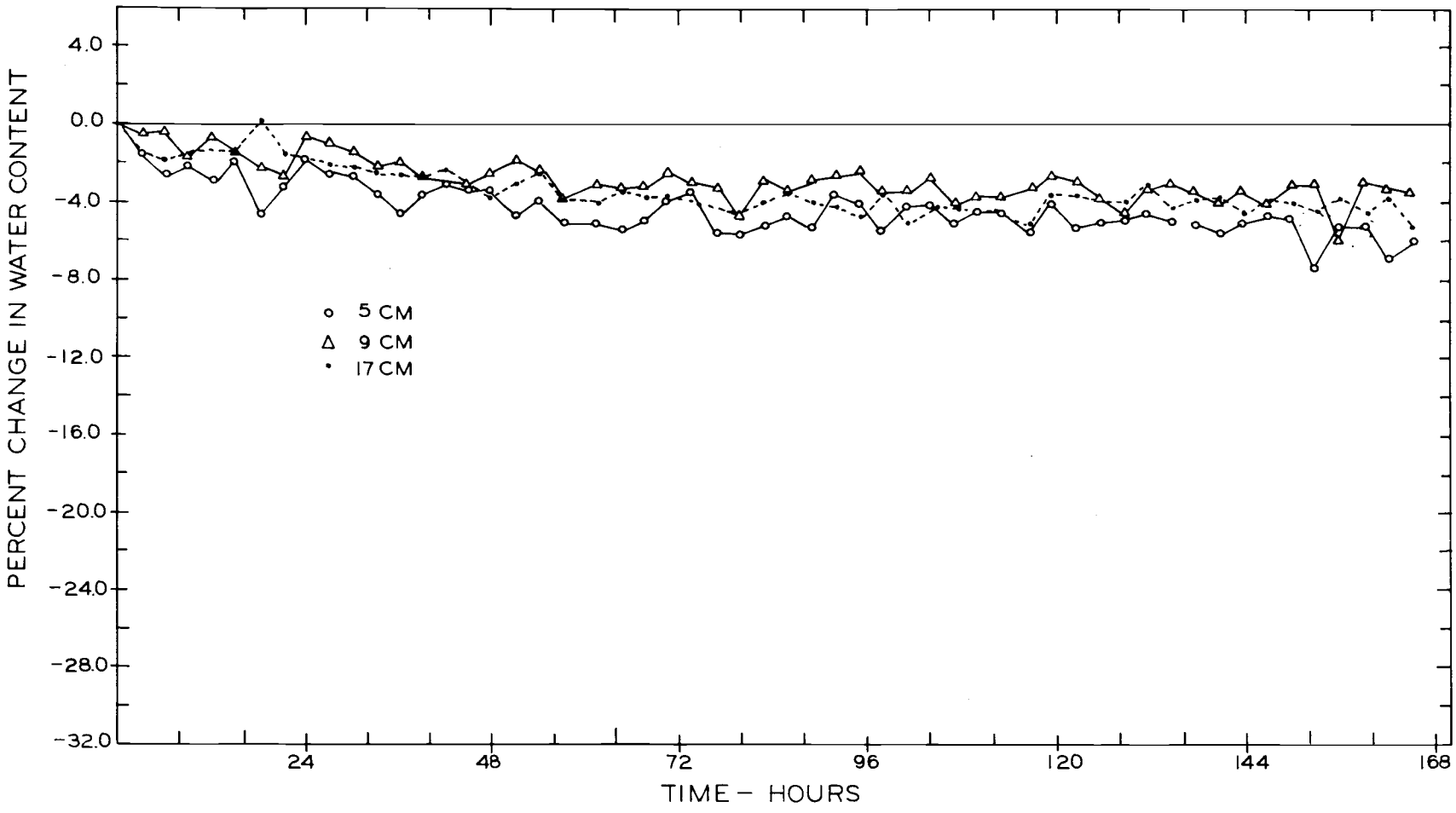

Figure 61. Percent change in water content as a function of time in initially unsaturated column of the 53-74 microns size glass beads at 5 cm, 9 cm, and 17 cm depths. Experiment IV.

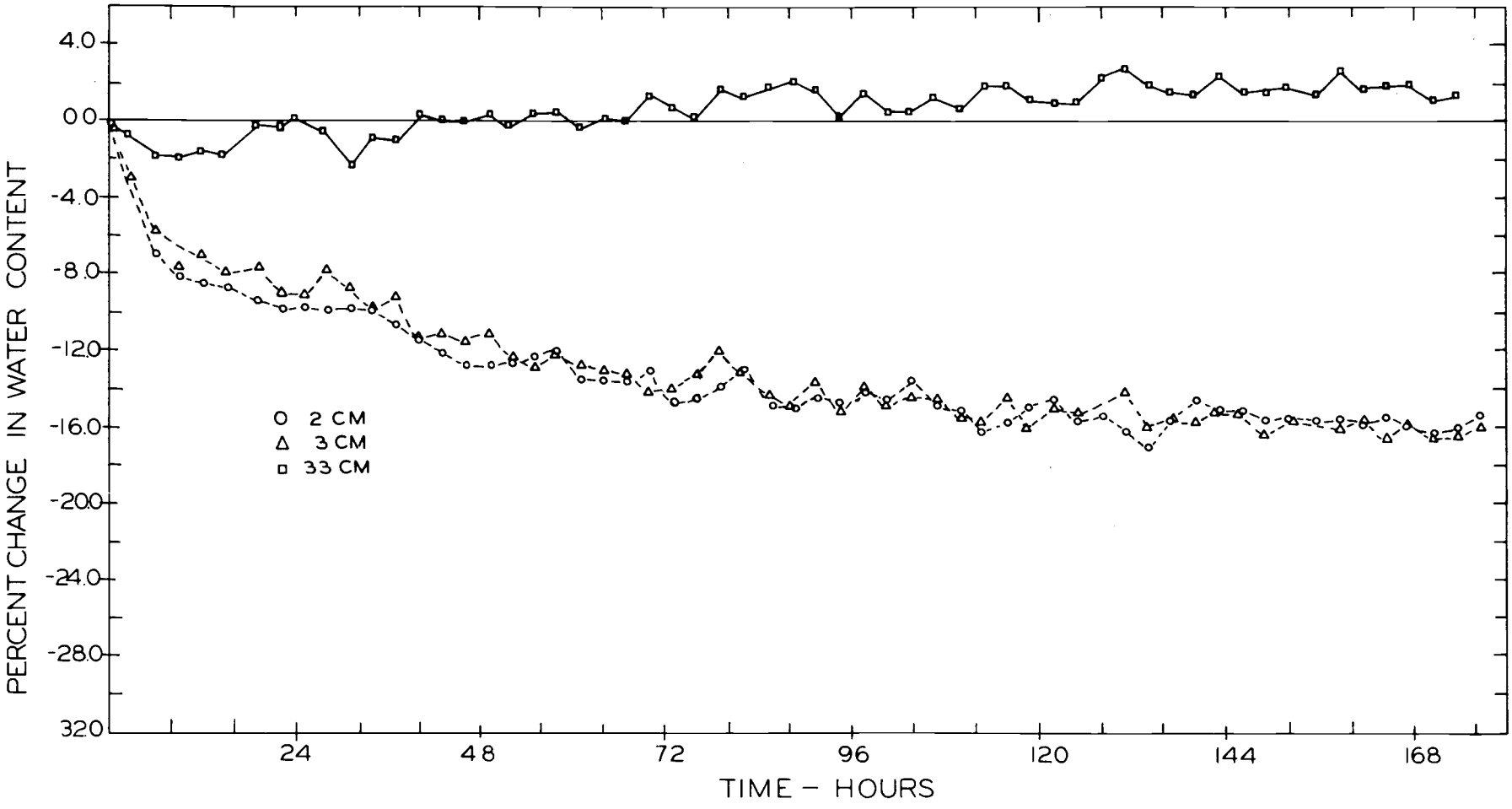

Figure 62. Percent change in water content as a function of time in initially unsaturated column of the 149-210 microns size glass beads at 2 cm, 3 cm, and 33 cm depths. Experiment VIII.

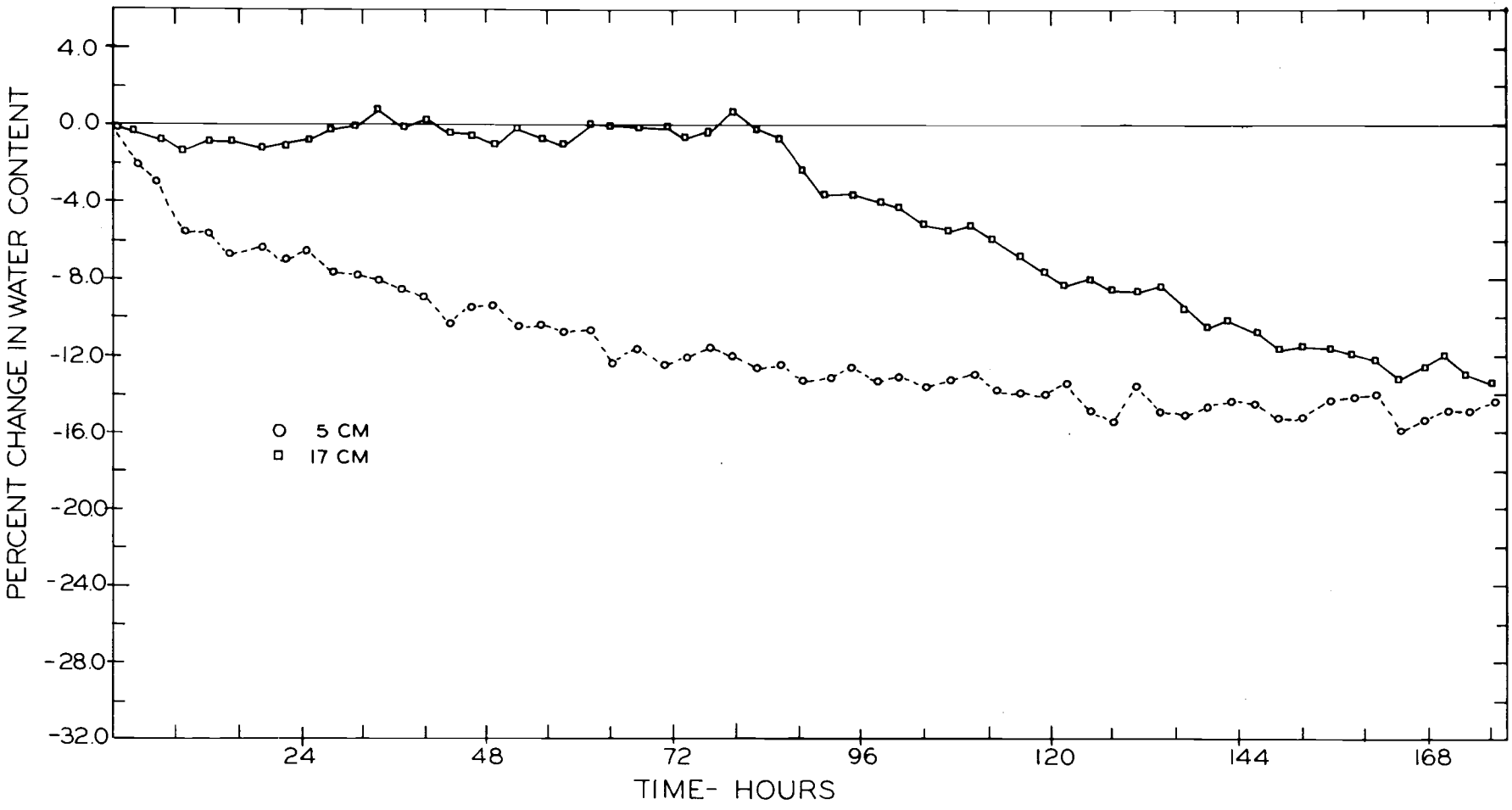

Figure 63. Percent change in water content as a function of time in initially unsaturated columns of the 149-210 microns size glass beads at 5 cm, and 17 cm depths. Experiment VIII.

149-210 μ size fraction at the 2 cm depth during the third day of the experiment. About the same amount of water was lost during the fifth day in the 53-74 μ size sample.

Figure 60 indicates a rather new rate of water loss at 2 cm and 3 cm depths at the end of the third day of the experiment for 53-74 μ size sample. The reason is not clearly understood. It appears to be a break in the continuity of water flow. It is apparent that the general trend, however, was the same.

The rate of evaporation was lower in the fine fraction of glass beads. At the end of the sixth day the zone of evaporation extended downward to a depth of 17 cm in the 149-210 μ size fraction beds, whereas little change in water content was observed in the 53-74 μ size glass beads beds. The results, also, show the influence of initial water content on the rate with which the zone of evaporation moves down into the bed. In the 149-210 size glass bead columns, the evaporation zone appears to reach a depth of 17 cm at the end of the fifth day in initially unsaturated samples, whereas no change in water content is indicated in the initially saturated samples during that period of time (experiments III and VII, Table 14).

Heat Flux

Heat absorbed by the column of glass beads was calculated using the model presented by Gardner and Hanks (1966). The heat flux into

a layer of thickness, ΔZ, is used to evaporate water and to raise the temperature of the material in this layer. The total heat flux, ΔH, into a layer of thickness, ΔZ, can be written as:

$$\Delta H = \frac{EQ + C\Delta T\Delta Z}{\Delta t},$$

$$\Delta H = Q\frac{\Delta \theta}{\Delta t}\Delta Z + C\frac{\Delta T}{\Delta t}\Delta Z, \tag{27}$$

where

ΔH = total heat flux (cal/cm^2 min),

E = evaporation ($cm = \Delta\theta \cdot \Delta Z$),

Q = heat of vaporization of water (cal/cm^3),

C = heat capacity of layer Z, including water ($cal/cm^3 °C$),

ΔT = change in temperature in time interval t (°C),

ΔZ = thickness of the layer (cm),

Δt = time interval (min), and

$\Delta \theta$ = change in moisture content (cm^3/cm^3).

The first member of the right hand side of Equation (27) represents the heat used for evaporation and the second member the heat used for increasing the temperature of the material.

For dry and completely saturated samples $\Delta\theta = 0$, and Equation (27) becomes:

$$\Delta H = C\frac{\Delta T}{\Delta t}\Delta Z . \tag{28}$$

The total heat flux, ΔH, was calculated by dividing the column into layers varying in thickness. The thickness, ΔZ, was varied according to the vertical temperature distribution. Smaller ΔZ's were chosen near the surface where the temperature gradient was steep. The temperature, $T_{\Delta Z}$, and the loss in water content, $\Delta\theta_{\Delta Z}$, of the layer, are given by:

$$T_{\Delta Z} = T_{(\frac{Z_1+Z_2}{2})}, \tag{29}$$

$$\Delta\theta_{\Delta Z} = \Delta\theta_{(\frac{Z_1+Z_2}{2})}. \tag{30}$$

For selected times, t, $T_{\Delta Z}$ and $\Delta\theta_{\Delta Z}$ were tabulated from temperature distribution and moisture distribution plots. The heat flux, ΔH, was then calculated according to Equations (27) and (28). The heat flux plotted as a function of time is shown in Figures 64 through 71.

Dry Samples

For dry samples no heat is used to evaporate water. The water content remained constant and the thermal conductivity did not change during the duration of the experiments. According to the thermal conductivity experiments, this parameter is independent of the size of

the glass beads. The heat flux into the beads, made up of two different glass bead sizes may, therefore, be expected to be the same. The rate of heat flux for the 53-74 μ, and the 149-210 μ fractions are shown in Figures 64 and 65. The actual amount of heat exchanged at the surface of the beads is shown in Table 18. These values were obtained by integration of the rate of heat flow graphs.

Table 18. Quantity of heat exchanged at the surface of dry glass beads beds.

Day No.	Material	Sensible Heat Flux	
		in	out
		cal/cm^2	
1	53-74 μ	36.0	46.2
2		43.4	43.4
1	149-210 μ	46.1	45.3
2		47.5	47.8

Table 18 indicates that the heat exchanged for the two size fractions was the same except for day one, when the amount of heat entering the 53-74 μ size bead bed was smaller. The anomaly for day one was the result of higher initial temperatures.

Saturated Samples

In these experiments a saturated sample of glass beads was used. Water was added at the surface of the column as it appeared to dry out. The water content was considered to be constant during the

course of the experiments. The amount of water held at saturation is the same for the two fractions of beads. According to the thermal conductivity experiments, this parameter is independent of the size of the glass beads. The heat flux into the beds may, therefore, be expected to be the same irrespective of the glass beads fraction. Figures 66 and 67 show the rates of heat flux for the 53-74 μ, and the 149-210 μ size fractions. The actual amount of heat exchanged at the surface of beads is shown in Table 19.

Table 19. Quantity of heat exchanged at the surface of saturated glass beads beds.

Day No.	Material	Sensible Heat Flux	
		in	out
		cal/cm^2	
1	53-74 μ	64.9	69.7
2		67.1	70.3
1	149-210 μ	65.0	71.8
2		70.4	73.8

These results indicate that the two fractions behaved in a manner similar to the one observed in the dry beads beds. The incoming and the outgoing heat flux was of the same magnitude for both size fractions. The total heat exchanged at the surface was about one and a half times more in the saturated samples. This difference in the observed heat exchange is the result of the larger heat capacity of saturated glass beads and the higher thermal conductivity.

Initially Saturated Samples

In these experiments the samples were initially saturated with water and then allowed to dry out by the imposed heat load. The rate of heat flux was calculated using Equation (27). The rate of heat flux as a function of time is shown in Figures 68 and 69. The actual amount of heat exchanged at the surface of the beds consisted of a sensible heat flux and an evaporative heat flux. The evaporative heat flux is also shown in Figures 68 and 69. A summary of the actual heat exchanged at the surface is shown in Table 20.

Table 20. Quantity of heat exchanged at the surface of initially saturated glass beads beds.

Day No.	Material	Sensible		Evaporative		Total
		in	out	out	out	out
		cal/cm^2		cal/cm^2		cal/cm^2
1	53-74 μ	87.8	68.8	69.2	69.9	120.1
2		65.8	62.1	61.7	94.6	152.6
1	149-210 μ	91.9	54.3	171.2	259.5	393.7
2				146.9	141.7	288.6

Examination of Figures 68 and 69 and Table 20 indicates that during the first cycle rapid evaporation occurred and that the evaporative flux was the major part of the total heat flux. About 11 hours after the initiation of the experiments, the evaporative flux actually exceeded the sensible heat flux. This means that more heat was

leaving the system than was being added. Due to a rapid loss of heat from the surface, upward temperature gradients were initiated during the cooling periods.

The evaporative flux for the two fractions showed an influence of the difference in size of glass beads. During the first cycle the total evaporative flux observed was 139.1 cal/cm^2 for the 53-74 μ size glass beads and 430.7 for the 149-210 μ size glass beads. According to the results of water content measurement experiments, the coarser fraction lost water at a faster rate than the finer fraction. During the second day the total evaporative flux for the coarser fraction decreased to 288.6 cal/cm^2 reflecting the reduction in the rate of evaporation from the system. An early rapid loss of water from the surface extended the zone of evaporation deeper into the bed, thereby introducing a larger resistance to upward vapor flow. As the observed evaporation was much slower in the 53-74 μ size glass bead beds, no significant change in the total evaporative flux was observed for this fraction during the second cycle. Table 20 indicates slightly higher values of the total evaporative flux during the second day of the experiment for the finer fraction of glass beads.

The net sensible heat exchanged at the surface was approximately zero during the second day for the finer fraction as it should be since the beds returned to the initial temperature distribution at the end of each day. This was, however, not true for either size fraction

during the first cycle. The reason for this discrepancy was that the initial temperatures in the beds were lower than the equilibrium temperatures. The temperature data confirm this observation. The quantity of sensible heat exchanged at the surface of each size fraction was approximately the same and similar to the heat flux observed in saturated samples (Table 19). This can be explained in terms of thermal conductivity of the systems. According to thermal conductivity experiments, this parameter would be the same for the two fractions. Rapid loss of water and high sensible heat flux suggest higher surface temperature for the coarse fraction. This observation can be made from the temperature data that showed an increase in the maximum temperature at the 2 cm depth during the second day of the experiments (Figure 50). No such increase in the maximum temperature attained at the 2 cm depth was observed for the 53-74 μ size glass bead beds.

Initially Unsaturated Samples

These experiments were conducted with initially unsaturated samples. No water was added during the course of the experiments and the system was allowed to dry out under the imposed diurnal temperature variations. The rate of heat flux, calculated with Equation (27), is shown in Figures 70 and 71. A daily summary of the heat flux for the two size fractions is shown in Table 21.

Table 21. Quantity of heat exchanged at the surface of initially unsaturated glass beads beds.

Day No.	Material	Sensible		Evaporative		Total
		in	out	out	out	out
		cal/cm^2		cal/cm^2		cal/cm^2
1	53-74 μ	68.0	68.0	165.2	88.3	253.5
2		77.0	82.6	64.3	184.7	254.6
3		71.8	70.7	44.9	77.0	120.8
1	149-210 μ	66.4	68.4	252.4	202.9	457.3
2		100.2	67.7	84.8	150.1	202.4
3		73.3	77.8	66.2	61.3	132.0

These results show a trend similar to the one observed for the initially saturated experiments. Rapid evaporative losses during the first cycle were followed by slow rates of evaporation in subsequent cycles and the evaporative flux was a major part of the total heat flux. About 11 hours after the initiation of the experiments, the evaporative heat flux exceeded the sensible heat flux and the system showed a net heat loss.

The net sensible heat flux exchanged at the surface was approximately zero during each day for both fractions. A discrepancy, however, was indicated for the 149-210 μ size fraction during the second day of experiment. Rapid evaporative losses from the coarse beds suggest an increase in the surface temperature. According to the temperature measurements this increase in the surface temperature was observed during the third day for the 149-210 μ size fraction.

Comparison of these results with those from the initially

saturated samples (Figures 68 and 69, Table 20) and completely saturated samples (Figures 66 and 67, Table 19), suggest the influence of initial water content on the heat exchanged at the surface of the beds. For the 53-74 μ size fraction, the evaporative flux for initially unsaturated beds was much larger than the evaporative flux observed for initially saturated samples. A similar observation was made by Gurr et al. (1952) who reported that maximum transfer of water under temperature gradients occurred in unsaturated soils with soil water content equal to one-third of the moisture equivalent. The transfer of water under thermal gradients takes place both in liquid and vapor forms. In saturated soils this movement occurs in the liquid phase only. The quantity of water that moves in liquid form is very small as compared to vapor flow.

The sensible heat flux did not show the influence of initial water content. This is because the thermal conductivity of completely saturated samples (40%) and unsaturated samples (30%) did not differ significantly (Figure 30).

Conclusions

The water content measurements at various depths in the sample beds give a good indication of the effect of pore size distributions on evaporation. The coarse fraction lost water much faster than the fine fraction. Water vapor passing through large pores encounters

less resistance per unit crosssectional area than vapor passing through small pores.

The rapid loss of water in the coarse samples with pore size distributions consisting of mainly large pores affected the temperature distribution in the columns. Since a large quantity of heat is used to change water from liquid to vapor state, evaporation constitutes a major portion of the heat budget of systems such as soils. Pore size distribution has been observed to influence the rate of water loss from porous media subjected to temperature fluctuations. This means, the heat exchanged at the surface of a moist porous material is dependent on its pore size distribution. The heat flux data showed a higher evaporative and total heat flux for the coarse samples than for the fine samples (Tables 20 and 21). The sensible heat flux, on the contrary, was similar in both size fraction. The sensible flux consists of heat transferred by conduction, convection, and vapor transfer. In unsaturated samples all three processes are expected to contribute to sensible heat flux in the system. The similarity of the sensible heat flux for each size fraction, in saturated and unsaturated experiments (Tables 19 and 21), however, clearly indicated that the vapor heat transfer is very small and does not showits dependence on pore size distributions. This is in accordance with the observation that has been made in the previous chapter with respect to thermal conductivity.

The incoming radiation is used more efficiently in saturated media than in dry materials. The total heat exchanged in moist beds, allowed to dry under temperature fluctuations is much larger. The major part of this flux, however, consists of the evaporative flux. The sensible heat flux, on the other hand, is quite similar to saturated samples. Because of the importance of simultaneous heat and water balance around the root zone, it is necessary that a continuous supply of water be maintained.

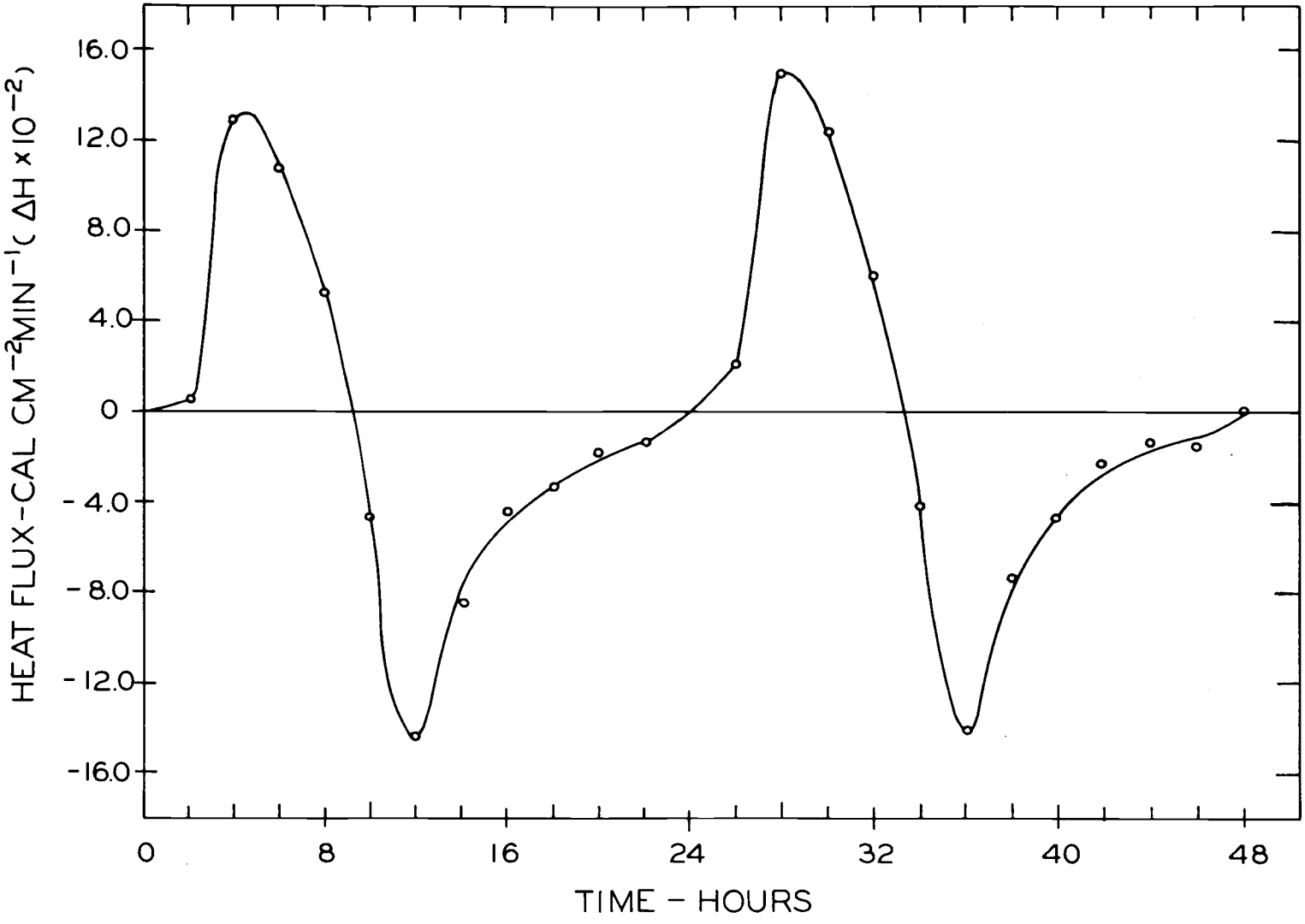

Figure 64. Heat flux variations in air dry column of the 53-74 microns size glass beads. Experiment I.

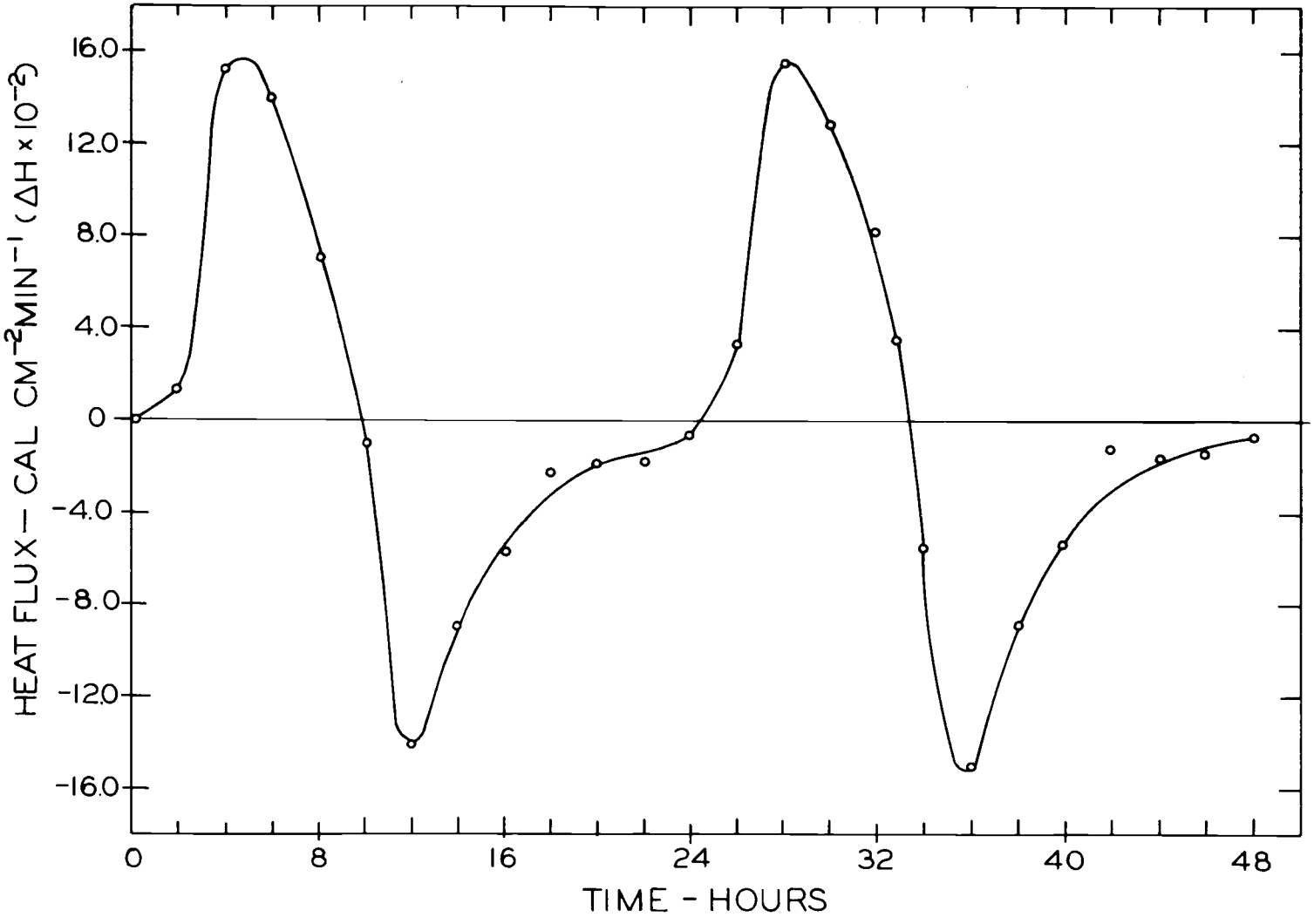

Figure 65. Heat flux variations in air dry column of the 149-210 microns size glass beads. Experiment V.

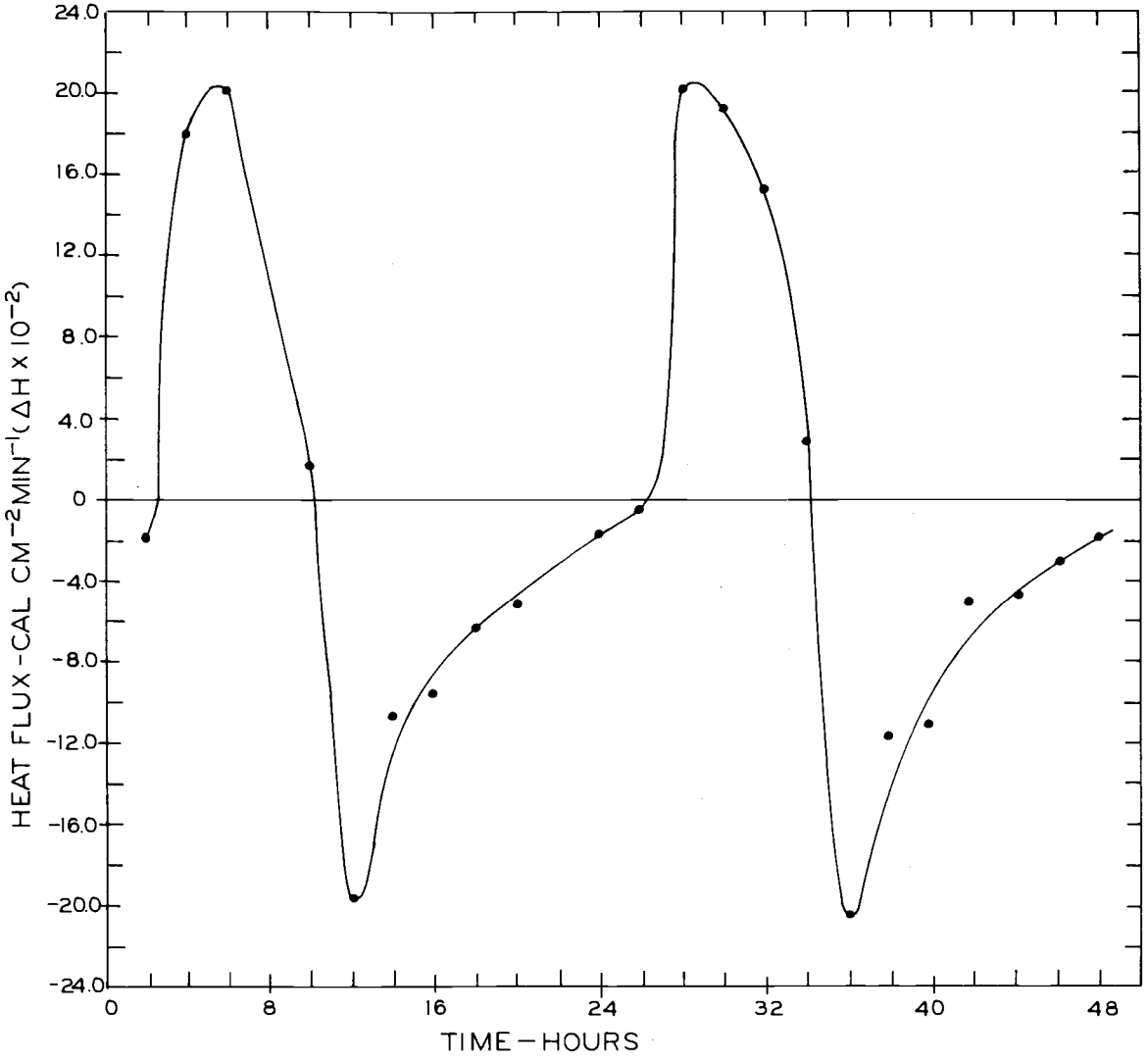

Figure 66. Heat flux variations in saturated column of the 53-74 microns size glass beads. Experiment II.

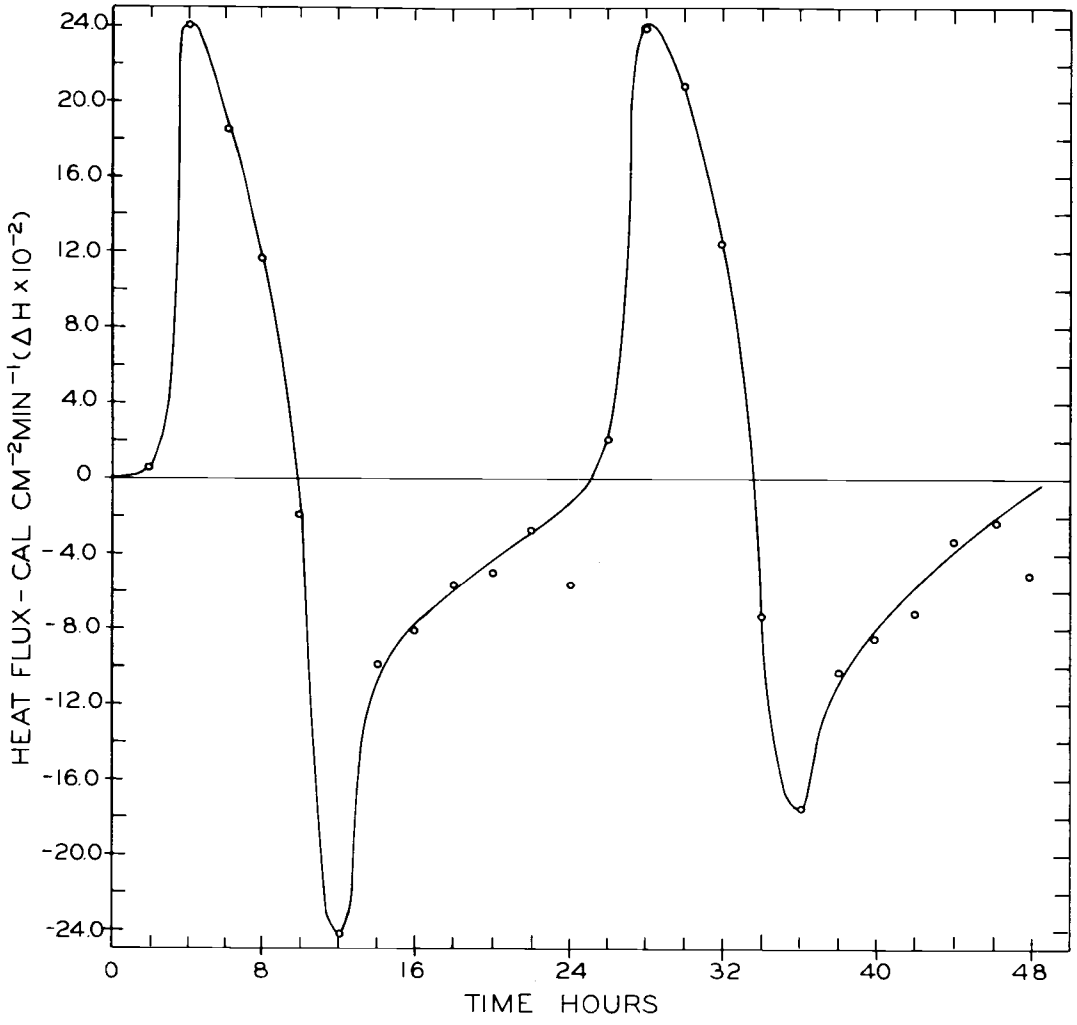

Figure 67. Heat flux variations in saturated column of the 149-210 microns size glass beads. Experiment VI.

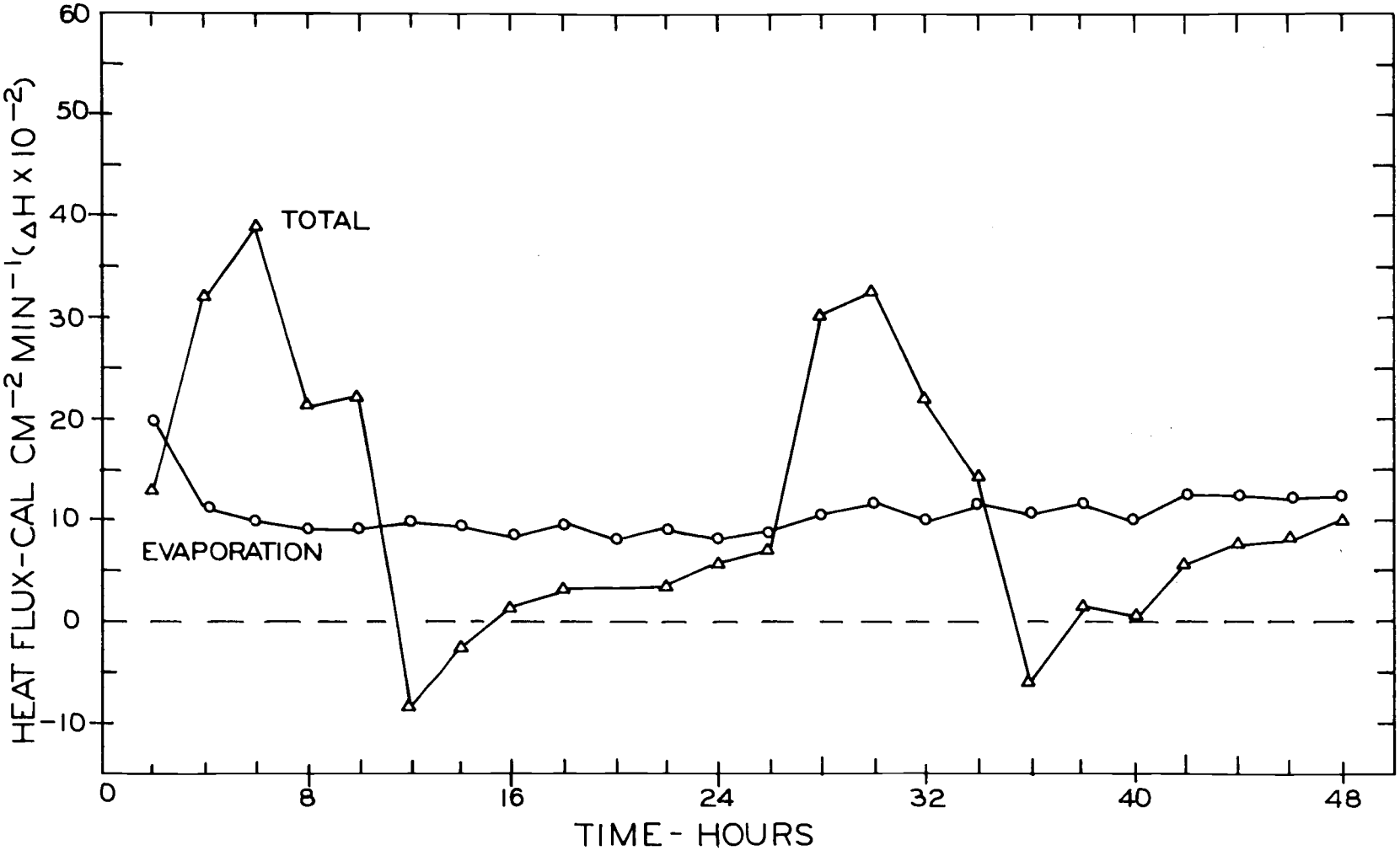

Figure 68. Heat flux variations in initially saturated column of the 53-74 microns size glass beads. Experiment III.

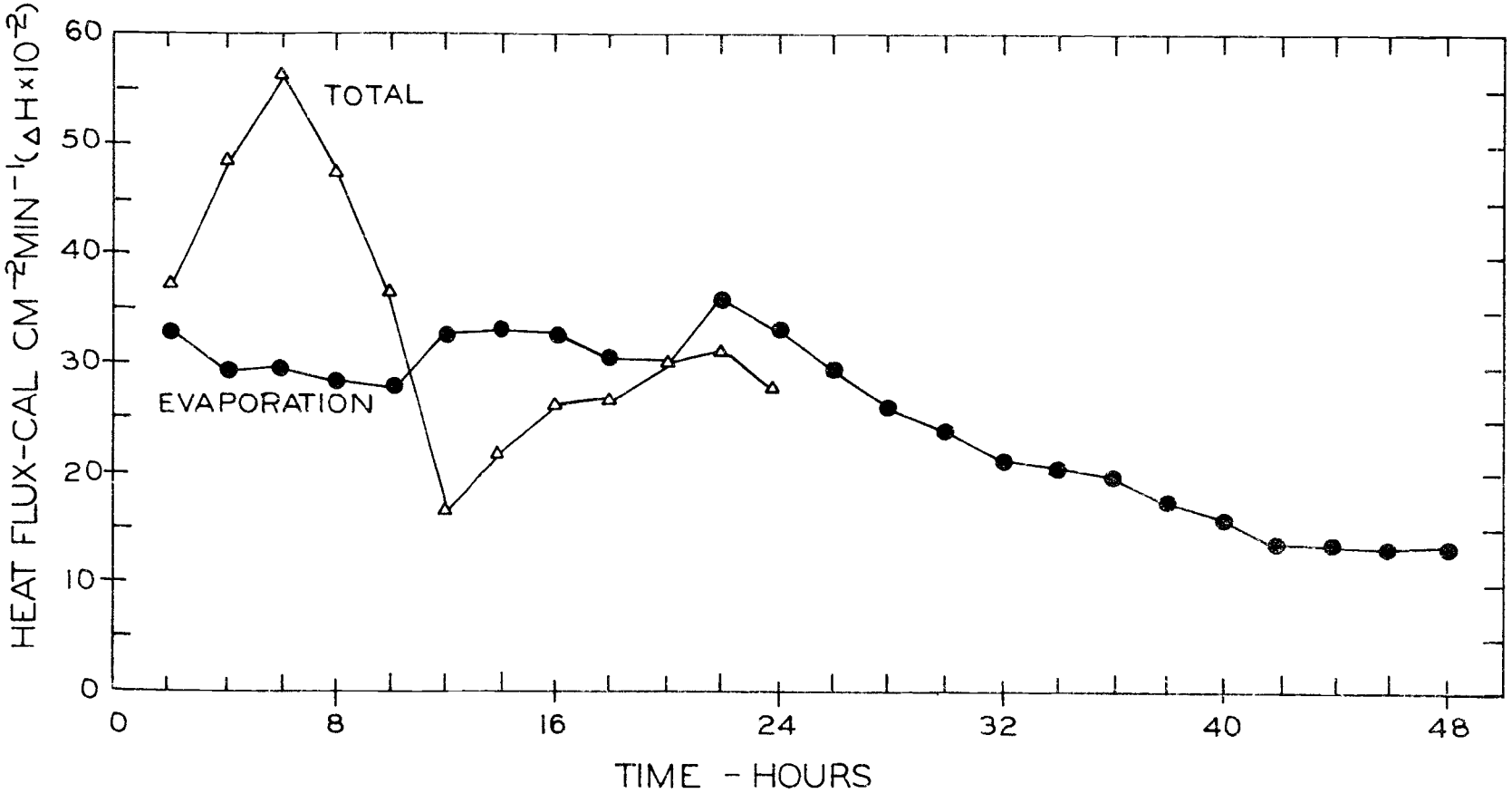

Figure 69. Heat flux variations in initially saturated column of the 149-210 microns size glass beads.

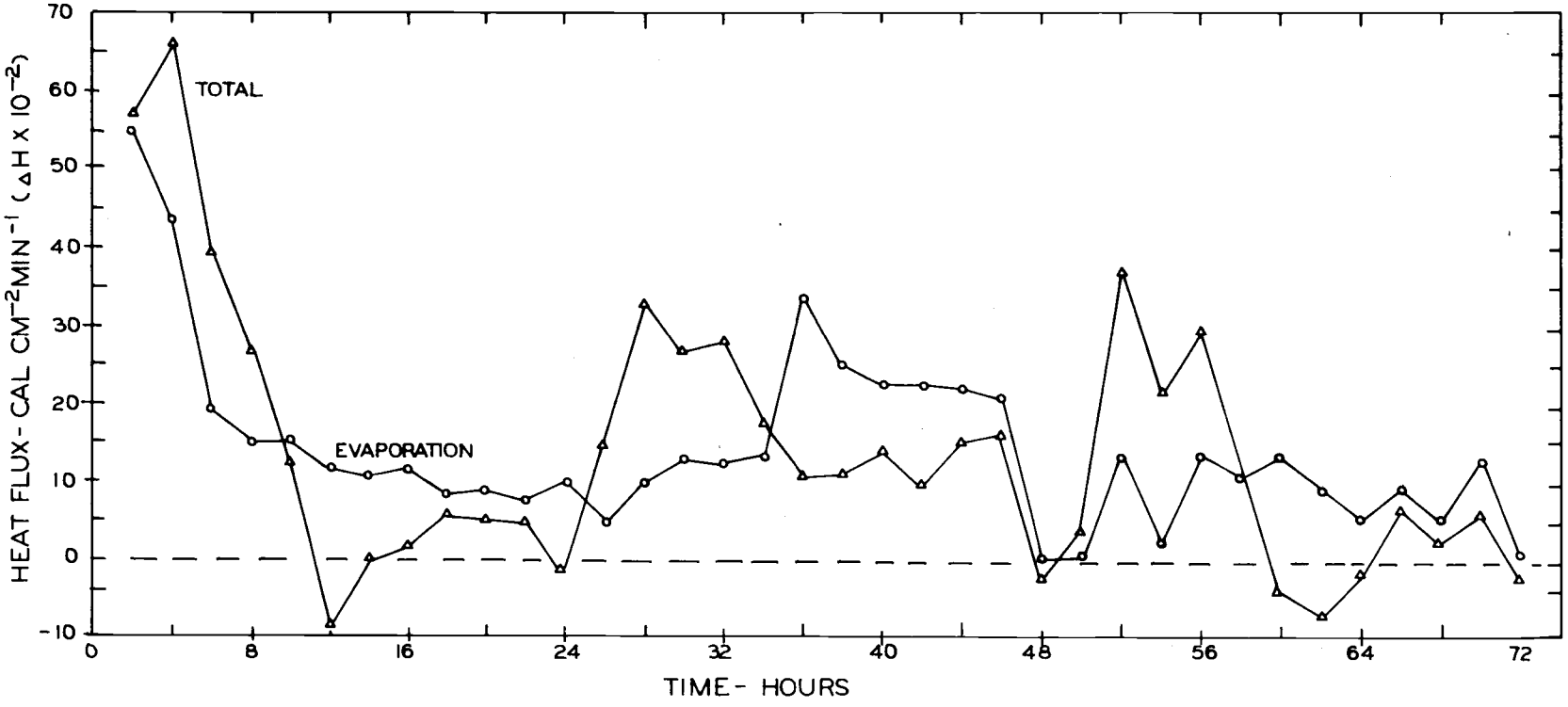

Figure 70. Heat flux variations in initially unsaturated column of the 53-74 microns size glass beads. Experiment IV.

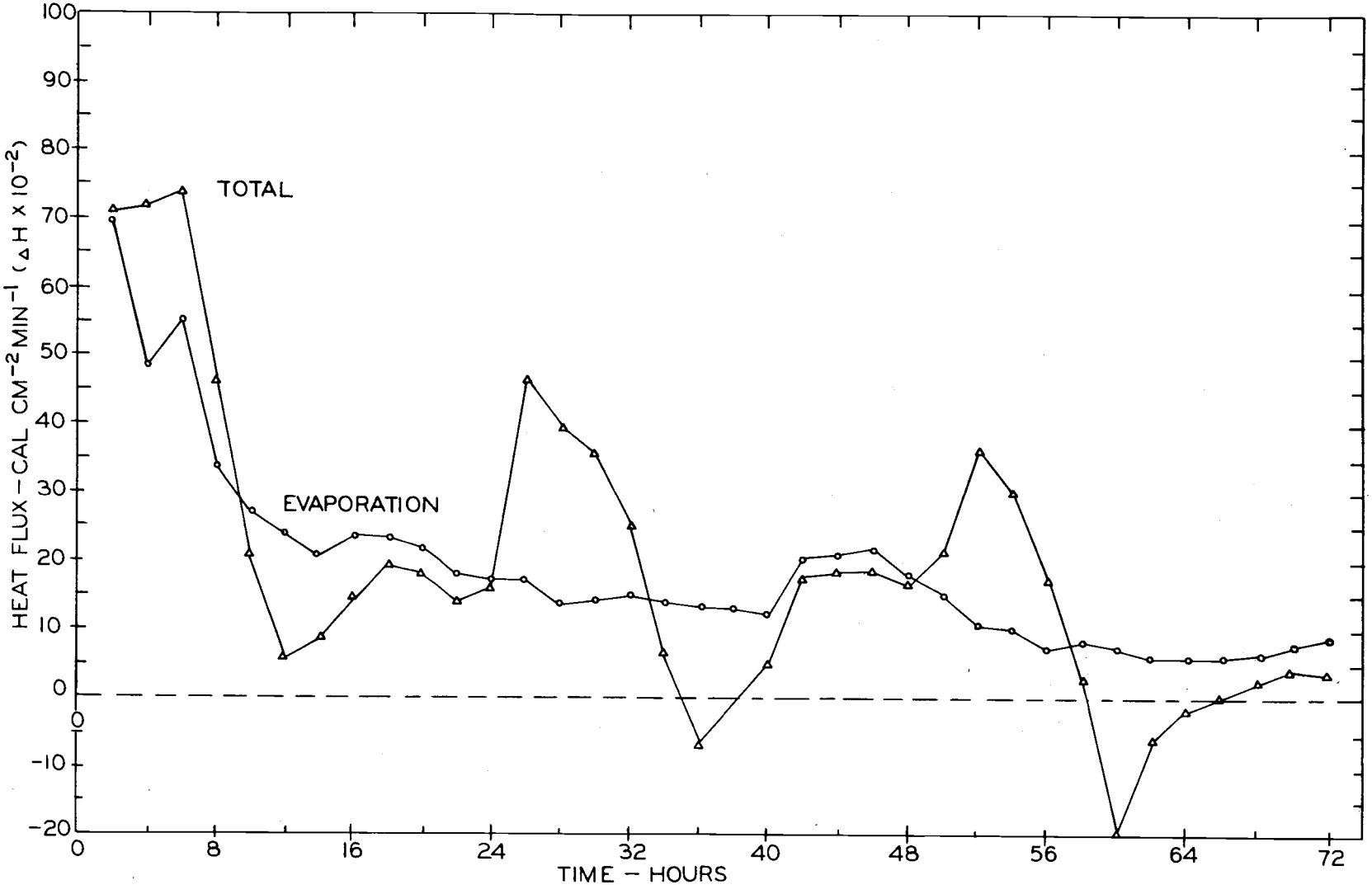

Figure 71. Heat flux variations in initially unsaturated column of the 149-210 microns size glass beads. Experiment VIII.

SUMMARY AND CONCLUSION

The importance of soil water characteristic curves necessitates a relatively easy and quick method to determine these curves. The use of a mercury intrusion porosimeter as compared to the standard technique of using porous plates has been evaluated for this purpose. Eight soils differing in clay content were tested. Although the porosimeter technique gives very reproducible results, the pore size distribution curves obtained from porosimeter and pressure plate methods do not agree. The degree of this discrepancy depends upon the clay content of the soil.

Two major reasons for the deviations encountered are due to (1) a computational procedure that does not account for the volume of pores larger than pore diameter corresponding to a pressure of 6.0 psi and smaller than the pore diameter corresponding to a pressure of 5000 psi, (2) the pore aperture size calculations based on the pressure displacement equation that underestimates the pore diameter and, therefore, require a correction factor (Klock, Boersma, and DeBacker, 1969). The adjustments for these two factors make the pore size distribution curves obtained from mercury intrusion and pressure plate methods coincide. The problem, however, gets more complicated in soils that contain swelling type of clays. A procedure to obtain soil water characteristic curves from porosimeter

has been given. It is suggested that the porosimeter technique be established as a routine laboratory procedure.

Several investigators have attempted to predict thermal conductivities of porous media based on the properties of their constituents. The model developed by de Vries (1966) has been tested. Three size fractions of glass beads are used. The predicted and the experimental values of thermal conductivity indicate a good agreement.

Heat is transferred from a hot to a cold region by three mechanisms: (i) conduction, (ii) convection, and (iii) vapor transfer. It was postulated that in porous materials with similar properties, vapor transfer component of heat transfer is pore size dependent. The results obtained with the three size fractions of glass beads (Figure 30), however, refute this hypothesis, indicating that the contribution of vapor transfer to heat transfer is insignificantly small as compared to the total thermal conductivity.

Two of the three size fractions of glass beads were used to further investigate the simultaneous flow of heat and water subjected to daily temperature fluctuations. Water content measurements indicate the influence of pore size distributions on rate of water loss from the porous beds. Large pores introduce low resistance to vapor flow and as expected rapid evaporation occurred in coarse beds. As a result the quantity of heat exchanged has been observed to be much

larger in coarse samples than in fine samples. The sensible heat flux, however, did not indicate any effect of pore size distribution. Again, the sensible heat flux was observed to be approximately the same in saturated, initially saturated and initially unsaturated beds. The results tend to confirm the previous observation that heat transfer is independent of pore size distribution and the vapor transfer component of heat transfer is insignificant.

Heat flux calculations, also, show that the incoming radiations were more efficiently used in moist systems than in dry systems. In moist beds that were allowed to dry during the experiments, the total heat flux consists mainly of evaporative flux. The sensible heat flux, however, has been observed to be similar to that in saturated samples. To maintain an adequate balance of water in agricultural soil, the results suggest the quantity of water lost must be replenished.

BIBLIOGRAPHY

Cary, J.W. 1963. Onsager's relations and non-isothermal diffusion of water vapor. Journal of Physical Chemistry 67:126-129.

Cary, J.W. 1964. An evaporation experiment and its irreversible thermodynamics. International Journal of Heat Mass Transfer 7:531-537.

Cary, J.W. 1965. Water flux in moist soil: Thermal versus suction gradients. Soil Science 100:168-175.

Cary, J.W. 1966. Soil moisture transport due to thermal gradients: Practical aspects. Soil Science Society of America, Proceedings 30:428-433.

Childs, E.C. 1940. The use of soil moisture characteristics in soil studies. Soil Science 50:239-252.

Cochran, P.H., L. Boersma and C.T. Youngberg. 1967. Thermal properties of a pumice soil. Soils Science Society of America, Proceedings 31:454-459.

de Vries, D.A. 1952. The thermal conductivity of soil. Mededelingen van de Landbouwhogeschool te Wageningen 52:1-73.

de Vries, D.A. 1966. Thermal properties of soils. In: Physics of Plant Environment. W.R. Van Wijk (ed.). North-Holland Publishing Company, Amsterdam. 379 p.

Dirksen, C. 1964. Water movement and frost heaving in unsaturated soil without an external source of water. Unpublished Ph.D. thesis, Cornell University. 140 pages.

Drake, L.E. and H.L. Ritter. 1945. Macropore size distribution in some typical porous substances. Industrial and Engineering Chemistry, Analytical ed. 17:781.

Gardner, H.R. and R.J. Hanks. 1966. Evaluation of the evaporation zone in soil by measurement of heat flux. Soil Science Society of America, Proceedings 30:425-428.

Gardner, H.R. and D.F. Hillel. 1962. The relations of external evaporative conditions to the drying of soils. Journal Geophysical Research 67:4319-4325.

Gement, A. 1950. The thermal conductivity of soil. Journal of Applied Physics 21:750-752.

Gurr, C.G., T.J. Marshall and J.T. Hutton. 1952. Movement of water in soil due to a temperature gradient. Soil Science 74:335-345.

Hanks, R.J. and H.R. Gardner. 1965. Influence of different diffusivity water content relations on evaporation of water from soils. Soil Science Society of America, Proceedings 29:495-498.

Hillel, D. and J. Mottes. 1966. Effect of plate impedance, wetting method and aging on soil moisture retention. Soil Science 102:135-139.

Jackson, R.D., R.J. Reginato and C.H.M. van Bavel. 1965. Comparison of measured and calculated hydraulic conductivities of unsaturated soils. Water Resources Research 1:375-380.

Jones, H.E. and H. Kohnke. 1952. The influence of soil moisture tension on vapor movement of soil water. Soil Science Society of America, Proceedings 16:245-248.

Juhola, A.J. and E.O. Wiig. 1949. Pore structure in activated charcoal. II. Determination of macro pore-size distribution. Journal of the American Chemical Society 71:2078-2080.

Klock, G.O. 1968. Pore size distribution as measured by the mercury intrusion method and their use in predicting permeability. Ph.D. thesis, Oregon State University. 91 numbered leaves.

Klock, G.O., L. Boersma and L.W. DeBacker. 1969. Pore size distribution as measured by the mercury intrusion method and their use in predicting permeability. Soil Science Society of America, Proceedings 33:12-15.

Kowsar, A. 1968. Effects of petroleum mulch on soil water content and soil temperature. M.S. thesis. Corvallis, Oregon State University. 103 numb. leaves.

Leamer, R.W. and J.F. Lutz. 1940. Determination of pore size distribution in soils. Soil Science 49:347-360.

Lebedeff, A.F. 1927. The movement of ground and soil water. First International Congress of Soil Science, Proceedings 1:459-494.

Lund, Z.F. 1959. Available water-holding capacity of alluvial soils in Louisiana. Soil Science Society of America, Proceedings 23:1-3.

Maclean, D.J. and P.M. Gwatkin. 1946. Moisture movements occurring in soil due to the existence of a temperature gradient. Road Research Laboratory, D.S.I.R. England, Note RN/761.

Nakshabandi, G. Al and H. Kohnke. 1965. Thermal conductivity and diffusivity of soils as related to moisture tension and other physical properties. Agricultural Meteorology 2:271-279.

Nielsen, D.R. and R.E. Phillips. 1958. Small fritted glass bead plates for determination of moisture retention. Soil Science Society of America, Proceedings 22:574-575.

Phillip, J.R. and D.A. de Vries. 1957. Moisture movement in porous materials under temperature gradients. American Geophysics Union, Transactions 38:222-232.

Purcell, W.R. 1949. Capillary pressures--Their measurement using mercury and the calculation of permeability therefrom. Petroleum Branch American Institute of Mining and Metalurgical Engineers, Transactions 186:39-50.

Richards, L.A. 1941. A pressure-membrane extraction apparatus for soil solution. Soil Science 51:377-386.

Richards, L.A. 1947. Pressure membrane apparatus, construction, and use. Agricultural Engineering 28:451-454.

Richards, L.A. 1948. Porous plate apparatus for measuring moisture retention and transmission by soil. Soil Science 66:105-110.

Richards, L.A. 1949a. Methods of measuring soil moisture tension. Soil Science 68:95-112.

Richards, L.A. 1949b. Methods for mounting porous plates used in moisture measurements. Agronomy Journal 41:487-490.

Ritter, L.C. and R.L. Drake. 1945. Pore size distributions in porous materials. Industrial and Engineering Chemistry, Analytical ed. 17:792.

Rose, C.W. 1966. Agricultural Physics. Printed in Great Britain by the Camelot Press Limited, London and Southampton. p. 230.

Schofield, R.K. 1939. Pore size distribution as revealed by the dependence of suction on moisture content. In: Transactions of the First Commission of the International Society of Soil Science. Bangor, Wales, 1939, ed. by G.W. Robinson. Vol. A. Aberystwyth. p. 54-57.

Skaggs, R.W. and E.M. Smith. 1967. Apparent thermal conductivity of soil as related to soil porosity. Paper No. 67-114 presented at the Annual Meeting of the ASAE at Saskatoon, Saskatchewan, June 27-30.

Smith, A. 1932. Seasonal subsoil temperature variations. Journal of Agricultural Research 44:421-428.

Smith, W.O. 1939. Thermal conductivities in moist soils. Soil Science Society of America, Proceedings 4:32-40.

Smith, W.O. and H.G. Byers. 1938. The thermal conductivity of dry soils of certain of the great soil groups. Soil Science Society of America, Proceedings 3:13-19.

Stakman, W.P. 1969. Jaarverslag 1969. Instituut voor Cultuurtechniek en Waterhuishouding. Staringgebouw, Wageningen, The Netherlands. p. 10.

Tanner, C.B., S.J. Bourget and W.E. Holmes. 1954. Moisture tension plates constructed from alundum filter discs. Soil Science Society of America, Proceedings 18:222-223.

Taylor, S.A. 1962. The influence of temperature upon the transfer of water in soil systems. Mededelingen Landbouwhogeschool Ghent 27:535-551.

Taylor, S.A. 1963. Simultaneous flows in soils and plants. Utah State University Monographs, Logan, Utah. 101 p.

Taylor, S.A. and J.W. Cary. 1960. Analysis of the simultaneous flow of water and heat with the thermodynamics of irreversible processes. Seventh International Congress of Soil Science, Transactions, Madison, Wisconsin 1:80-90.

Taylor, S.A. and J.W. Cary. 1964. Linear equations for the simultaneous flow of matter and energy in a continuous soil system. Soil Science Society of America, Proceedings 28:167-172.

Taylor, S.A. and J.W. Cary. 1965. Soil water movement in vapor and liquid phases. In: Eckardt, F.E., (ed.). Methodology of Plant Eco-physiology. UNESCO Arid Zone Research 25:159-165.

U.S. Soil Conservation Service. 1967. Supplement to the soil classification system (7th approximation). Washington, D.C. 207 p.

Van Wijk, W.R. and D.A. de Vries. 1966. Periodic temperature variations in a homogeneous soil. In: Physics of Plant Environment. North-Holland Publishing Company, Amsterdam. 379 p.

Washburn, E.W. 1921. Note on a method of determining the distribution of pore sizes in a porous media. National Academy of Science, Proceedings 7:115.

Weast, R.C. (ed.). 1964. Handbook of chemistry and physics. 45th ed. Cleveland, The Chemical Rubber Company.

Webb, J. 1956. The thermal conductivity of soil. Nature 177:989.

Weigand, C.L. and S.A. Taylor. 1962. Temperature depressions and temperature distribution in drying soil columns. Soil Science 94:75-79.

Winslow, N.M. and J.J. Shapiro. 1959. An instrument for the measurement of pore-size distribution by mercury penetration. ASTM Bulletin 49:39-44.

Woodside, William. 1958. Calculation of the thermal conductivity of porous media. Canadian Journal of Physics 36:815-923.

Woodside, J. and J.B. Cliffe. 1959. Heat and moisture transfer in closed systems of two granular materials. Soil Science 87:75-82.

APPENDIX

APPENDIX I

Calculations of Pressure Correction for Hanging Mercury Column in Penetrometer Assembly

Length of penetrometer = 26 cm

Density of mercury = 13.6 g/cm^3

1 lb = 453.6 g

1 in^2 = 6.452 cm^2

Let the penetrometer reading be 0.02. The length of mercury column at this point was measured to be 24.62 cm.

Pressure exerted by the hanging mercury column

$$= 24.62 \text{ cm} \times 13.6 \frac{g}{cm^3} \times \frac{1}{453.6 \frac{g}{lb}} \times 6.452 \frac{cm^2}{in^2}$$

$$= 4.764 \frac{lb}{in^2}$$